International Journal of Applied Mathematics
Volume 38 No. 4s, 2025
ISSN: 1311-1728 (printed version); ISSN: 1314-8060 (on-line version)

REVISITING FINITE DIFFERENCE SOLUTIONS FOR HEAT-TYPE EQUATIONS. PART III. DIFFUSION-ADVECTION TRANSFER

G. Garrido [1,§] , J. L. G. Pestaña [2]

[1] Departamento de Informática, Universidad de Jaén
Campus Las Lagunillas, 23071 Jaén, Spain
e-mail: ggluque@ujaen.es

[2] Departamento de Física, Universidad de Jaén
Campus Las Lagunillas, 23071 Jaén, Spain
e-mail: jlg@ujaen.es

August 26, 2025

Abstract

In this third paper of a series, we revisit all major systematic uncertainties that affect a complete and unbiased sample of twelve finite difference schemes for diffusion-advection-like equations. In order to provide the coherent picture, unlike the existing way, we use as the key tenets both the

Received: August 04, 2025

International Journal of Applied Mathematics
Volume 38 No. 4s, 2025
ISSN: 1311-1728 (printed version); ISSN: 1314-8060 (on-line version)

reverse Taylor's analysis and the discrete Fourier's analysis, as well as the monotonicity analysis. For every type of scheme, their theoretical uncertainties are examined. A detailed graphical investigation is also provided. We find that no scheme considered in this study resolves the smaller length scales well. We report numerous unexpected results, almost all of them related to the stability issue. Furthermore, we present several numerical experiments on an equal footing corroborating our demonstrations and proving to what degree the accuracy of each scheme is impaired by the discontinuities in the data. A comparison with each other is made as well. We definitively establish that the Crank-Nicolson scheme is preferred by experiments.

Math. Subject Classification: 35Q68, 35K05, 35K10, 65M06, 65N22, 97N40

Key Words and Phrases: PDEs in connection with computer science; Heat equation; Second-order parabolic equations; Finite difference methods for initial value and initial-boundary value problems involving PDEs; Numerical solution of discretized equations for boundary value problems involving PDEs; Numerical analysis (educational aspects)

1 Introduction

The old finite difference method is presently used in numerous compute resources and courses, not only in mathematics, but also in natural sciences, engineering, and noticeably even in social sciences. However it is not easy to find the why similar schemes on a given partial differential equation provide dissimilar results, and even a given scheme on comparable partial differential equations offers disparate results. By relying on general diagnostic tools Parts I and II find the first why, and this study aims to find the second one.

In this third review paper in a series of four papers (following [6, 7], Part I and II, respectively), we re-investigated how well finite

Received: August 04, 2025

International Journal of Applied Mathematics
Volume 38 No. 4s, 2025
ISSN: 1311-1728 (printed version); ISSN: 1314-8060 (on-line version)

difference schemes solve the diffusive-advective transfer in linearized form. In the last paper in the series, we shall extend this Part III by including nonlinearities of a first order variable velocity and source term.

The scope of this Part III is exactly to integrate the simplest (Dirichlet, linear and unidimensional) diffusion-advection parabolic differential equation, $\frac{\partial T}{\partial t} = -v\frac{\partial T}{\partial x} + \alpha\frac{\partial^2 T}{\partial x^2}$ (Eq. (2.23) of Part I), using all at most three-level, low-order schemes. While doing so, we explain all the methodological insights and concerns of the difference equation. Also, we do it in the chronological sequence in which they were developed. However, in what follows we will not review the principles of this finite difference approach but refer the reader to Part I for their details and clarification of notation.

The paper is organized as follows. In Section 2 we rigorously investigate all twelve pioneering schemes which our topical current understanding of parabolic differential equations involving both the first and the second spatial derivative (see both Part I and Part II) is based on, namely the Richardson's, Schmidt's, Crank-Nicolson, Laasonen's, Courant-Isaacson-Rees, Du Fort-Frankel, Wendroff's, Lax-Wendroff, Molenkamp's, Runchal's, Lerat's and Crouzeix's schemes. In this study we do not select mixture schemes (see Part I); and hence this sample as a whole, however, does not include neither a possible mixture of the Lax's and Du Fort-Frankel schemes nor their ill-defined Lax-Richtmyer counterpart (see Part II). In Section 3 we implement all of these schemes. Then, as a proof of concept, we both discuss their performance properties and eventually compare them with each other. Finally Section 4 presents a short summary and conclusive remarks, highlighting the differences between the dissipative couplings of Part I and the dynamical couplings of Part II. Motivated in particular by discontinuities in the data, A shows the exemplary initial value problem, as simple as it is very interesting, we apply in Section 4.

Received: August 04, 2025

International Journal of Applied Mathematics
Volume 38 No. 4s, 2025
ISSN: 1311-1728 (printed version); ISSN: 1314-8060 (on-line version)

2 The difference equations

In this Section we lay groundwork for detailed follow-up performance tests. We thoroughly revisit the finite difference equations for canonical linear diffusion-advection equation, Eq. (2.23) of Part I, up to second order in the derivatives and also carefully examine the sources and form of their theoretical uncertainties, i.e. we answer analytically to consistency, stability and convergence criteria. We highlight the conceptual differences between not only hierarchical and monolithic schemes but also notably two and three level hierarchical schemes. We also show for the first time the risk of spatial oscillations throughout the entire range of wavenumbers, that is to say we examine separately all the Fourier components of the spatial variation. We sort the exposition, motivated by technical considerations lacking in literature, by chronology and acknowledging their authors.

To aid comparison with our canonical linear diffusion-advection equation we note that the exact growth factor in one of the Fourier modes is equal to $\exp(-\alpha\, k^2\, \Delta t)$, the exact propagation velocity is the constant v and we shall represent exact phase angle, $-C\, k\Delta x$, in every scheme.

Building on our previous studies, which demonstrated the complementarity of Hirt's and von Neumann's analysis, we present new analyses on the resulting properties of these difference equations. Indeed, the diffusion-advection equation is fascinating, but somewhat notorious for the difficulty of its numeric formulation; which is particularly true for the stability criteria [18].

2.1 The Richardson's 1910 three-time-level explicit scheme

2.1.1 Construction

In 1910 Richardson [14] devised the pioneering scheme which was explicit in time and gave values at any time level in terms of values at the previous two time levels. To achieved this, he discretized

Received: August 04, 2025

International Journal of Applied Mathematics
Volume 38 No. 4s, 2025
ISSN: 1311-1728 (printed version); ISSN: 1314-8060 (on-line version)

Table 1: Schemes analysed in this work. Note that n represents the temperature at the current time step whereas $n+1$ (colored in red) represents the new (future) temperature. Note also the temperature one time step in the past, $n-1$ (colored in violet).

Author	Algorithm
Richardson [14]	$T_j^{n+1} = T_j^{n-1} + (2\,F + C)\,T_{j-1}^n - 4\,F\,T_j^n + (2\,F - C)\,T_{j+1}^n$
Schmidt [16]	$T_j^{n+1} = (F + 0.5\,C)\,T_{j-1}^n + (1 - 2\,F)T_j^n + (F - 0.5\,C)\,T_{j+1}^n$
Crank-Nicolson [2]	$(-0.5\,F - 0.25\,C)\,T_{j-1}^{n+1} + (1 + F)\,T_j^{n+1} + (-0.5\,F + 0.25\,C)\,T_{j+1}^{n+1}$ $= (0.5\,F + 0.25\,C)\,T_{j-1}^n + (1 - F)\,T_j^n + (0.5\,F - 0.25\,C)\,T_{j+1}^n$
Laasonen [8]	$(-F - 0.5\,C)\,T_{j-1}^{n+1} + (1 + 2\,F)\,T_j^{n+1} + (-F + 0.5\,C)\,T_{j+1}^{n+1} = T_j^n$
Courant-Isaccson-Rees [1]	$T_j^{n+1} = (F + C)\,T_{j-1}^n + (1 - 2\,F - C)\,T_j^n + F\,T_{j+1}^n$
Du Fort-Frankel [5]	$T_j^{n+1} = \left(\frac{1-2\,F}{1+2\,F}\right)T_j^{n-1} + \left(\frac{2\,F+C}{1+2\,F}\right)T_{j-1}^n + \left(\frac{2\,F-C}{1+2\,F}\right)T_{j+1}^n)$
Wendroff [19]	$(1 - F - C)\,T_{j-1}^{n+1} + (1 + 2\,F + C)\,T_j^{n+1} - F\,T_{j+1}^{n+1} = (1 + F + C)\,T_{j-1}^n$ $+(1 - 2\,F - C)\,T_j^n + F\,T_{j+1}^n$
Lax-Wendroff [10]	$T_j^{n+1} = (F + 0.5\,C + 0.5\,C^2)\,T_{j-1}^n + (1 - 2\,F - C^2)\,T_j^n$ $+(F - 0.5\,C + 0.5\,C^2)\,T_{j+1}^n$
Molenkamp [12]	$(-F - C)\,T_{j-1}^{n+1} + (1 + 2\,F + C)\,T_j^{n+1} - F\,T_{j+1}^{n+1} = T_j^n$
Runchal [15]	$-0.5\,F\,T_{j-1}^{n+1} + (1 + F)\,T_j^{n+1} - 0.5\,F\,T_{j+1}^{n+1} = (0.5\,F + C)\,T_{j-1}^n$ $+(1 - F - C)\,T_j^n + 0.5\,F\,T_{j+1}^n$
Lerat [11]	$(-F - 0.5\,C - 0.5\,C^2)\,T_{j-1}^{n+1} + (1 + 2\,F + C^2)\,T_j^{n+1}$ $+(-F + 0.5\,C - 0.5\,C^2)\,T_{j+1}^{n+1} = T_j^n$
Crouzeix [3]	$-F\,T_{j-1}^{n+1} + (1 + 2\,F)\,T_j^{n+1} - F\,T_{j+1}^{n+1} = 0.5\,C\,T_{j-1}^n + T_j^n - 0.5\,C\,T_{j+1}^n$

both time and space derivatives by second order central differences, Eqs. (2.9) and (2.10) of Part I respectively, i.e.,

$$\frac{T_j^{n+1} - T_j^{n-1}}{2\Delta t} = -v\frac{T_{j+1}^n - T_{j-1}^n}{2\,\Delta x} + \alpha\frac{T_{j-1}^n - 2\,T_j^n + T_{j+1}^n}{(\Delta x)^2}. \qquad (2.1)$$

However, as a three-time-level bottom-up scheme that it is, the Richardson's scheme has the problem of setting the initial grid function value; i.e. we have to decide how start the process. The solution is to use any other single-step scheme, as shortly discussed.

For easy reference we reformulate Eq. (2.1) in the second column in Table 1 introducing, for convenience, the F dimensionless Fourier number ($F = \alpha\frac{\Delta t}{(\Delta x)^2}$, Eq. (3.2) of Part I) and the C dimensionless Courant-Isaacson-Rees number ($C = v\frac{\Delta t}{\Delta x}$, Eq. (2.2) of Part II), both of which provide a measurement for the spatiotemporal discretization and whose ratio $\frac{C}{F} = \frac{v}{\alpha}\Delta x = P$, the so-called Péclet number, is an indicator of the relative importance of advection versus diffusion.

Received: August 04, 2025

International Journal of Applied Mathematics
Volume 38 No. 4s, 2025
ISSN: 1311-1728 (printed version); ISSN: 1314-8060 (on-line version)

2.1.2 Stability

We firstly analyze the stability using the von Neumann's method. Substituting a term of Eq. (2.1) of Part I into each term in Eq. (2.1) we get the equation for the growth factor (Eq. (2.15) of Part I),

$$G = \frac{1}{G} - 4\,F\,(1 - \cos{(k\Delta x)}) - 2\,i\,C\sin{(k\Delta x)}, \qquad (2.2)$$

whose complex solutions are

$$\begin{aligned} G_{\pm} &= -2\,F(1-\cos{(k\Delta x)}) - i\,C\sin{(k\Delta x)} \\ &\pm \sqrt{[2\,F(1-\cos{(k\Delta x)})]^2 - [C\,\sin{(k\Delta x)}]^2 + 1 + 4\,i\,F\,C(1-\cos{(k\Delta x)})\sin{(k\Delta x)}} \\ &= \frac{1}{2}[-a_1 \pm a_4 - i\,(a_2 \pm a_5)]; \end{aligned} \qquad (2.3)$$

and whose magnitude components take the form

$$|G_{\pm}| = \frac{1}{4}[(-a_1 \pm a_4)^2 + (-a_2 \mp a_5)^2], \qquad (2.4)$$

where

$$a_1 = 4\,F\,(1-\cos{(k\Delta x)}), \qquad (2.5)$$
$$a_2 = 2\,C\sin{(k\Delta x)}, \qquad (2.6)$$
$$a_3 = a_1^2 - a_2^2 + 4, \qquad (2.7)$$
$$a_4 = \sqrt{\sqrt{a_3^2 + 4\,a_1^2\,a_2^2} + a_3}, \qquad (2.8)$$
$$a_5 = \frac{a_1\,a_2}{|a_1\,a_2|}\sqrt{\sqrt{a_3^2 + 4\,a_1^2\,a_2^2} - a_3}. \qquad (2.9)$$

That is to say, as a three time level that it is, this scheme has two temporal modes. Note, the solution G_+ corresponds to the physical mode because for well resolved components ($k\Delta x \ll 1$) its real (observable) part is as it should be; and vice versa:

$$\lim_{k\Delta x \to 0} \Re(G_{\pm}) = \pm\sqrt{2}. \qquad (2.10)$$

Received: August 04, 2025

International Journal of Applied Mathematics
Volume 38 No. 4s, 2025
ISSN: 1311-1728 (printed version); ISSN: 1314-8060 (on-line version)

However, the most important of what happens to the Richardson's growth factor is that the magnitude of its modes take the start values

$$\lim_{k\Delta x \to 0} |G_\pm| = 2 > 1, \tag{2.11}$$

which means that the low frequency (physical and spurious) modes do not satisfy Eq. (2.16) of Part I, implying that the Richardson's scheme is unconditionally unstable for the diffusion-advection equation. The same as in Part I. In fact, this in turn tells us all about Eq. (2.1): it is a no go scheme which can not be applied to any problem involving diffusion.

2.2 The Schmidt's 1924 single-step explicit scheme

2.2.1 Construction

In 1924 Schmidt [16] proposed a second order approximation for the spatial derivatives but forward in time, i.e.

$$\frac{T_j^{n+1} - T_j^n}{\Delta t} = -v \frac{T_{j+1}^n - T_{j-1}^n}{2\,\Delta x} + \alpha \frac{T_{j-1}^n - 2T_j^n + T_{i+1}^n}{(\Delta x)^2}, \tag{2.12}$$

which is also reformulated in Table 1 using F and C.

2.2.2 Consistency and order of accuracy

We firstly analyze the consistency of the scheme using the Hirt's method. Substituting each value of T at points other than point (x_j, t^n) in the scheme in a Taylor series around the value T_j^n at that point (x_j, t^n), i.e. we substitute Eqs. (2.6), (2.12) and (2.13) of Part I in Eq. (2.12), gives

$$\begin{aligned} \frac{\partial T}{\partial t} + v\frac{\partial T}{\partial x} - \alpha \frac{\partial^2 T}{\partial x^2} = & -\frac{\Delta t}{2}\frac{\partial^2 T}{\partial t^2} - \frac{(\Delta t)^2}{6}\frac{\partial^3 T}{\partial t^3} - v\frac{(\Delta x)^2}{6}\frac{\partial^3 T}{\partial x^3} \\ & - \frac{(\Delta t)^3}{24}\frac{\partial^4 T}{\partial t^4} + \frac{\alpha\,(\Delta x)^2}{12}\frac{\partial^4 T}{\partial x^4} + \cdots . \end{aligned} \tag{2.13}$$

Received: August 04, 2025

International Journal of Applied Mathematics
Volume 38 No. 4s, 2025
ISSN: 1311-1728 (printed version); ISSN: 1314-8060 (on-line version)

We then see from that equation, which is not the modified equation, that the right hand side vanishes when $\Delta t \to 0$ and $\Delta x \to 0$ and therefore the Schmidt's scheme of calculation is consistent. In addition, this side goes to zero as the first power of Δt and the second power of Δx, implying that the scheme is of first order accuracy in time and second order accuracy in space as well. Indeed, this result further verifies what would otherwise be expected because the way this scheme is based on Taylor series expansions.

We furthermore provide here the evolution equation with only space derivatives, i.e. the modified equation. In order to achieve it, we firstly find expressions for $\frac{\partial^2 T}{\partial t^2}$, $\frac{\partial^3 T}{\partial t^3}$ and $\frac{\partial^4 T}{\partial t^4}$, and secondly (be careful with this) for $\frac{\partial^2 T}{\partial x \partial t}$, $\frac{\partial^3 T}{\partial x^2 \partial t}$ and $\frac{\partial^4 T}{\partial x^3 \partial t}$, by differentiating Eq. (2.13); all of which we use systematically to eliminate the time derivatives in it. This implies that the modified equation associated with the Schmidt scheme, the equation of the grid function from Schmidt difference equation, is:

$$
\begin{aligned}
\frac{\partial T}{\partial t} + v\frac{\partial T}{\partial x} - \alpha\frac{\partial^2 T}{\partial x^2} = & -\frac{C^2}{2}\frac{(\Delta x)^2}{\Delta t}\frac{\partial^2 T}{\partial x^2} \\
& + \frac{1}{6}(-C + 6\,F\,C - 2\,C^3)\frac{(\Delta x)^3}{\Delta t}\frac{\partial^3 T}{\partial x^3} \\
& + \frac{1}{12}(-C^2 + F - 6\,F^2 + 4\,F\,C^2)\frac{(\Delta x)^4}{\Delta t}\frac{\partial^4 T}{\partial x^4} \\
& + \mathcal{O}((\Delta x)^5),
\end{aligned}
\tag{2.14}
$$

which is one of two ways to next not only calculate the local error but also estimate the stability (see below). Notice that this modified equation reduces to Eq. (3.11) of Part I when $C \to 0$ and Eq. (2.16) of Part II when $F \to 0$, as it must be.

2.2.3 Stability

We secondly analyze the stability using the von Neumann's method. Substituting a term of Eq. (2.1) of Part I into each term in Eq. (2.12) we get the complex valued growth factor (Eq. (2.15) of Part

Received: August 04, 2025

International Journal of Applied Mathematics
Volume 38 No. 4s, 2025
ISSN: 1311-1728 (printed version); ISSN: 1314-8060 (on-line version)

I) associated with the Schmidt's scheme,

$$G = 1 - 2\,F\,(1 - \cos{(k\Delta x)}) - i\,C\sin{(k\Delta x)}, \tag{2.15}$$

whose magnitude component takes the form

$$|G| = \sqrt{[1 - 2\,F\,(1 - \cos{(k\Delta x)})]^2 + (C\sin{(k\Delta x)})^2}, \tag{2.16}$$

which has to satisfy Eq. (2.16) of Part I in order to prevent numerical modes from growing faster than the physical modes of the differential equation; i.e. we must consider the end values of $\cos{(k\Delta x)}$:

1. for the case of $k\Delta x = \pi$, we have $|G|^2 = (1 - 2\,F)^2 \leq 1$ which implies
$$2\,F \leq 1; \tag{2.17}$$
2. for the limiting case $k\Delta x \to 0$, we have (neglecting high-order terms)
$$\lim_{k\Delta x \to 0} |G| = 1 - \frac{1}{2}\,(2\,F - C^2)\,(k\Delta x)^2 \tag{2.18}$$
which implies $2\,F - C^2 \geq 0$, i.e.
$$C^2 \leq 2\,F. \tag{2.19}$$

We plot these conditions for avoiding an instability, Eqs. (2.17) and (2.19), in Fig. 1. Eq. (2.17) is the same as Eq. (3.13) of Part I, as it must be; and, unlike Eq. (2.16) of Part II, the Schmidt's scheme is conditionally stable for the diffusion-advection parabolic differential equation. See also Fig. 2.

Alternatively, the Hirt's method is another way to obtain or confirm this result. Now, if the first (even) term of modified equation (2.14) acting as a diffusion term, which is equal to $\frac{1}{2}(2\,F - C^2)\frac{(\Delta x)^2}{\Delta t}\frac{\partial^2 T}{\partial x^2}$, has to be positive for T_j^n to be damped in time, must have what is coded in Eq. (2.19). Now, unlike Eq. (2.16) of Part II, this possibility does exist. Furthermore, since the even, first term on the right hand of modified equation Eq. (2.14) acting as a dispersive term (is an odd-order derivative) is always negative, for the second diffusive derivative to also be positive then we need what is coded in Eq. (3.15) of Part I as C approaches 0, which certainly implies the same as Eq. (2.17), $F \leq 1/2$.

Received: August 04, 2025

International Journal of Applied Mathematics
Volume 38 No. 4s, 2025
ISSN: 1311-1728 (printed version); ISSN: 1314-8060 (on-line version)

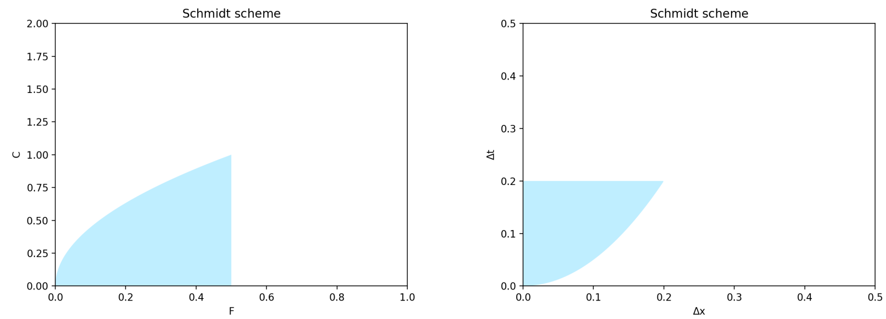

Figure 1: Stability region (by blue colour) of the Schmidt's scheme in both FC and resolution planes, using $\alpha = 0.1$ and $v = 1$ as an example.

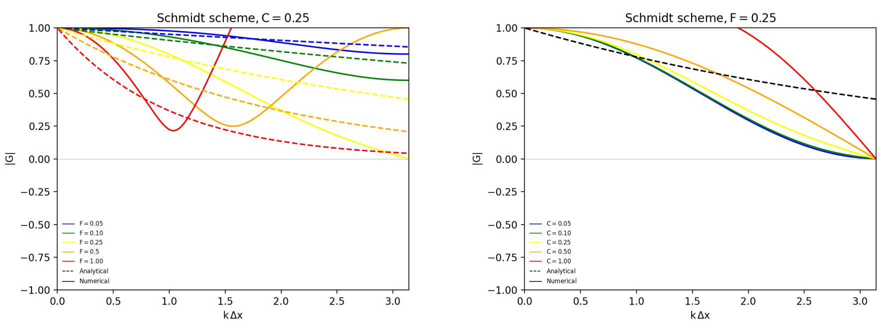

Figure 2: The growth factors of the Schmidt's scheme, Eq. (2.16) vs. frequency in radians, for a specific a nd i llustrative v alue of F (indicated in the legend) with low and high constant C values (left panel); and vice versa (right panel). The growth factor of the analytic solution, $\exp(-\alpha\, k^2\, \Delta t)$ vs. frequency in radians, for the same F values are distinguished by dashed line colors. We show the stability region, Eq. (2.16) of Part I or $[-1, 1]$, and the value "0" that represents the oscillation threshold.

Received: August 04, 2025

International Journal of Applied Mathematics
Volume 38 No. 4s, 2025
ISSN: 1311-1728 (printed version); ISSN: 1314-8060 (on-line version)

2.2.4 Accuracy

We thirdly investigate how accurate, both in magnitude and in phase, the numerical solution is using the Hirt's and von Neumann's complementary analysis.

On the one hand, by applying the discrete Fourier series grid solution of Eq. (2.1) of Part I to the Schmidt's modified equation (2.14) including terms up to the next-to-leading order, the damping term of the numerical solution becomes (see Eq. (2.27) of Part I):

$$\exp\left\{\left[\frac{1}{2}(C^2-2\,F)\,\frac{(\Delta x)^2}{\Delta t}+\frac{1}{24}(-2\,C^2+2\,F-12\,F^2+8\,F\,C^2)\,\frac{(\Delta x)^4}{\Delta t}k^2\right]k^2\,\Delta t\right\}. \tag{2.20}$$

Like its analytical counterpart (see Eq. (2.24) of Part I), we (again) notice that there is a little dissipation for $k=0$ and it will be greater at higher wavenumbers. We now present the search for stiffness in the left panel of Fig. 3 by comparing Eq. (2.20) to Eq. (2.24) of Part I in all the Fourier modes on the grid (Eq. (2.3) of Part I) evaluated for specific F values. Indeed, in this panel we observe the underdamped regime when F is low (note the blue and green lines in the panel) and how for progressively higher values of F, depending of the frequency of the Fourier mode, shift gradually to an anomalous overdamped process, which causes the stiffness. Coincidentally, the right panel shows approximately the case threshold for specific C values. We conclude that the damping factor offers an average description of evolutionary behaviors of amplitudes that is valid at least qualitatively.

Alternatively, since the exact growth factor in one of the Fourier modes is equal to $\exp(-\alpha\,k^2\,\Delta t)$, the Schmidt's relative amplitude error, Eq. (2.29) of Part I, is given by

$$\delta A=e^{\alpha\,k^2\,\Delta t}\sqrt{[1-2\,F\,(1-\cos(k\Delta x))]^2+(C\sin(k\Delta x))^2}-1. \tag{2.21}$$

In the left panel of Fig. 4 we show this error in all the Fourier modes on the grid (Eq. (2.3) of Part I) evaluated for for a specific and illustrative value of C (indicated in the legend) with low and

Received: August 04, 2025

International Journal of Applied Mathematics
Volume 38 No. 4s, 2025
ISSN: 1311-1728 (printed version); ISSN: 1314-8060 (on-line version)

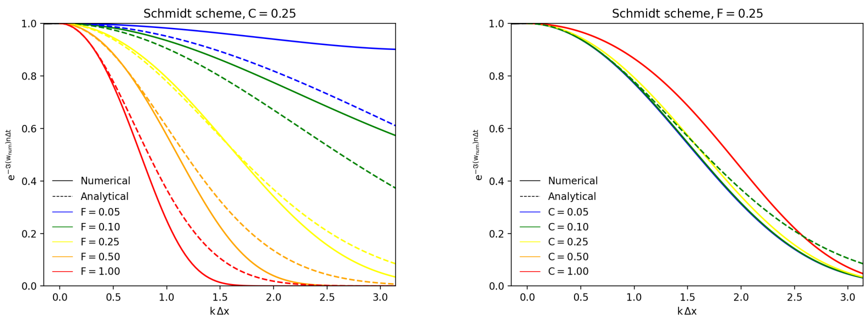

Figure 3: Damping factors (approximated to the four-order derivatives) vs. frequency in radians, for a specific and illustrative value of C (indicated in the legend) with low and high constant F values (left panel); and vice versa (right panel).

high constant F values, where we observe (apart from the region of instability) both the under-damped (note the blue and green lines in the panel, consistent with the underdamped regimen from Eq. (2.20)) and over-damped (note the yellow line in the panel, consistent with the overdamped regimen from Eq. (2.20)) modes and, consequently, the Schmidt's scheme will lose some accuracy. In fact, the right panel of Fig. 4 shows the case when Eq. (2.21) has its largest value from this dissipative point of view, equal to -1. We shall point out later that this dissipative decrease is typically seen in first order schemes.

We thus show that the dispersive numerical behavior of Schmidt's scheme is similar from that shown in the Part I.

On the other hand, by applying the discrete Fourier series grid solution of Eq. (2.1) of Part I to the Schmidt's modified equation (2.14) truncated up to the five-order derivatives, then we see that the dispersive term is given by

$$\exp\left\{i\,k\,\left[x - v\,t + \frac{1}{6}(C - 6\,F\,C + 2\,C^3)\,\frac{(\Delta x)^3}{\Delta t}\,k^2\,t\right]\right\}, \qquad (2.22)$$

implying the dispersive phase velocity shown in Fig. 5, where we

Received: August 04, 2025

International Journal of Applied Mathematics
Volume 38 No. 4s, 2025
ISSN: 1311-1728 (printed version); ISSN: 1314-8060 (on-line version)

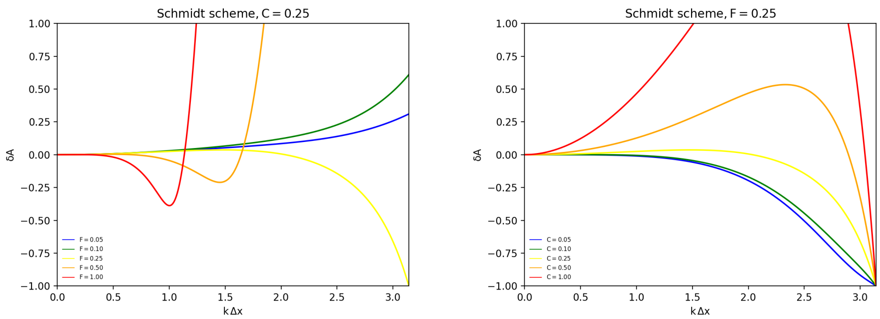

Figure 4: The corresponding relative amplitude errors, Eq. (2.21).

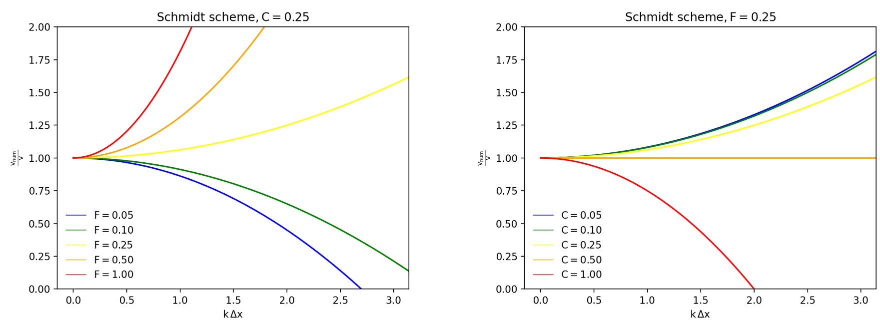

Figure 5: The phase velocity of the Schmidt's solution (approximated to the four-order derivatives), Eq. (2.22) vs. frequency in radians, for specific F and C values which are distinguished by line colors.

find that the instantaneous velocity flips sign when the polynomial of Eq. (2.22) cancels out, i.e. once a stability-threshold is reached.

Alternatively, from the von Neumann's complementary analysis point of view, the numerical phase component of the Schmidt's growth factor, Eq. (2.15), is given by

$$\phi = \arctan\left(\frac{\Im(G)}{\Re(G)}\right) = \arctan\left(\frac{-C\,\sin(k\Delta x)}{1 - 2\,F\,[1-\cos(k\Delta x)]}\right), \quad (2.23)$$

which we show in the Fig. 6.

Received: August 04, 2025

International Journal of Applied Mathematics
Volume 38 No. 4s, 2025
ISSN: 1311-1728 (printed version); ISSN: 1314-8060 (on-line version)

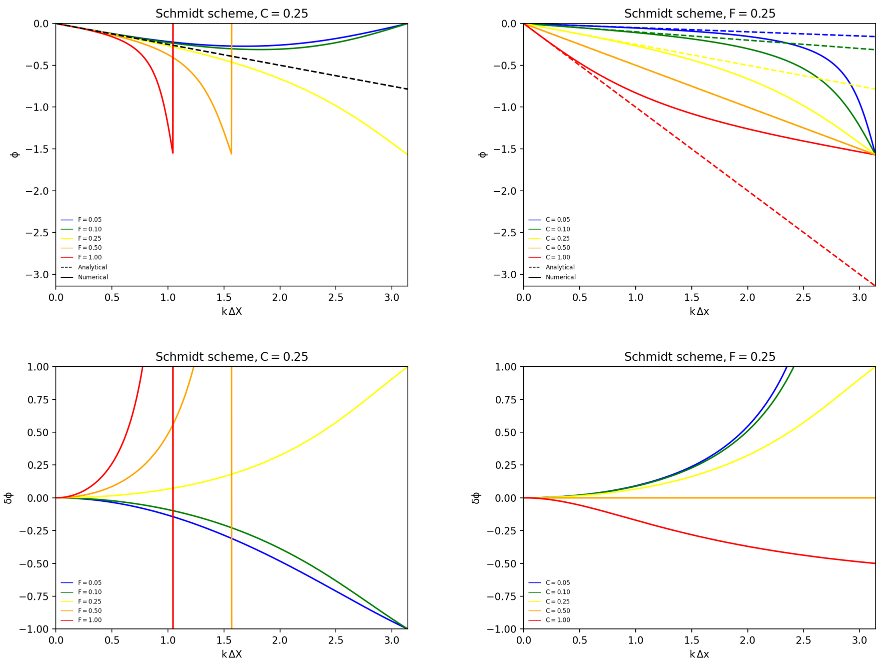

Figure 6: Upper: the phase components of the Schmidt's scheme, Eq. (2.107) vs. frequency in radians, for specific F values as indicated in the legend with low and high constant C values (left panels); and vice versa (right panels). The phase component of the analytic solution, $-C\,k\Delta x$ vs. frequency in radians, for the same F values are distinguished by dashed line colors. Lower: the corresponding numerical relative phase errors, Eq. (2.30) of Part I.

Therefore, since the exact phase speed is the $-v$, we present in the Fig. 6 the numerical relative phase error (see Eq. (2.30) of Part I) of the Schmidt's scheme plotted against the phase angle for specific C and F values.

To shed light on the stability issue is key to consider upper right panel in Fig. 6 where we find, in perfect agreement with findings from Fig. 5, that for $C < 0.5$ waves have leading shift but shift away from the $\delta\phi = 0$ (note the lower right panel in Fig. 6) up

International Journal of Applied Mathematics
Volume 38 No. 4s, 2025
ISSN: 1311-1728 (printed version); ISSN: 1314-8060 (on-line version)

to the stability threshold is reached when we have no dispersion error (although there is an amplitude error, let's not forget), and the relative phase shift error flips sign and the Fourier modes have just the opposite, i.e. lagging shift. Here only short waves with $C < 0.5$ are poorly resolved, quasi-stationary waves. Nevertheless, the upper left panel shows us that for F values less than or below the stability threshold we have leading shift, the relative phase error is less than 0 (note the lower left panel), indicating a numerical propagation speed smaller than the physical one; but shift a little to the line $\delta\phi = 0$ up to the stability threshold is reached when we have no dispersion error, and the relative phase shift error flips sign and the Fourier modes have lagging shift driving the solution to instability.

Note that the orange and red lines in the left panels of 6, which are outside the stability region, have phase jumps. Further on, a more in-depth explanation of this effect is found.

We thus show that the dispersive numerical behavior of Schmidt's scheme is very different from that shown in the Part II.

2.2.5 Monotonicity

Finally, from the Eq. (2.12) the coefficients of the new solution are $F + 0.5\,C$, $1 - 2\,F$ and $F - 0.5\,C$. That is, they are all positive in the stability region, left panel of the Fig. 1. Hence, this Schmidt's scheme behaves monotonically.

2.3 The Crank-Nicolson 1947 single-step semi-explicit scheme

2.3.1 Construction

In 1947 Crank and Nicolson [2] achieved a forward in time scheme using, to say the least, the average of the scheme formerly proposed by Schmidt and the Laasonen's scheme described below. In this way

Received: August 04, 2025

International Journal of Applied Mathematics
Volume 38 No. 4s, 2025
ISSN: 1311-1728 (printed version); ISSN: 1314-8060 (on-line version)

they obtained the semi-explicit scheme (see e.g. Part II):

$$\frac{T_j^{n+1}-T_j^n}{\Delta t} = -v\,\frac{1}{2}\left(\frac{T_{j+1}^{n+1}-T_{j-1}^{n+1}}{2\Delta x}+\frac{T_{j+1}^{n}-T_{i-1}^{n}}{2\Delta x}\right) + \alpha\left(\frac{1}{2}\right)\left(\frac{T_{j-1}^{n+1}-2T_j^{n+1}+T_{j+1}^{n+1}}{(\Delta x)^2}+\frac{T_{j-1}^{n}-2T_j^{n}+T_{j+1}^{n}}{(\Delta x)^2}\right), \tag{2.24}$$

which is again reformulated in Table 1 using F and C.

2.3.2 Consistency and order of accuracy

Eq. (2.24) now poses a significant challenge to deriving consistency because we must reduce the number of indexes in it before raising and/or lowering them. Thus, in this situation we reformulate Eq. (2.24) once more so it would be suitable to derive an equation with derivatives only. Specifically, we rewrite Eq. (2.24) as $(1+F)\,T_j^{n+1} = (1-F)\,T_j^n + (F+0.5\,C)\,T_{j-1}^{n+1/2} + (F-0.5\,C)\,T_{j+1}^{n+1/2}$. Next, substituting each value of T at points other than point $(x_j, t^{n+1/2})$ in this equation in a Taylor series around the value T_j^n at that point $(x_j, t^{n+1/2})$, gives

$$\frac{\partial T}{\partial t}+v\frac{\partial T}{\partial x}-\alpha\frac{\partial^2 T}{\partial x^2} = -\frac{\alpha}{4}\frac{(\Delta t)^2}{(\Delta x)^2}\frac{\partial^2 T}{\partial t^2}-\frac{v\,(\Delta x)^2}{6}\frac{\partial^3 T}{\partial x^3}-\frac{(\Delta t)^2}{48}\frac{\partial^3 T}{\partial t^3}+\cdots. \tag{2.25}$$

We then see from that equation (which is not the modified equation) that, due to the first term on the right hand side, the Crank-Nicolson scheme of calculation is consistent only if $\Delta t \to 0$ and $\Delta x \to 0$ are taken such that $\frac{\Delta t}{\Delta x} \to 0$. In other words,

1. if a time step $\Delta t \sim (\Delta x)^2$ is used we then achieve second order accuracy in both time and space as well;

2. however, for any value of $\frac{\Delta t}{\Delta x}$ the solution is not quite parabolic but nearly hyperbolic (i.e. it converges to that of a wave equation).

Received: August 04, 2025

International Journal of Applied Mathematics
Volume 38 No. 4s, 2025
ISSN: 1311-1728 (printed version); ISSN: 1314-8060 (on-line version)

That is to say, interestingly, the Crank-Nicolson scheme is conditionally consistent for the diffusion-advection equation, i.e. we must now to be careful in choosing the time step to assure the consistency of the scheme (if we want to use it, as suggested for its many other virtues). The same as found in Part I using the Du Fort-Frankel scheme for the diffusion differential equation.

We furthermore provide here the evolution equation with only space derivatives, i.e. the modified equation. In order to achieve it, we firstly find expressions for $\frac{\partial^2 T}{\partial t^2}$ and $\frac{\partial^3 T}{\partial t^3}$, and secondly (be careful with this) for $\frac{\partial^2 T}{\partial x \partial t}$ and $\frac{\partial^3 T}{\partial x^2 \partial t}$, by differentiating Eq. (2.25); all of which we use systematically to eliminate the time derivatives in it. This implies that the modified equation associated with the Crank and Nicolson scheme, the equation of the grid function from Crank and Nicolson difference equation, is:

$$\begin{aligned}\frac{\partial T}{\partial t} + v\frac{\partial T}{\partial x} - \alpha\frac{\partial^2 T}{\partial x^2} = \frac{1}{12}(-2\,C - C^3)\frac{(\Delta x)^3}{\Delta t}\frac{\partial^3 T}{\partial x^3} \\ + \frac{1}{12}(F + F\,C^2)\frac{(\Delta x)^4}{\Delta t}\frac{\partial^4 T}{\partial x^4} + \mathcal{O}((\Delta x)^5),\end{aligned} \tag{2.26}$$

which is one of two ways to next not only calculate the local error but also estimate the stability (see below). Notice that this modified equation reduces to Eq. (3.20) of Part I when $C \to 0$ and Eq. (2.21) of Part II when $F \to 0$, as it must be.

2.3.3 Stability

We secondly now analyze the stability using the von Neumann's method. Substituting a term of Eq. (2.1) of Part I into each term in Eq. (2.24) we get the following complex valued, growth factor associated with the Crank-Nicolson scheme:

$$G = \frac{1 - F + F\,\cos(k\Delta x) - i\,\frac{C}{2}\sin(k\Delta x)}{1 + F - F\,\cos(k\Delta x) + i\,\frac{C}{2}\sin(k\Delta x)}, \tag{2.27}$$

Received: August 04, 2025

International Journal of Applied Mathematics
Volume 38 No. 4s, 2025
ISSN: 1311-1728 (printed version); ISSN: 1314-8060 (on-line version)

whose magnitude component takes the form

$$|G| = \sqrt{\frac{[1 - F^2(1 - 2\,\cos{(k\Delta x)} + \cos^2{(k\Delta x)}) - \frac{C^2}{4}\sin^2{(k\Delta x)}]^2 + [C\sin{(k\Delta x)}]^2}{[(1 + F - F\,\cos{(k\Delta x)})^2 + (\frac{C}{2}\sin{(k\Delta x)})^2]^2}}, \tag{2.28}$$

which satisfies Eq. (2.16) of Part I for the end values of $\cos{(k\Delta x)}$. Specifically, $|G| = \frac{1-4\,F^2}{1+2\,F} < 1$ for $k\Delta x = \pi$ and $|G| = 1$ for $k\Delta x = 0$. Hence, the Crank-Nicolson scheme is stable for the diffusion-advection equation even at large time step size, although (be careful with this) this will not necessarily give accurate solution. This is because, the non-explicit schemes use the information from neighboring cell of the current time step to find the solution. This can already be seen in Fig. 7. However, the solution is now oscillatory, $|G| < 0$, when F number is above 0.8 (see Fig. 7); i.e. the low and high (oscillatory) wavelengths are propagated as weakly damped oscillations in time and therefore may persist for a long time, thereby implying (not a condition or constraint but) a prominent shortcoming in such cases.

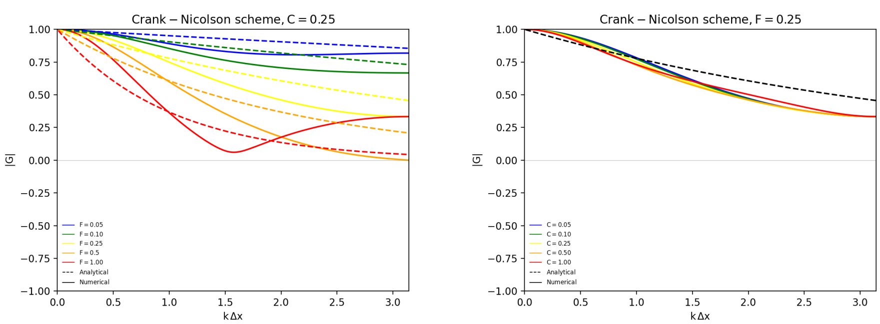

Figure 7: The same as Fig. 2 but for the Crank-Nicolson scheme.

Alternatively, the Hirt's method is another way to obtain this. The even, first t erm o n t he r ight h and o f m odified eq uation Eq. (2.26), which acts as a dispersive term (is an odd-order derivative), is always negative and also there is no diffusive derivatives implying that the Crank-Nicolson scheme is indeed unconditionally stable.

International Journal of Applied Mathematics
Volume 38 No. 4s, 2025
ISSN: 1311-1728 (printed version); ISSN: 1314-8060 (on-line version)

2.3.4 Accuracy

We thirdly investigate how accurate, both in magnitude and in phase, the numerical solution is using the Hirt's and von Neumann's complementary analysis.

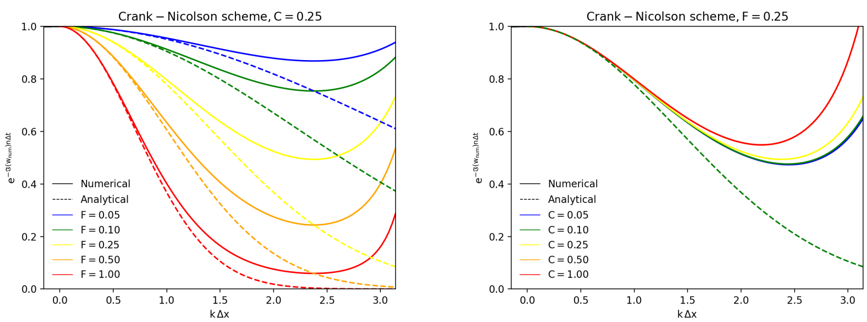

Figure 8: The same as Fig. 3 but for the Crank-Nicolson scheme.

On the one hand, by applying the discrete Fourier series grid solution of Eq. (2.1) of Part I to the Schmidt's modified equation (2.26) including terms up to the next-to-leading order, the damping term of the numerical solution becomes (see Eq. (2.27) of Part I):

$$\exp\left\{\left[-F\,\frac{(\Delta x)^2}{\Delta t}+\frac{1}{12}(F+F\,C^2)\,\frac{(\Delta x)^4}{\Delta t}k^2\right]k^2\,\Delta t\right\}. \tag{2.29}$$

Like its analytical counterpart (see Eq. (2.24) of Part I), we (again) notice that there is a little dissipation for $k = 0$ and it will be greater at higher wavenumbers. We now present the search for stiffness in the left panel of Fig. 8 by comparing Eq. (2.29) to Eq. (2.24) of Part I in all the Fourier modes on the grid (Eq. (2.3) of Part I) evaluated for specific F values. We now do not observe stiffness because the next-to-leading term in Eq. (2.29) is indeed anti-damping. In all cases, we observe that the Crank-Nicolson high wavelengths dissipate more slowly than those in the the analytical solution do, implying there is no overdamped or stiff regime. However, we do observe that for progressively higher values

Received: August 04, 2025

International Journal of Applied Mathematics
Volume 38 No. 4s, 2025
ISSN: 1311-1728 (printed version); ISSN: 1314-8060 (on-line version)

of F the Crank-Nicolson dissipation is further apart than the one from the analytical solution; i.e. the Crank-Nicolson grid function has just one underdamped regimen. The right panel of Fig. 8 shows the same for specific C values. Next, a more in-depth explanation of this effect is found.

Alternatively, since the exact growth factor in one of the Fourier modes is equal to $\exp(-\alpha\, k^2\, \Delta t)$, the Crank-Nicolson relative amplitude error, Eq. 2.29 of Part I, is given by

$$\delta A = e^{\alpha k^2 \Delta t}\sqrt{\frac{[1 - F^2(1 - 2\,\cos{(k\Delta x)} + \cos^2{(k\Delta x)}) - \frac{C^2}{4}\sin^2{(k\Delta x)}]^2 + [C\sin{(k\Delta x)}]^2}{[(1 + F - F\,\cos{(k\Delta x)})^2 + (\frac{C}{2}\sin{(k\Delta x)})^2]^2}} - 1, \tag{2.30}$$

In the left panel of Fig. 9 we show this relative error in all the Fourier modes on the grid (Eq. (2.3) of Part I) evaluated for a specific and illustrative value of F (indicated in the legend) with low and high constant C values, where we observe the marked preference for F values below 0.5. Indeed, for $F < 0.5$ the low wavelengths are underdamped (in agreement with the underdamped regimen from Eq. (2.29)) while for $F \geq 0.5$ they undergo an oscillating damping (consistent with the discussion in the previous Section), giving rise to an oscillatory behavior, $\delta A < -1$. Only for $F < 0.5$ the spurious oscillating modes are completely dissipated, implying low computational efficiency. These undesired oscillations, scarcely recognized or underestimated in the literature [2], are accordingly due to instability involved in the explicit half step of the not purely implicit Crank-Nicolson method. As is intuitively understood, and as seen in the right panel of Fig. 9, the C values have very little influence on the dissipative behavior of the equation.

We thus show that the dissipative numerical behavior of Crank-Nicolson's scheme is similar to that shown in the Part I.

On the other hand, by applying the discrete Fourier series grid solution of Eq. (2.1) of Part I to the Crank-Nicolson's modified equation (2.26) truncated up to the five-order derivatives, then we

International Journal of Applied Mathematics
Volume 38 No. 4s, 2025
ISSN: 1311-1728 (printed version); ISSN: 1314-8060 (on-line version)

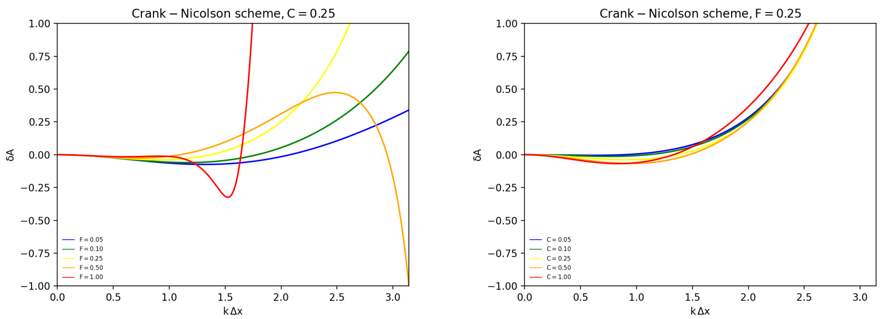

Figure 9: The same as Fig. 4 but for the Crank-Nicolson scheme.

see that the dispersive term is given by

$$\exp\left\{i\,k\,\left[x - v\,t + \frac{1}{12}(2\,C + C^3)\,\frac{(\Delta x)^3}{\Delta t}\,k^2\,t\right]\right\}, \tag{2.31}$$

implying the dispersive phase velocity shown in Fig. 10. First and foremost, and although it is intuitive as we have just pointed out, it is still surprising that Eq. (2.31) does not depend on F (up to second order of accuracy). We therefore find a numerical propagation speed smaller than the physical one, but shifting away from the physical one with increasing C's. This leads to the fact that the instantaneous velocity does not flip sign because the numerical speed never reaches exact value, implying the Crank-Nicolson scheme don't have instability issue. More on this later.

Alternatively, from the von Neumann's complementary analysis point of view, the numerical phase component of the Crank-Nicolson growth factor, Eq. (2.27), is given by

$$\phi = \arctan\left(\frac{-C\,\sin(k\Delta x)}{1 - F^2(1 - 2\,\cos(k\Delta x) + \cos^2(k\Delta x)) - (C/2\,\sin(k\Delta x))^2}\right), \tag{2.32}$$

which we show in the left panel of the Fig. 11.

Examining the phase component of the scheme for the resolvable wave number components of the numerical solution evaluated for a

International Journal of Applied Mathematics
Volume 38 No. 4s, 2025
ISSN: 1311-1728 (printed version); ISSN: 1314-8060 (on-line version)

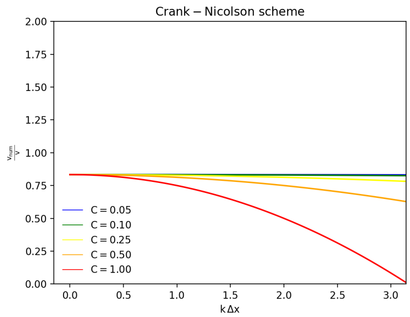

Figure 10: The same as Fig. 5 but for the Crank-Nicolson scheme.

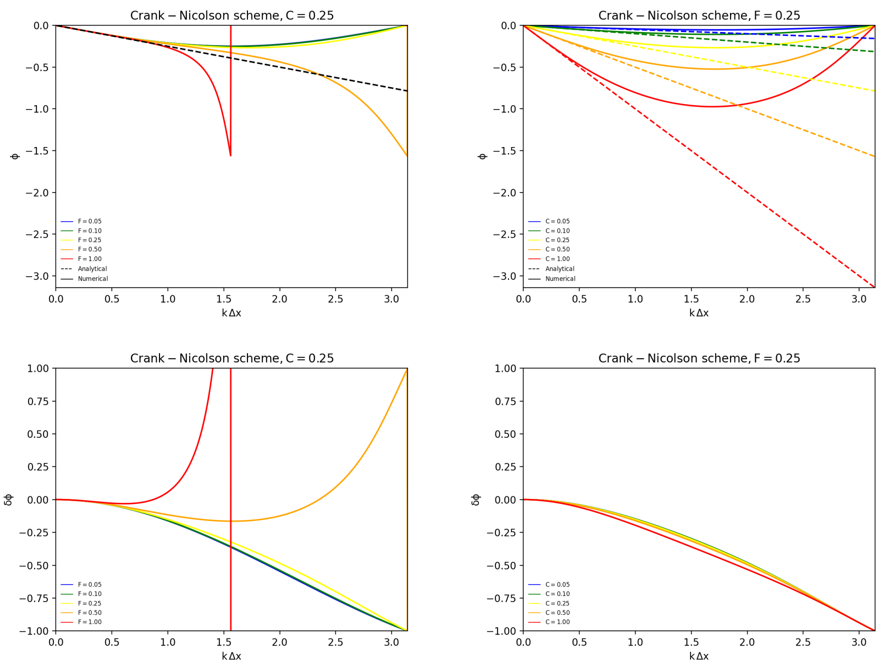

Figure 11: The same as Fig. 6 but for the Crank-Nicolson scheme.

specific and illustrative value of F (indicated in the legend) with low and high constant C values, and shown in the right panel of Fig. 11, we can now see that although both low and high frequency harmon-

Received: August 04, 2025

International Journal of Applied Mathematics
Volume 38 No. 4s, 2025
ISSN: 1311-1728 (printed version); ISSN: 1314-8060 (on-line version)

ics are nearly stationary, the mid oscillatory waves are propagated with different speeds, implying that the Crank-Nicolson scheme is also selectively dispersive. Specifically, this implies that whilst the low frequency waves are well resolved, those with high frequency will be poorly resolved ($\delta\phi \simeq -1$ in the right panel). Also, for all values of C we have leading shift, the relative phase error is less than 0 (see the right panel of Fig. 11), indicating a numerical propagation speed smaller than the physical one; but shift away from the line $\delta\phi = 0$ or the physical speed (see the left panel), implying the Crank-Nicolson scheme don't have instability issue. Finally, the left panels of Fig. 11 (especially the right upper panel) also shows us that relative phase is very strongly affected by the value of F for values above 0.5 corresponding to spurious oscillating modes discussed above.

Finally, note that Eq. (2.32) can only be applied where its denominator is non-zero as there will be a discontinuity in phase at certain values of ϕ (see red line on the left panels in the Fig. 11). We will address this phase jump in a later Section and show it here as a record of the issue.

We thus show that the dispersive numerical behavior of Crank-Nicolson's scheme is similar to that shown in the Part II.

2.3.5 Monotonicity

Finally, from the Eq. (2.24) the coefficients of the new solution are $-0.5\,F - 0.25\,C$, $1 + F$, $-0.5\,F + 0.25\,C$, $0.5\,F + 0.25\,C$, $1 - F$ and $0.5\,F - 0.25\,C$. Hence, the Crank-Nicolson's scheme is nonmonotone, i.e. it also may produce spurious oscillations.

2.4 The Laasonen's 1949 single-step implicit scheme

2.4.1 Construction

In 1949 Laasonen [8] used the same approximation as Schmidt did, but evaluating the space derivatives forwards in time, at time step

Received: August 04, 2025

International Journal of Applied Mathematics
Volume 38 No. 4s, 2025
ISSN: 1311-1728 (printed version); ISSN: 1314-8060 (on-line version)

$n+1$ instead of at time step n; i.e.,

$$\frac{T_j^{n+1}-T_j^n}{\Delta t} = -v\frac{T_{j+1}^{n+1}-T_{j-1}^{n+1}}{2\Delta x} + \alpha\frac{T_{j-1}^{n+1}-2T_j^{n+1}+T_{j+1}^{n+1}}{(\Delta x)^2}. \quad (2.33)$$

Table 1 emphasizes that Eq. (2.33) is purely time-implicit.

2.4.2 Consistency and order of accuracy

We firstly analyze the consistency of the scheme using the Hirt's method. Substituting each value of T at points other than point (x_j, t^n) in the scheme in a Taylor series around the value T_j^n at that point (x_j, t^n), i.e. we substitute Eqs. 2.8, 2.12 and 2.13 in Eq. (2.33), gives

$$\begin{aligned}\frac{\partial T}{\partial t} + v\frac{\partial T}{\partial x} - \alpha\frac{\partial^2 T}{\partial x^2} = \frac{\Delta t}{2}\frac{\partial^2 T}{\partial t^2} - \frac{(\Delta t)^2}{6}\frac{\partial^3 T}{\partial t^3} - \frac{v\,(\Delta x)^2}{6}\frac{\partial^3 T}{\partial x^3} \\ + \frac{(\Delta t)^3}{24}\frac{\partial^4 T}{\partial t^4} + \frac{\alpha\,(\Delta x)^2}{12}\frac{\partial^4 T}{\partial x^4} + \cdots.\end{aligned} \quad (2.34)$$

We then see from that equation, which is not the modified equation, that the right hand side vanishes when $\Delta t \to 0$ and $\Delta x \to 0$ and therefore the Laasonen's scheme of calculation is consistent. In addition, this side goes to zero as the first power of Δt and the second power of Δx, implying that the scheme is of first order accuracy in time and second order accuracy in space as well. Indeed, this result further verifies what would otherwise be expected because the way this scheme is based on Taylor series expansions.

We furthermore provide here the evolution equation with only space derivatives, i.e. the modified equation. In order to achieve it, we firstly find expressions for $\frac{\partial^2 T}{\partial t^2}$, $\frac{\partial^3 T}{\partial t^3}$ and $\frac{\partial^4 T}{\partial t^4}$, and secondly (be careful with this) for $\frac{\partial^2 T}{\partial x \partial t}$, $\frac{\partial^3 T}{\partial x^2 \partial t}$ and $\frac{\partial^4 T}{\partial x^3 \partial t}$, by differentiating Eq. (2.34); all of which we use systematically to eliminate the time derivatives in it. This implies that the modified equation associated with the Laasonen scheme, the equation of the grid function from

International Journal of Applied Mathematics
Volume 38 No. 4s, 2025
ISSN: 1311-1728 (printed version); ISSN: 1314-8060 (on-line version)

Laasonen difference equation, is:

$$\begin{aligned}\frac{\partial T}{\partial t} + v\frac{\partial T}{\partial x} - \alpha\frac{\partial^2 T}{\partial x^2} = &\frac{C^2}{2}\frac{(\Delta x)^2}{\Delta t}\frac{\partial^2 T}{\partial x^2}\\ &+ \frac{1}{6}(-C - 6\,F\,C - 2\,C^3)\frac{(\Delta x)^3}{\Delta t}\frac{\partial^3 T}{\partial x^3}\\ &+ \frac{1}{12}(C^2 + F + 6\,F^2 + 4\,F\,C^2)\frac{(\Delta x)^4}{\Delta t}\frac{\partial^4 T}{\partial x^4}\\ &+ \mathcal{O}((\Delta x)^5),\end{aligned} \tag{2.35}$$

which is one of two ways to next not only calculate the local error but also estimate the stability (see below). Notice that this modified equation reduces to Eq. (3.27) of Part I when $C \to 0$ and Eq. (2.28) of Part II when $F \to 0$, as it must be.

2.4.3 Stability

We secondly analyze the stability using the von Neumann's method. Substituting a term of Eq. 2.1 of Part I into each term in Eq. (2.12) we get the complex valued growth factor (Eq. 2.15 of Part I) associated with the Laasonen's scheme:

$$G = \frac{1}{1 + 2\,F\,(1 - \cos(k\Delta x)) + i\,C\sin(k\Delta x)}, \tag{2.36}$$

whose magnitude component takes the form

$$|G| = \frac{1}{\sqrt{[1 + 2\,F\,(1 - \cos(k\Delta x))]^2 + (C\sin(k\Delta x))^2}} < 1, \tag{2.37}$$

which satisfies Eq. (2.16) of Part I for the end values of $\cos(k\Delta x)$:

1. for the case of $k\Delta x = \pi$, we have $|G| = \frac{1}{(1+4\,F)^2} < 1$; and

2. for the limiting case $k\Delta x \to 0$, we have (neglecting high-order terms)

$$\lim_{k\Delta x \to \pi} |G| = 1 - \frac{1}{2}\,(2\,F + C^2)\,(k\Delta x)^2 < 1. \tag{2.38}$$

Received: August 04, 2025

International Journal of Applied Mathematics
Volume 38 No. 4s, 2025
ISSN: 1311-1728 (printed version); ISSN: 1314-8060 (on-line version)

Thus, the Laasonen's scheme is stable for the diffusion-advection equation, as corresponds to an implicit scheme. See Fig. 12.

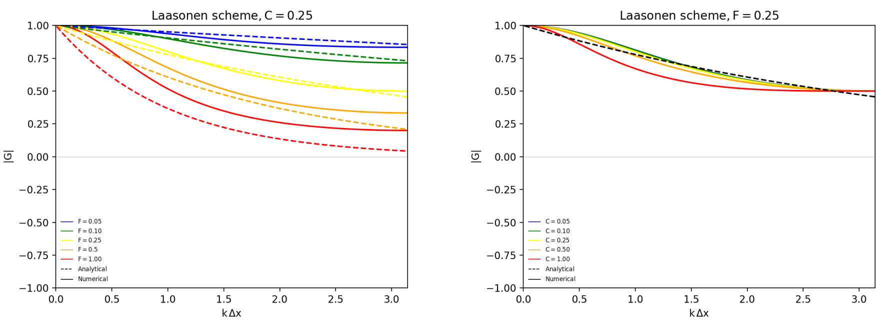

Figure 12: The same as Fig. 2 but for the Laasonen's scheme.

2.4.4 Accuracy

We thirdly investigate how accurate, both in magnitude and in phase, the numerical solution is using the Hirt's and von Neumann's complementary analysis.

On the one hand, by applying the discrete Fourier series grid solution of Eq. (2.1) of Part I to the Laasonen's modified equation (2.35) including terms up to the next-to-leading order, the damping term of the numerical solution becomes (see Eq. (2.27) of Part I):

$$\exp\left\{\left[(-C^2-F)\,\frac{(\Delta x)^2}{\Delta t}+\frac{1}{12}(C^2+F+6\,F^2+4\,F\,C^2)\,\frac{(\Delta x)^4}{\Delta t}k^2\right]k^2\,\Delta t\right\}. \tag{2.39}$$

Like its analytical counterpart (see Eq. (2.24) of Part I), we (again) notice that there is a little dissipation for $k=0$ and it will be greater at higher wavenumbers. We now present the search for stiffness in the left panel of Fig. 13 by comparing Eq. (2.39) to Eq. (2.24) of Part I in all the Fourier modes on the grid (Eq. (2.3) of Part I) evaluated for specific F v alues. We now do not observe s tiffness. All next-to-leading terms in Eq. 2.39 are indeed anti-damping. In all cases, we observe that the Laasonen's long wavelengths dissipate

Received: August 04, 2025

International Journal of Applied Mathematics
Volume 38 No. 4s, 2025
ISSN: 1311-1728 (printed version); ISSN: 1314-8060 (on-line version)

more slowly (indeed, too slowly) that those in the the analytical solution do, and do so equally for progressively higher values of F. The Laasonen's grid function has also just one underdamped regimen. Next, a more in-depth explanation of this effect is found. The right panel of Fig. 13 shows the same for specific C values. Next, a more in-depth explanation of this effect is found.

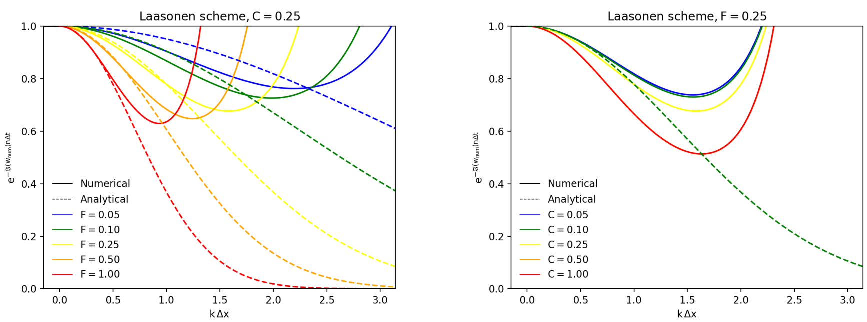

Figure 13: The same as Fig. 3 but for the Laasonen's scheme.

Alternatively, since the exact growth factor in one of the Fourier modes is equal to $\exp(-\alpha\, k^2\, \Delta t)$, the Laasonen's relative amplitude error, Eq. (2.29) of Part I, is given by

$$\delta A = \frac{e^{\alpha\, k^2\, \Delta t}}{\sqrt{[1 + 2\, F(1 - \cos{(k\Delta x)}]^2 + [C \sin{(k\Delta x)}]^2}} - 1, \qquad (2.40)$$

In the left panel of Fig. 14 we show this error in all the Fourier modes on the grid (Eq. (2.3) of Part I) evaluated for for a specific and illustrative value of F (indicated in the legend) with low and high constant C values, where we observe that almost all the modes, but especially those of high frequency (say, the worst modes), are excesively under-damped (in agreement with the underdamped regimen from Eq. 2.39) and, consequently, the Laasonen's scheme is going to lose a lot of accuracy. In fact (as the right panel of Fig. 14 confirms) we need very low values of F for high computational efficiency from this dissipative point of view.

Received: August 04, 2025

International Journal of Applied Mathematics
Volume 38 No. 4s, 2025
ISSN: 1311-1728 (printed version); ISSN: 1314-8060 (on-line version)

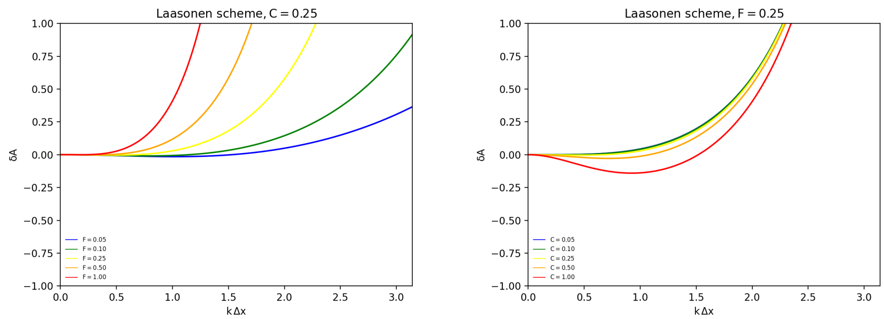

Figure 14: The same as Fig. 4 but for the Laasonen's scheme.

We thus show that the dissipative numerical behavior of Laasonen's scheme is different to that shown in the Part I.

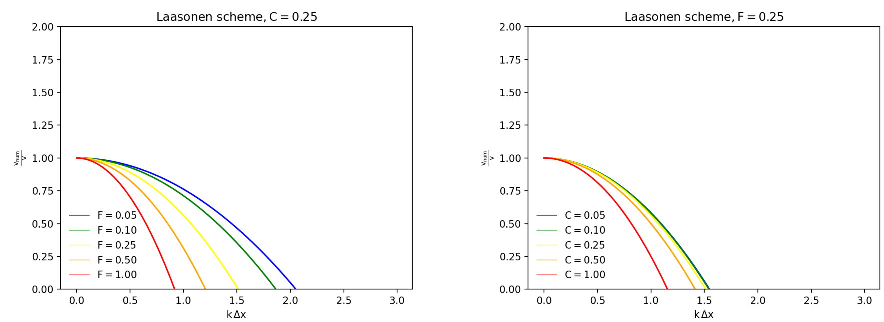

Figure 15: The same as Fig. 5 but for the Laasonen's scheme.

On the other hand, by applying the discrete Fourier series grid solution of Eq. (2.1) of Part I to the Laasonen's modified equation (2.35) truncated up to the five-order derivatives, then we see that the dispersive term is given by

$$\exp\left\{i\,k\,\left[x - v\,t + \frac{1}{6}(C + 6\,F\,C + 2\,C^3)\,\frac{(\Delta x)^3}{\Delta t}\,k^2\,t\right]\right\}, \qquad (2.41)$$

implying the dispersive phase velocity shown in Fig. 15; where we find a numerical propagation speed much lower than the physical

International Journal of Applied Mathematics
Volume 38 No. 4s, 2025
ISSN: 1311-1728 (printed version); ISSN: 1314-8060 (on-line version)

one causing phase lag, but shifting away from the physical one as C increases for fixed F and likewise as F increases for fixed C. This leads to the fact that the instantaneous velocity does not flip sign because the numerical speed never reaches exact value, implying the Laasonen's scheme don't have instability issue. More on this later.

Alternatively, from the von Neumann's complementary analysis point of view, the numerical phase component of the Laasonen's growth factor, Eq. (2.15), is given by

$$\phi = \arctan\left(\frac{\Im(G)}{\Re(G)}\right) = \arctan\left(\frac{-C\,\sin(k\Delta x)}{1+2\,F\,[1-\cos(k\Delta x)]}\right), \quad (2.42)$$

which we show in the Fig. 16.

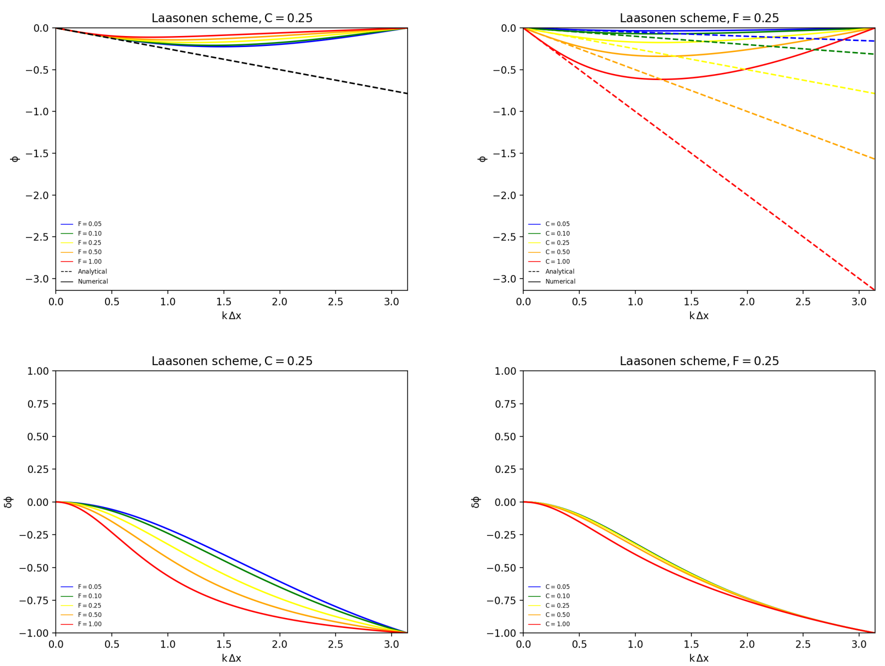

Figure 16: The same as Fig. 6 but for the Laasonen's scheme.

We find that the (dispersive) behavior is similar to that using the Crank-Nicolson scheme for fixed F. Indeed, the upper right panel

Received: August 04, 2025

International Journal of Applied Mathematics
Volume 38 No. 4s, 2025
ISSN: 1311-1728 (printed version); ISSN: 1314-8060 (on-line version)

of Fig. 16 shows us that for all values of C we have leading shift, the relative phase error is less than 0 (see the lower right panel of Fig. 16), indicating a numerical propagation speed smaller than the physical one; but shift away from the line $\delta\phi = 0$, implying again the Laasonen's scheme don't have instability issue, either. However, let's not forget that the Crank-Nicolson dispersive behavior with increasing F's is much worse than that using the Laasonen's scheme (see the left panels of Fig. 16).

We thus show that the dispersive numerical behavior of Laasonen's scheme is very similar to that shown in the Part II.

2.4.5 Monotonicity

The Laasonen's scheme is an implicit scheme. Since T_j^{n+1} depends only on T_j^n, then we cannot use the convex combination technique. Therefore we must demonstrate Eq. (2.31) of Part I. From Eq. (2.33) (see Table 1) we also get

$$(-F - 0.5\,C)\,T_{j-2}^{n+1} + (1 + 2\,F)\,T_{j-1}^{n+1} + (-F + 0.5\,C)\,T_j^{n+1} = T_{j-1}^n, \tag{2.43}$$

which subtracted from Eq. (2.33) gives

$$\begin{aligned} T_j^{n+1} - T_{j-1}^{n+1} = T_j^n - T_{j-1}^n &+ (F - 0.5\,C)\,(T_{j+1}^{n+1} - T_j^{n+1}) \\ &+ (F + 0.5\,C)\,(T_{j-1}^{n+1} - T_{j-2}^{n+1}) \\ &- 2\,F\,(T_j^{n+1} - T_{j-1}^{n+1}), \end{aligned} \tag{2.44}$$

and if in this equation we take the absolute value of both sides, use the triangle inequality on the right-side and sum the two sides over all j then we get Eq. (2.31) of Part I. Hence, the Laasonen's scheme is monotone and does not introduce oscillations.

Received: August 04, 2025

International Journal of Applied Mathematics
Volume 38 No. 4s, 2025
ISSN: 1311-1728 (printed version); ISSN: 1314-8060 (on-line version)

2.5 The Courant-Isaacson-Rees 1952 single-step explicit scheme

2.5.1 Construction

In 1952 Courant, Isaacson and Rees [1] used the forward in time approximation, Eq. (2.6) of Part I, to replace the time rate of change and the one-sided in the correct direction Eq. (2.10) of Part I for the first order derivative in space. In this way they obtained the following one-step, explicit scheme:

$$\frac{T_j^{n+1} - T_j^n}{\Delta t} = -v\frac{T_j^n - T_{j-1}^n}{\Delta x} + \alpha\frac{T_{j-1}^n - 2T_j^n + T_{j+1}^n}{(\Delta x)^2}, \qquad (2.45)$$

which is reformulated in Table 1 using the F and C numbers.

2.5.2 Consistency and order of accuracy

We firstly analyze the consistency of the scheme using the Hirt's method. Substituting each value of T at points other than point (x_j, t^n) in the scheme in a Taylor series around the value T_j^n at that point (x_j, t^n), i.e. we substitute Eqs. 2.6, 2.12 and 2.13 of Part I in Eq. (2.45), gives

$$\frac{\partial T}{\partial t}+v\frac{\partial T}{\partial x}-\alpha\frac{\partial^2 T}{\partial x^2} = \frac{v\,\Delta x}{2}\frac{\partial^2 T}{\partial x^2}-\frac{\Delta t}{2}\frac{\partial^2 T}{\partial t^2}-\frac{v\,(\Delta x)^2}{6}\frac{\partial^3 T}{\partial x^3}-\frac{(\Delta t)^2}{6}\frac{\partial^3 T}{\partial t^3}+\cdots . \qquad (2.46)$$

We then see from that equation, which is not the modified equation, that the right hand side vanishes when $\Delta t \to 0$ and $\Delta x \to 0$ and therefore the Courant-Isaacson-Rees scheme of calculation is consistent. In addition, this side goes to zero as the first power of Δt and the first power of Δx, implying that the scheme is of first order accuracy in both time and space as well. Indeed, this result further verifies what would otherwise be expected because the way this scheme is based on Taylor series expansions.

We furthermore provide here the evolution equation with only space derivatives, i.e. the modified equation. In order to achieve

Received: August 04, 2025

International Journal of Applied Mathematics
Volume 38 No. 4s, 2025
ISSN: 1311-1728 (printed version); ISSN: 1314-8060 (on-line version)

it, we firstly find expressions for $\frac{\partial^2 T}{\partial t^2}$ and $\frac{\partial^3 T}{\partial t^3}$, and secondly (be careful with this) for $\frac{\partial^2 T}{\partial x \partial t}$ and $\frac{\partial^3 T}{\partial x^2 \partial t}$, by differentiating Eq. (2.25); all of which we use systematically to eliminate the time derivatives in it. This implies that the modified equation associated with the Courant, Isaacson and Rees scheme, the equation of the grid function from Courant, Isaacson and Rees difference equation, is:

$$\frac{\partial T}{\partial t} + v\frac{\partial T}{\partial x} - \alpha\frac{\partial^2 T}{\partial x^2} = \frac{C - C^2}{2}\frac{(\Delta x)^2}{\Delta t}\frac{\partial^2 T}{\partial x^2} + \left(\frac{-C + 6\,F\,C + 3\,C^2 - 2\,C^3}{6}\right)\frac{(\Delta x)^3}{\Delta t}\frac{\partial^3 T}{\partial x^3}$$
$$+ \left(\frac{-2\,C^2 + 2\,F + C - 12\,F^2 - 12\,F\,C - 3\,C^2 + 8\,F\,C^2 + 4\,C^3}{24}\right)\frac{(\Delta x)^4}{\Delta t}\frac{\partial^4 T}{\partial x^4} + \mathcal{O}((\Delta x)^5), \tag{2.47}$$

which is one of two ways to next not only calculate the local error but also estimate the stability (see below). Notice that this modified equation reduces to Eq. (2.40) of Part II when $F \to 0$, as it must be.

2.5.3 Stability

We secondly analyze the stability using the von Neumann's method. Substituting a term of Eq. (2.1) of Part I into each term in Eq. (2.12) we get the complex valued growth factor (Eq. (2.15) of Part I) associated with the Courant-Isaacson-Rees scheme,

$$G = 1 - (2\,F + C)\,(1 - \cos{(k\Delta x)}) - i\,C\sin{(k\Delta x)}, \tag{2.48}$$

whose magnitude component takes the form

$$|G| = \sqrt{[1 - (2\,F + C)\,(1 - \cos{(k\Delta x)})]^2 + (C\sin{(k\Delta x)})^2}, \tag{2.49}$$

which has to satisfy Eq. (2.16) of Part I for all Eq. (2.3) of Part I in order to prevent numerical modes from growing faster than the physical modes of the differential equation; i.e. we must consider the end values of $\cos{(k\Delta x)}$:

1. for the case of $k\Delta x = \pi$, we have $|G|^2 = [1 - 2\,(2\,F + C)]^2 \leq 1$ which implies
$$C \leq 1 - 2\,F; \tag{2.50}$$

Received: August 04, 2025

International Journal of Applied Mathematics
Volume 38 No. 4s, 2025
ISSN: 1311-1728 (printed version); ISSN: 1314-8060 (on-line version)

2. for the limiting case $k\Delta x \to 0$, we have (neglecting high-order terms)

$$\lim_{k\Delta x \to 0} |G| = 1 - \frac{1}{2}\left(2\,F + C - C^2\right)(k\Delta x)^2 \tag{2.51}$$

which implies $2\,F + C - C^2 \geq 0$, i.e.

$$C^2 - C \leq 2\,F. \tag{2.52}$$

We plot these conditions, Eqs. (2.50) and (2.52), in Fig. 17. Hence, the Courant-Isaacson-Rees explicit scheme is conditionally stable for the diffusion-advection parabolic differential equation, as Fig. 18 confirms.

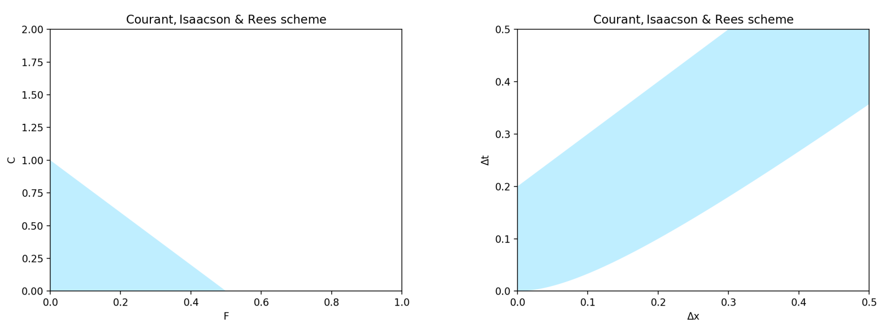

Figure 17: Stability region (by blue colour) of the Courant-Isaacson-Rees scheme in both FC and resolution planes, using $\alpha = 0.1$ and $v = 1$ as an example.

2.5.4 Accuracy

We thirdly investigate how accurate, both in magnitude and in phase, the numerical solution is using the Hirt's and von Neumann's complementary analysis.

On the one hand, by applying the discrete Fourier series grid solution of Eq. (2.1) of Part I to the Courant-Isaacson-Rees modified

Received: August 04, 2025

International Journal of Applied Mathematics
Volume 38 No. 4s, 2025
ISSN: 1311-1728 (printed version); ISSN: 1314-8060 (on-line version)

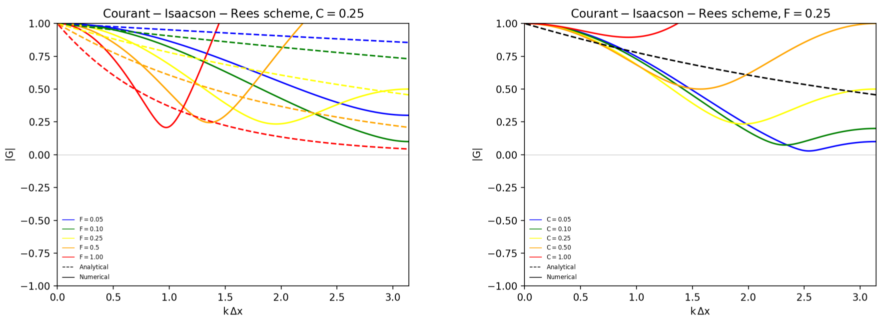

Figure 18: The same as Fig. 2 but for the Courant-Isaacson-Rees scheme.

equation (2.47) including terms up to the next-to-leading order, the damping term of the numerical solution becomes (see Eq. (2.27) of Part I):

$$\exp\Big\{\Big[(-C^2 - C - F)\,\frac{(\Delta x)^2}{\Delta t} + \frac{1}{24}(-2\,C^2 + 2\,F + C - 12\,F^2 - 12\,F\,C - 3\,C^2 + 8\,F\,C^2 + 4\,C^3)\,\frac{(\Delta x)^4}{\Delta t}k^2\Big]k^2\,\Delta t\Big\}. \tag{2.53}$$

Like its analytical counterpart (see Eq. (2.24) of Part I), we (again) notice that there is a little dissipation for $k = 0$ and it will be greater at higher wavenumbers. We now present the search for stiffness in the left panel of Fig. 19 by comparing Eq. (2.53) to Eq. (2.24) of Part I in all the Fourier modes on the grid (Eq. (2.3) of Part I) evaluated for specific F values. We now do not observe stiffness. Now in all cases we observe that the Courant-Isaacson-Rees wavelengths dissipate more rapidly (in fact too rapidly) than those in the analytical solution do. The Courant-Isaacson-Rees grid function has just one overdamped regimen, as the right panel of Fig. 19 confirms. Next, a more in-depth explanation of this effect is found.

Alternatively, since the exact growth factor in one of the Fourier

International Journal of Applied Mathematics
Volume 38 No. 4s, 2025
ISSN: 1311-1728 (printed version); ISSN: 1314-8060 (on-line version)

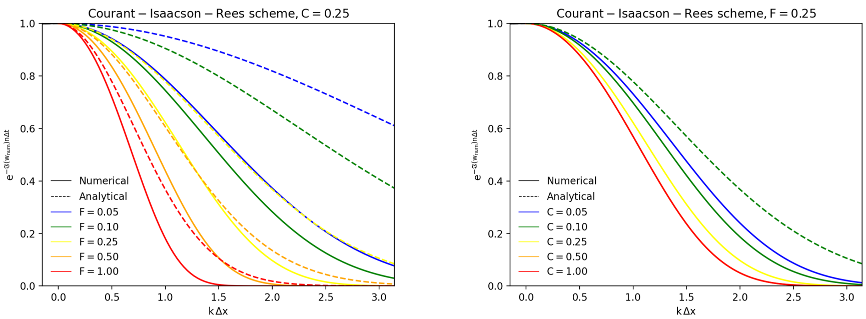

Figure 19: The same as Fig. 3 but for the Courant-Isaacson-Rees scheme.

modes is equal to $\exp(-\alpha\, k^2\, \Delta t)$, the Courant-Isaacson-Rees relative amplitude error, Eq. (2.29) of Part I, is given by

$$\delta A = e^{\alpha\, k^2\, \Delta t}\sqrt{[1-(2\,F+C)\,(1-\cos{(k\Delta x)})]^2+(C\sin{(k\Delta x)})^2}-1, \tag{2.54}$$

In Fig. 20 we show this error in all the Fourier modes on the grid (Eq. (2.3) of Part I) evaluated for a specific and illustrative value of F (indicated in the legend) with low and high C-constant values, and vice versa; where we observe (apart from the region of instability) that almost all the modes, but especially those of high frequency (say, the worst modes), are excesively over-damped (in agreement with the overdamped regimen from Eq. (2.53)) and, consequently, the Courant-Isaacson-Rees scheme is going to lose accuracy.

On the other hand, by applying the discrete Fourier series grid solution of Eq. (2.1) of Part I to the Courant-Isaacson-Rees modified equation (2.47) truncated up to the five-order derivatives, then we see that the dispersive term is given by

$$\exp\left\{i\,k\,\left[x-v\,t+\frac{1}{6}(C-6\,F\,C-3\,C^2+2\,C^3)\,\frac{(\Delta x)^3}{\Delta t}\,k^2\,t\right]\right\}, \tag{2.55}$$

implying the dispersive phase velocity shown in Fig. 21, where we

International Journal of Applied Mathematics
Volume 38 No. 4s, 2025
ISSN: 1311-1728 (printed version); ISSN: 1314-8060 (on-line version)

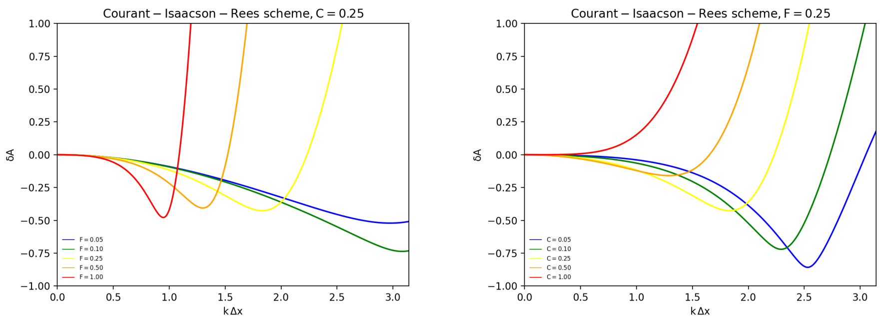

Figure 20: The same as Fig. 4 but for the Courant-Isaacson-Rees scheme.

find that the instantaneous velocity flips sign as it corresponds to a scheme that has a stability issue. Specifically, in the left panel of the Fig. 21 we find a numerical propagation speed smaller than the physical one (the blue curve) up to the polynomial of Eq. (2.55) cancels out when the numerical speed reaches exact value at $F = 0.06$ but while the damping is strong enough (see the right panel in the Fig. 19) to prevent unstable numerical growth. Then the trend reverses and we find a numerical propagation speed greater than the physical one and shifting away from the physical one with increasing F's. The right panel of the Fig. 21 shows the same behavior for a constant F number of $F = 0.25$. More on this later.

Alternatively, from the von Neumann's complementary analysis point of view, the numerical phase component of the Courant-Isaacson-Rees growth factor, Eq. (2.15), is given by

$$\phi = \arctan\left(\frac{\Im(G)}{\Re(G)}\right) = \arctan\left(\frac{-C\,\sin(k\Delta x)}{1-(2\,F+C)\,[1-\cos(k\Delta x)]}\right), \tag{2.56}$$

which we show very carefully in the Fig. 22. As we already noticed in Crank-Nicolson's scheme, this Eq. (2.56) presents phase jumps and so, to compare the magnitudes of error, we have to evaluate it using the two-argument arctangent.

Therefore, since the exact phase speed is the $-v$, we present in

Received: August 04, 2025

International Journal of Applied Mathematics
Volume 38 No. 4s, 2025
ISSN: 1311-1728 (printed version); ISSN: 1314-8060 (on-line version)

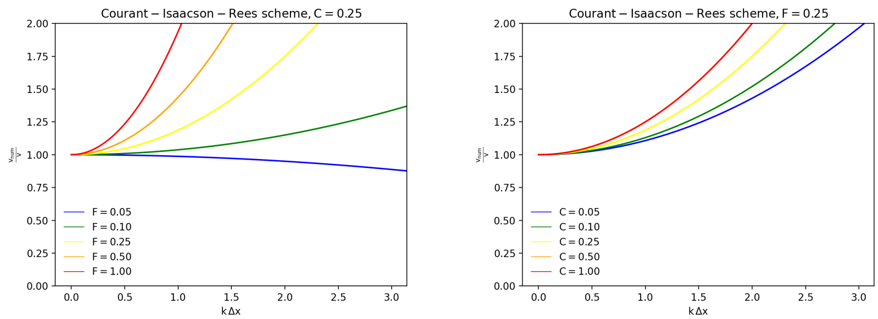

Figure 21: The same as Fig. 5 but for the Courant-Isaacson-Rees scheme.

the Fig. 22 both the phase and the numerical relative phase error (see Eq. (2.30) of Part I) of the Courant-Isaacson-Rees scheme plotted against the phase angle for specific C and F values.

Consistent with Fig. 21, the upper left panel of Fig. 22 shows us that for $F < 0.06$ we have lagging shift, the relative phase error is smaller than 0 (see the lower left panel of Fig. 22), indicating a numerical propagation speed smaller than the physical one; but shift closer to the line $\delta\phi = 0$ up to a threshold is reached when we have no dispersion error, the relative phase shift error flips sign and the Fourier modes have just the opposite, i.e. leading shift. In contrast, and also consistent with Fig. 21, the left panels of Fig. 22 show that for a constant F number of $F = 0.25$ we have leading shift but also shift closer to the line $\delta\phi = 0$, although without reaching it because of damping.

We thus show that the dispersive numerical behavior of Courant-Isaacson-Rees scheme is completely different to that shown in the Part II.

2.5.5 Monotonicity

Finally, from the Eq. (2.45) the coefficients of the new solution are $F + C$, $1 - 2F - C$ and F. That is, they are all positive in the

Received: August 04, 2025

International Journal of Applied Mathematics
Volume 38 No. 4s, 2025
ISSN: 1311-1728 (printed version); ISSN: 1314-8060 (on-line version)

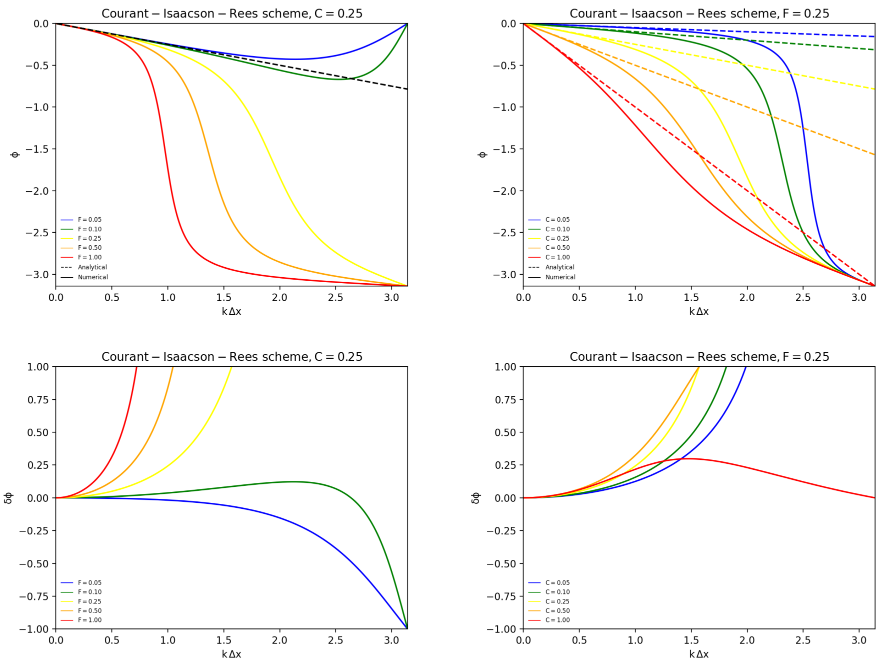

Figure 22: The same as Fig. 6 but for the Courant-Isaacson-Rees scheme. We use the `atan2` function, as defined in `Python`.

stability region, left panel of the Fig. 17. Hence, this Courant-Isaacson-Rees scheme behaves monotonically.

2.6 The Du Fort-Frankel 1953 three-time-level explicit scheme

2.6.1 Construction

In 1953 Du Fort and Frankel [5] (who were working with the wave equation) proposed the following scheme by taking the time average

Received: August 04, 2025

International Journal of Applied Mathematics
Volume 38 No. 4s, 2025
ISSN: 1311-1728 (printed version); ISSN: 1314-8060 (on-line version)

of T_j^n at $(x_j,\, t^n)$, i.e.,

$$\frac{T_j^{n+1}-T_j^{n-1}}{2\,\Delta t} = -v\frac{T_{j+1}^n - T_{j-1}^n}{2\,\Delta x} + \alpha\frac{T_{j-1}^n - (T_j^{n+1}+T_j^{n-1}) + T_{j+1}^n}{(\Delta x)^2}, \tag{2.57}$$

which is reformulated in Table 1 using the F and C numbers.

2.6.2 Consistency and order of accuracy

We firstly analyze the consistency of the scheme using the Hirt's method. Substituting each value of T at points other than point (x_j, t^n) in the scheme in a Taylor series around the value T_j^n at that point (x_j, t^n), i.e. we substitute Eqs. 2.6, 2.12 and 2.13 of Part I in Eq. (2.57), gives

$$\begin{aligned}\frac{\partial T}{\partial t} + v\frac{\partial T}{\partial x} - \alpha\frac{\partial^2 T}{\partial x^2} = &-\alpha\frac{(\Delta t)^2}{(\Delta x)^2}\frac{\partial^2 T}{\partial t^2} - v\frac{(\Delta x)^2}{6}\frac{\partial^3 T}{\partial x^3} - \frac{(\Delta t)^2}{6}\frac{\partial^3 T}{\partial t^3}\\ &- \alpha\frac{(\Delta t)^4}{(\Delta x)^2}\frac{\partial^4 T}{\partial t^4} + \alpha\frac{(\Delta x)^2}{12}\frac{\partial^4 T}{\partial x^4} + \cdots .\end{aligned} \tag{2.58}$$

We then see from that equation (which is not the modified equation) that, due to the first term on the right hand side, the Du Fort-Frankel scheme of calculation is consistent only if $\Delta t \to 0$ and $\Delta x \to 0$ are taken such that $\frac{\Delta t}{\Delta x} \to 0$. In other words,

1. if a time step $\Delta t \sim (\Delta x)^2$ is used we then achieve second order accuracy (on space and consequently in time as well);
2. however, for any value of $\frac{\Delta t}{\Delta x}$ the solution is not quite parabolic but nearly hyperbolic (i.e. it converges to that of a wave equation).

That is to say, the Du Fort-Frankel scheme is conditionally consistent, i.e. we must now to be careful in choosing the time step to assure the consistency of the scheme (if we want to use it, as suggested for its other virtues). The same as found in Part I for the diffusion d ifferential eq uation, an d th e sa me as us ing th e Crank-Nicolson here.

Received: August 04, 2025

International Journal of Applied Mathematics
Volume 38 No. 4s, 2025
ISSN: 1311-1728 (printed version); ISSN: 1314-8060 (on-line version)

2.6.3 Stability

We secondly analyze the stability using the von Neumann's method. Substituting a term of Eq. (2.1) of Part I into each term in Eq. (2.57) we get the equation for the growth factor (Eq. (2.15) of Part I),

$$(1+2\,F)\,G = \frac{-1+2\,F}{G} + 4\,F\,\cos(k\Delta x) - 2\,i\,C\sin(k\Delta x), \quad (2.59)$$

whose complex solutions are

$$G_{\pm} = \frac{4\,F\cos(k\Delta x) - i\,C\sin(k\Delta x) \pm \sqrt{4\,[1-(4\,F^2+C^2)(\sin(k\Delta x))^2] - i\,8\,F\,C\sin(2\,k\Delta x)}}{2+4\,F}; \quad (2.60)$$

i.e.,

$$G_{\pm} = \frac{-b_1 \pm b_4 + i\,(-b_2 \pm b_5)}{2+4\,F}, \quad (2.61)$$

where

$$b_1 = -4\,F\,\cos(k\Delta x), \quad (2.62)$$
$$b_2 = 2\,C\sin(k\Delta x), \quad (2.63)$$
$$b_3 = b_1^2 - b_2^2 - 16\,F^2 + 4, \quad (2.64)$$
$$b_4 = \sqrt{\sqrt{b_3^2 + 4\,b_1^2\,b_2^2} + b_3}, \quad (2.65)$$
$$b_5 = \frac{b_1\,b_2}{|b_1\,b_2|}\sqrt{\sqrt{b_3^2 + 4\,b_1^2\,b_2^2} - b_3}. \quad (2.66)$$

That is to say, as a three time level that it is, this scheme has two temporal modes. Note, the solution G_+ corresponds to the physical mode because for well resolved components ($k\Delta x \ll 1$) its real (observable) part is as it should be; and vice versa:

$$\lim_{k\Delta x\to 0} \Re(G_+) = \frac{\sqrt{2}+2\,F}{1+2\,F}, \quad (2.67)$$
$$\lim_{k\Delta x\to 0} \Re(G_-) = \frac{-2\sqrt{2}+4\,F}{2+4\,F}. \quad (2.68)$$

Received: August 04, 2025

International Journal of Applied Mathematics
Volume 38 No. 4s, 2025
ISSN: 1311-1728 (printed version); ISSN: 1314-8060 (on-line version)

However, the most important of what happens to the Du Fort-Frankel's growth factor is that the magnitude of its physical mode takes the start value

$$\lim_{k\Delta x\to 0}|G_+| = \frac{\sqrt{2}+2\,F}{1+2\,F} > 1, \tag{2.69}$$

which means that the low frequency physical mode do not satisfy Eq. (2.16) of Part I, implying that the Du Fort-Frankel's scheme is unconditionally unstable for the diffusion-advection parabolic differential equation and cannot be applied to it. This outcome is both unexpected and in broad inconsistency with the literature. On the one hand, the scheme is unconditionally stable for pure diffusive transfer (Part I). On the other hand, the very few existing works on the scheme with both advective and diffusive transfers [13, 4] agree, although with different stability outcomes, that it is conditionally stable. However, none of these works takes, as we do for the first time, the square root of its complex growth factor.

2.7 The Wendroff's 1958 single-step semi-explicit scheme

2.7.1 Construction

In 1958 Wendroff [19] was the first to come up with an alternative to the Crank-Nicolson scheme by averaging between n and n+1 time levels the following semi-discretized, forward approximation (to diffusion-advection equation)

$$\frac{1}{2}\left(\frac{\partial T_j}{\partial t}+\frac{\partial T_{j-1}}{\partial t}\right) = -v\,\left(\frac{T_j-T_{j-1}}{\Delta x}\right)+\alpha\frac{T_{j-1}-2T_j+T_{j+1}}{(\Delta x)^2}, \tag{2.70}$$

Received: August 04, 2025

International Journal of Applied Mathematics
Volume 38 No. 4s, 2025
ISSN: 1311-1728 (printed version); ISSN: 1314-8060 (on-line version)

to obtain the following compact scheme:

$$\frac{1}{2}\left(\frac{T_j^{n+1}-T_j^n}{\Delta t}+\frac{T_{j-1}^{n+1}-T_{j-1}^n}{\Delta t}\right)=-\,v\,\frac{1}{2}\left(\frac{T_j^{n+1}-T_{j-1}^{n+1}}{\Delta x}+\frac{T_j^n-T_{j-1}^n}{\Delta x}\right)$$
$$+\,\alpha\,\frac{1}{2}\left(\frac{T_{j-1}^{n+1}-2T_j^{n+1}+T_{j+1}^{n+1}}{(\Delta x)^2}+\frac{T_{j-1}^n-2T_j^n+T_{j+1}^n}{(\Delta x)^2}\right). \tag{2.71}$$

Table 1 emphasizes that Eq. (2.71) is time-implicit. The same as the Crank-Nicolson scheme.

2.7.2 Consistency and order of accuracy

We firstly analyze the consistency of the scheme using the Hirt's method. Substituting each value of T at points other than point (x_j, t^n) in the right hand side of Eq. (2.71) in Table 1 in a Taylor series around the value T_j^n at that point (x_j, t^n), around the value T_j^{n+1} at the point (x_j, t^{n+1}) in the left hand side, and finally expanding the value T_j^{n+1} around (x_j, t^n), i.e. we substitute Eqs. 2.6, 2.12 and 2.13 of Part I in Eq. (2.71), gives

$$\frac{\partial T}{\partial t}+v\frac{\partial T}{\partial x}-\alpha\frac{\partial^2 T}{\partial x^2}=\frac{v\,\Delta x}{2}\frac{\partial^2 T}{\partial x^2}-\frac{\Delta t}{2}\frac{\partial^2 T}{\partial t^2}-\frac{v\,(\Delta x)^2}{6}\frac{\partial^3 T}{\partial x^3}-\frac{(\Delta t)^2}{6}\frac{\partial^3 T}{\partial t^3}+\cdots. \tag{2.72}$$

which is the same equation as that of the Courant-Isaacson-Rees scheme. Interestingly, we then see from that equation, which is not the modified equation, that the right hand side vanishes when $\Delta t \to 0$ and $\Delta x \to 0$ and therefore the Wendroff's scheme of calculation is consistent. In addition, this side goes to zero as the first power of Δt and the first power of Δx, implying that the scheme is of first order accuracy in both time and space as well, as expected by construction.

We furthermore provide here the evolution equation with only space derivatives, i.e. the modified equation. In order to achieve it, we firstly find expressions for $\frac{\partial^2 T}{\partial t^2}$ and $\frac{\partial^3 T}{\partial t^3}$, and secondly (be

Received: August 04, 2025

International Journal of Applied Mathematics
Volume 38 No. 4s, 2025
ISSN: 1311-1728 (printed version); ISSN: 1314-8060 (on-line version)

careful with this) for $\frac{\partial^2 T}{\partial x \partial t}$ and $\frac{\partial^3 T}{\partial x^2 \partial t}$, by differentiating Eq. (2.72); all of which we use systematically to eliminate the time derivatives in it. This implies that the modified equation associated with the Wendroff's scheme, the equation of the grid function from Wendroff difference equation, is:

$$\frac{\partial T}{\partial t} + 2C\frac{\Delta x}{\Delta t}\frac{\partial T}{\partial x} + (-2\,F + C)\frac{(\Delta x)^2}{\Delta t}\alpha\frac{\partial^2 T}{\partial x^2} = \left(\frac{-2\,C + 12\,F - 4\,C^3}{6}\right)\frac{(\Delta x)^3}{\Delta t}\frac{\partial^3 T}{\partial x^3} + \left(\frac{6\,C + 28\,F + 16\,F\,C^2 + 8\,C^3}{24}\right)\frac{(\Delta x)^4}{\Delta t}\frac{\partial^4 T}{\partial x^4} + \mathcal{O}((\Delta x)^5), \tag{2.73}$$

which is one of two ways to next not only calculate the local error but also estimate the stability (see below). Notice that this modified equation reduces to Eq. (2.73) of Part II when $F \to 0$, as it must be.

2.7.3 Stability

We secondly now analyze the stability using the von Neumann's method. Substituting a term of Eq. (2.1) of Part I into each term in Eq. (2.71) we get the following complex valued, growth factor associated with the Wendroff's scheme:

$$G = \frac{1 - 2\,F - C + (1 + 2\,F + C)\,\cos(k\Delta x) - i\,(1 + C)\sin(k\Delta x)}{1 + 2\,F + C + (1 - 2\,F - C)\,\cos(k\Delta x) - i\,(1 - C)\sin(k\Delta x)}, \tag{2.74}$$

whose magnitude component takes the form

$$|G| = \sqrt{\left(\frac{c_1c_2 + c_3c_4}{c_2^2 + c_4^2}\right)^2 + \left(\frac{c_1c_4 - c_2c_3}{c_2^2 + c_4^2}\right)^2}, \tag{2.75}$$

where

$$c_1 = 1 - 2\,F - C + (1 + 2\,F + C)\,\cos(k\Delta x), \tag{2.76}$$
$$c_2 = 1 + 2\,F + C + (1 - 2\,F - C)\,\cos(k\Delta x), \tag{2.77}$$
$$c_3 = (1 + C)\sin(k\Delta x), \tag{2.78}$$
$$c_4 = (1 - C)\sin(k\Delta x); \tag{2.79}$$

Received: August 04, 2025

International Journal of Applied Mathematics
Volume 38 No. 4s, 2025
ISSN: 1311-1728 (printed version); ISSN: 1314-8060 (on-line version)

which has to satisfy Eq. (2.16) of Part I for the end values of $\cos(k\Delta x)$:

1. for the limiting case $k\Delta x \to 0$, we have (neglecting high-order terms)
$$\lim_{k\Delta x \to 0} |G| = 1 - F\,(k\Delta x)^2 < 1, \tag{2.80}$$
which means that the longest wavelengths are stable.

2. but for the case of $k\Delta x = \pi$, we have $|G| = -1$; and
$$\lim_{k\Delta x \to \pi} |G| = C + 2\,F < 1, \tag{2.81}$$
which implies $C \leq 1 - 2\,F$.

We plot this condition, Eq. (2.81), in Fig. 23. Hence, the Wendroff semi-explicit scheme is conditionally stable for the diffusion-advection parabolic differential equation, as Fig. 24 confirms; which is not only unexpected but also nothing sort of a surprise as it does not correspond at all to what is expected from a semi-explicit scheme. Indeed, we find that the longest wavelengths do not need any condition, but the shortest ones need a new condition (Eq. (2.81)). We introduce for the first time in the literature this outcome, which profoundly challenge the established understanding of implicit schemes and enrich our comprehension of stability.

2.7.4 Accuracy

We thirdly investigate how accurate, both in magnitude and in phase, the numerical solution is using the von Neumann's analysis.

On the one hand, by applying the discrete Fourier series grid solution of Eq. (2.1) of Part I to the Wendroff's modified equation (2.73) including terms up to the next-to-leading order, the damping term of the numerical solution becomes (see Eq. (2.27) of Part I):

$$\exp\Big\{\Big[(-2\,F+C)\,\frac{(\Delta x)^2}{\Delta t}+\frac{1}{24}(6\,C+28\,F+16\,F\,C^2+8\,C^3)\,\frac{(\Delta x)^4}{\Delta t}k^2\Big]k^2\,\Delta t\Big\}. \tag{2.82}$$

International Journal of Applied Mathematics
Volume 38 No. 4s, 2025
ISSN: 1311-1728 (printed version); ISSN: 1314-8060 (on-line version)

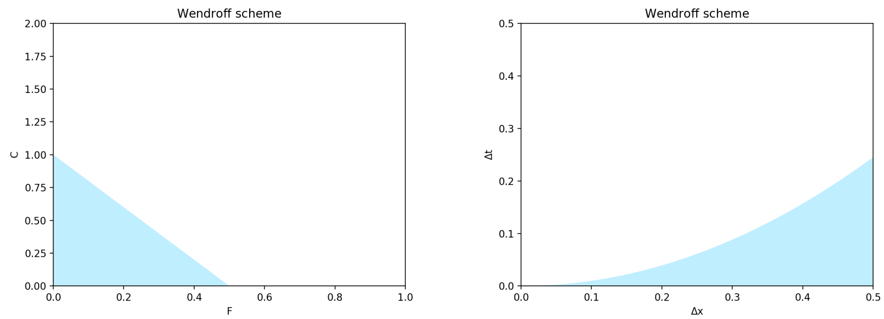

Figure 23: Stability region (by blue colour) of the Wendroff scheme in both FC and resolution planes, using $\alpha = 0.1$ and $v = 1$ as an example.

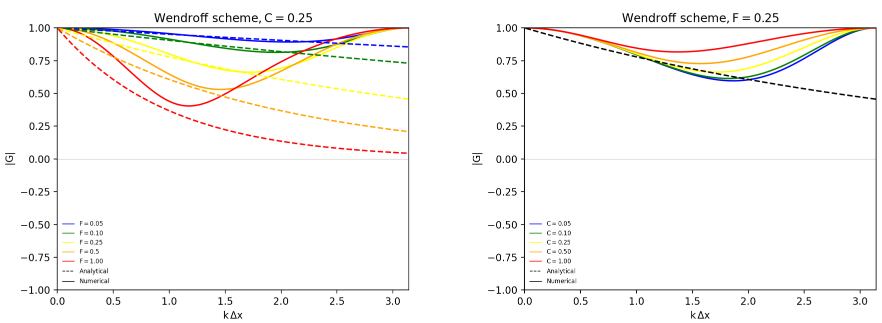

Figure 24: The same as Fig. 2 but for the Wendroff scheme.

Like its analytical counterpart (see Eq. (2.24) of Part I), we (again) notice that there is a little dissipation for $k = 0$ and it will be greater at higher wavenumbers. We now present the search for stiffness in the left panel of Fig. 25 by comparing Eq. (2.82) to Eq. (2.24) of Part I in all the Fourier modes on the grid (Eq. (2.3) of Part I) evaluated for specific F values. We now do not observe stiffness. Now in all cases we observe that the Wendroff wavelengths dissipate much less rapidly than those in the analytical solution do, as the right panel of Fig. 31 also confirms. The Wendroff grid function has just one very underdamped regimen. Next, a more in-depth

International Journal of Applied Mathematics
Volume 38 No. 4s, 2025
ISSN: 1311-1728 (printed version); ISSN: 1314-8060 (on-line version)

explanation of this effect is found.

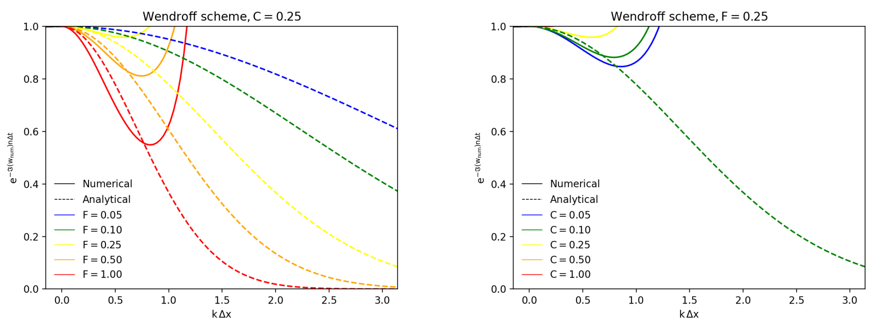

Figure 25: The same as Fig. 3 but for the Wendroff's scheme.

Alternatively, since the exact growth factor in one of the Fourier modes is equal to $\exp(-\alpha\, k^2\, \Delta t)$, the Wendroff's relative amplitude error, Eq. (2.29) of Part I, is given by

$$\delta A = e^{\alpha\, k^2\, \Delta t} \sqrt{\left(\frac{c_1 c_2 + c_3 c_4}{c_2^2 + c_4^2}\right)^2 + \left(\frac{c_1 c_4 - c_2 c_3}{c_2^2 + c_4^2}\right)^2} - 1, \qquad (2.83)$$

In Fig. 26 we show this error in all the Fourier modes on the grid (Eq. (2.3) of Part I) evaluated for a specific and illustrative value of F (indicated in the legend) with low and high C-constant values, and vice versa; where we observe (apart from the region of instability) that almost all the modes, but especially those of high frequency (say, the worst modes), are under-damped (in close agreement with the underdamped regimen from Eq. (2.82)) and, consequently, the Wendroff's scheme will lose a lot of accuracy due to this effect.

On the other hand, by applying the discrete Fourier series grid solution of Eq. (2.1) of Part I to the Wendroff's modified equation (2.73) truncated up to the five-order derivatives, then we see that the dispersive term is given by

$$\exp\left\{i\, k \left[x - 2\, v\, t + \frac{1}{6}(-2\, C + 12\, F - 4\, C^2)\, \frac{(\Delta x)^3}{\Delta t}\, k^2\, t\right]\right\}, \quad (2.84)$$

Received: August 04, 2025

International Journal of Applied Mathematics
Volume 38 No. 4s, 2025
ISSN: 1311-1728 (printed version); ISSN: 1314-8060 (on-line version)

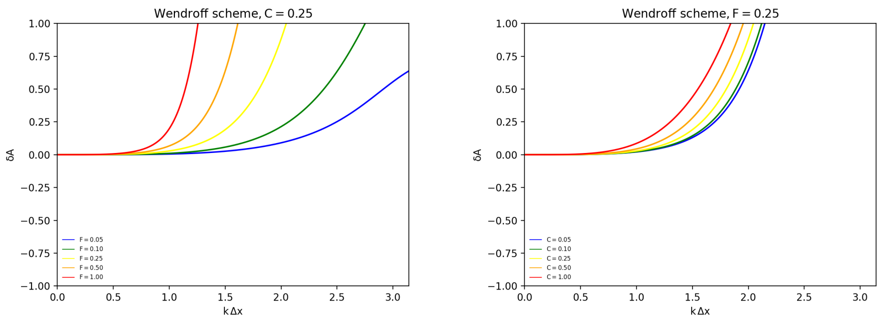

Figure 26: The same as Fig. 4 but for the Wendroff's scheme.

implying the dispersive phase velocity shown in Fig. 27; where we find a numerical propagation speed much greater than the physical one causing phase advance, but shifting away from the physical one as C increases for fixed F and, naturally, the opposite as F increases for fixed C. This behavior shown in the right panel of Fig. 27 leads to the fact that the instantaneous velocity flips sign when the stability threshold (Eq. (2.81)) is reached. This demonstrate that the Wendroff's scheme has instability issue. More on this later.

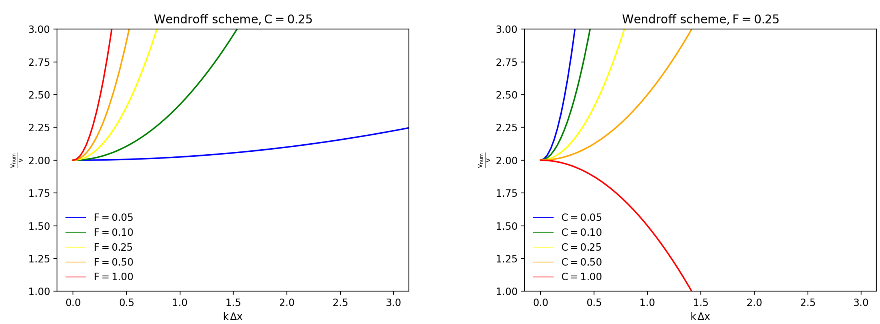

Figure 27: The same as Fig. 5 but for the Wendroff's scheme.

Alternatively, from the von Neumann's complementary analysis point of view, the numerical phase component of the Wendroff's

Received: August 04, 2025

International Journal of Applied Mathematics
Volume 38 No. 4s, 2025
ISSN: 1311-1728 (printed version); ISSN: 1314-8060 (on-line version)

growth factor, Eq. (2.75), is given by

$$\phi = \arctan\left(\frac{\Im(G)}{\Re(G)}\right) = \arctan\left(\frac{c_1\,c_4 - c_2\,c_3}{c_1\,c_2 + c_3\,c_4}\right), \tag{2.85}$$

which we show in the Fig. 28.

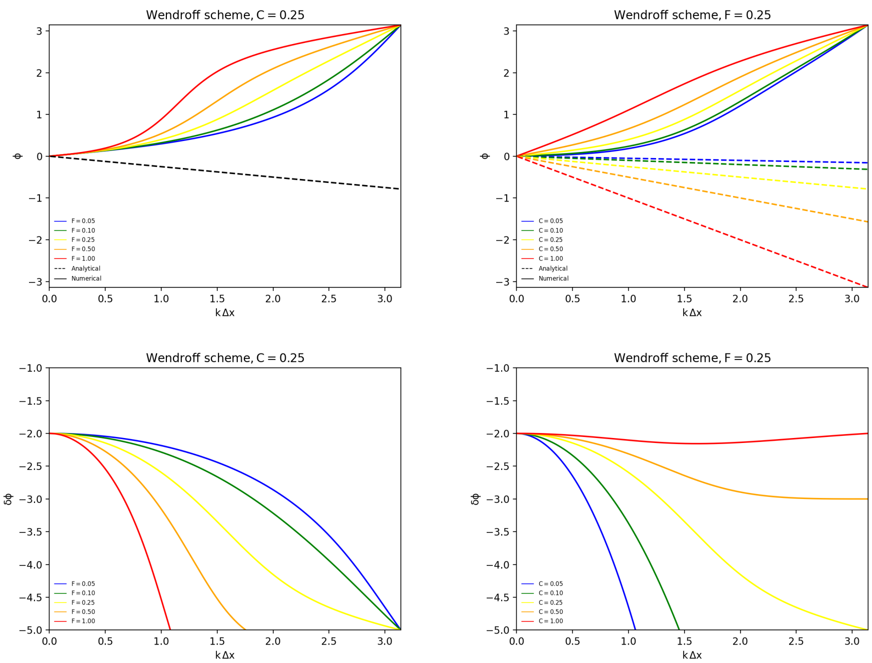

Figure 28: The same as Fig. 6 but for the Wendroff's scheme. We use the `atan2` function, as defined in `Python`.

We find that the (dispersive) behavior is very special. Indeed, the upper left panel of Fig. 39 shows us, in line with Fig. 27, not only that for all values of F we have leading shift (the relative phase error is less than 0 (see the lower left panel of Fig. 39), indicating a numerical propagation speed smaller than the physical one), but it is much smaller than it. In contrast, the right panels of Fig. 39 shows us, also in line with Fig. 27, that the same thing happens for

International Journal of Applied Mathematics
Volume 38 No. 4s, 2025
ISSN: 1311-1728 (printed version); ISSN: 1314-8060 (on-line version)

all values of C, but now shift closer from the line $\delta\phi = 0$, implying again the Wendroff's scheme has instability issue.

This dispersive behavior is bad for the numerical solution. However, let's not forget that the Wendroff's diffusive behavior has the opposite effect on the solution and we will see whether or not the result is satisfactory.

2.7.5 Monotonicity

Finally, from the Eq. (2.71) the coefficients of the new solution are $1 - F - C$, $1 + 2\,F + C$, $-F$, $1 + F + C$, $1 - 2\,F - C$ and F. Hence, the Wendroff's scheme is nonmonotone, i.e. it also may produce spurious oscillations.

2.8 The Lax-Wendroff 1960 single-step explicit algorithm

2.8.1 Construction

In 1960 Lax and Wendroff [10] looked for a (second order) accurate scheme but not by introducing additional terms that compensated for the bias caused by the second order spatial discretizations, as both Richardson and especially Crank and Nicolson did, but in a general way. Their derivation rests on the Taylor series expansion (up to the second-order derivatives) of the numerical solution T_i^{n+1} around the node $(x_i,\, t^n)$, Eq. (2.6) of Part I, and the replacement of its time derivatives by space derivatives by using both the linear (for now this is the way it is in this Part II), differential equation we wish to solve and its derivative (valid up to the second order in the x-derivative),

$$\frac{\partial^2 T}{\partial t^2} = v^2\,\frac{\partial^2 T}{\partial x^2}, \tag{2.86}$$

International Journal of Applied Mathematics
Volume 38 No. 4s, 2025
ISSN: 1311-1728 (printed version); ISSN: 1314-8060 (on-line version)

so that they invented:

$$
\begin{aligned}
T_j^{n+1} = T_j^n - \Delta t\, v\, \frac{T_{j+1}^n - T_{j-1}^n}{2\Delta x} + \Delta t\, \alpha\, \frac{T_{j-1}^n - 2T_j^n + T_{j+1}^n}{(\Delta x)^2} \\
+ \frac{1}{2}(\Delta t)^2\, v^2\, \frac{T_{j-1}^n - 2T_j^n + T_{j+1}^n}{(\Delta x)^2}.
\end{aligned}
\tag{2.87}
$$

which is the explicit scheme reformulated in Table 1.

2.8.2 Consistency and order of accuracy

We firstly analyze the consistency of the scheme using the Hirt's method. Substituting each value of T at points other than point (x_j, t^n) in the scheme in a Taylor series around the value T_j^n at that point (x_j, t^n), i.e. we substitute Eqs. 2.6, 2.12 and 2.13 of Part I in Eq. (2.87), gives (using Eq. (2.86))

$$
\frac{\partial T}{\partial t} + v\frac{\partial T}{\partial x} - \alpha\frac{\partial^2 T}{\partial x^2} = -\frac{v\,(\Delta x)^2}{6}\frac{\partial^3 T}{\partial x^3} - \frac{(\Delta t)^2}{6}\frac{\partial^3 T}{\partial t^3} + \cdots . \tag{2.88}
$$

We then see from that equation, which is not the modified equation, that the right hand side vanishes when $\Delta t \to 0$ and $\Delta x \to 0$ and therefore the Lax-Wendroff scheme of calculation is consistent. In addition, interestingly, this side goes to zero approximately as the second power of Δt and the second power of Δx, implying that the scheme is of approximately second order accuracy in both time and space.

We furthermore provide here the evolution equation with only space derivatives, i.e. the modified equation. In order to achieve it, we firstly find expressions for $\frac{\partial^2 T}{\partial t^2}$ and $\frac{\partial^3 T}{\partial t^3}$, and secondly (be careful with this) for $\frac{\partial^2 T}{\partial x \partial t}$ and $\frac{\partial^3 T}{\partial x^2 \partial t}$, by differentiating Eq. (2.88); all of which we use systematically to eliminate the time derivatives in it. This implies that the modified equation associated with the Lax-Wendroff scheme, the equation of the grid function from Lax-

International Journal of Applied Mathematics
Volume 38 No. 4s, 2025
ISSN: 1311-1728 (printed version); ISSN: 1314-8060 (on-line version)

Wendroff difference equation, is:

$$\frac{\partial T}{\partial t} + v\frac{\partial T}{\partial x} - \alpha\frac{\partial^2 T}{\partial x^2} = \left(\frac{-C + 6\,F\,C + C^3}{6}\right)\frac{(\Delta x)^3}{\Delta t}\frac{\partial^3 T}{\partial x^3} + \left(\frac{2\,F - 12\,F^2 - 4\,F\,C^2 - C^2 + C^4}{24}\right)\frac{(\Delta x)^4}{\Delta t}\frac{\partial^4 T}{\partial x^4} + \mathcal{O}((\Delta x)^5), \tag{2.89}$$

which is one of two ways to next not only calculate the local error but also estimate the stability (see below). Notice that this modified equation reduces to Eq. (2.81) of Part II when $F \to 0$, as it must be.

2.8.3 Stability

We secondly analyze the stability using the von Neumann's method. Substituting a term of Eq. (2.1) of Part I into each term in Eq. (2.12) we get the complex valued growth factor (Eq. (2.15) of Part I) associated with the Lax-Wendroff scheme,

$$G = 1 - 2\,F - C^2 + (2\,F + C^2)\,\cos(k\Delta x) - i\,C\sin(k\Delta x), \tag{2.90}$$

whose magnitude component takes the form

$$|G| = \sqrt{[1 - 2\,F - C^2 + (2\,F + C^2)\,\cos(k\Delta x)]^2 + (C\sin(k\Delta x))^2}, \tag{2.91}$$

which has to satisfy Eq. (2.16) of Part I for all Eq. (2.3) of Part I in order to prevent numerical modes from growing faster than the physical modes of the differential equation; i.e. we must consider the end values of $\cos(k\Delta x)$:

1. for the case of $k\Delta x = \pi$, we have $|G|^2 = [1 - 2\,(2\,F + C^2)]^2 \le 1$ which implies
$$C^2 \le 1 - 2\,F; \tag{2.92}$$
2. for the limiting case $k\Delta x \to 0$, we have (neglecting high-order terms)
$$\lim_{k\Delta x \to \pi} |G| = 1 - 2\,F\,(k\Delta x)^2 < 1, \tag{2.93}$$
which satisfies Eq. (2.16) of Part I.

International Journal of Applied Mathematics
Volume 38 No. 4s, 2025
ISSN: 1311-1728 (printed version); ISSN: 1314-8060 (on-line version)

We plot this condition, Eq. (2.92), in Fig. 29 (which is consistent with the literature [17]). Hence, the Lax-Wendroff explicit scheme is conditionally stable for the diffusion-advection parabolic differential equation, as Fig. 30 confirms.

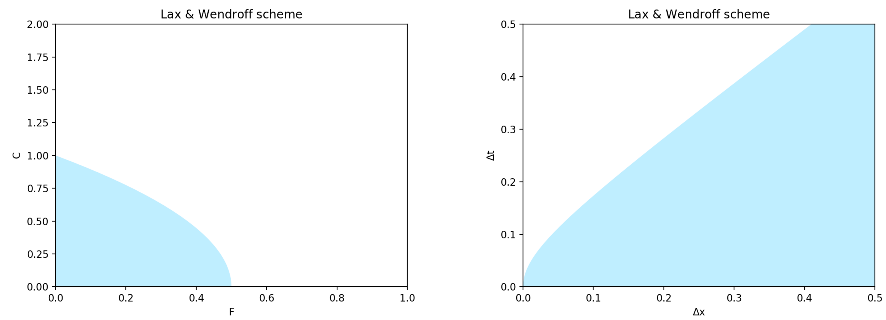

Figure 29: Stability region (by blue colour) of the Lax-Wendroff scheme in both FC and resolution planes, using $\alpha = 0.1$ and $v = 1$ as an example.

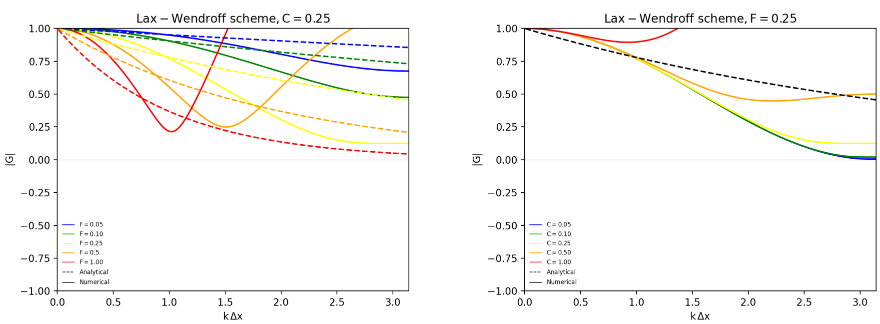

Figure 30: The same as Fig. 2 but for the Lax-Wendroff scheme.

2.8.4 Accuracy

We thirdly investigate how accurate, both in magnitude and in phase, the numerical solution is using the von Neumann's analysis.

Received: August 04, 2025

International Journal of Applied Mathematics
Volume 38 No. 4s, 2025
ISSN: 1311-1728 (printed version); ISSN: 1314-8060 (on-line version)

On the one hand, by applying the discrete Fourier series grid solution of Eq. (2.1) of Part I to the Lax-Wendroff modified equation (2.89) including terms up to the next-to-leading order, the damping term of the numerical solution becomes (see Eq. (2.27) of Part I):

$$\exp\Big\{\Big[(-F)\,\frac{(\Delta x)^2}{\Delta t}+\frac{1}{24}(-C^2+2\,F-12\,F^2-4\,F\,C^2+C^4)\,\frac{(\Delta x)^4}{\Delta t}k^2\Big]k^2\,\Delta t\Big\}. \tag{2.94}$$

Like its analytical counterpart (see Eq. (2.24) of Part I), we (again) notice that there is a little dissipation for $k = 0$ and it will be greater at higher wavenumbers. We now present the search for stiffness in the left panel of Fig. 31 by comparing Eq. (2.94) to Eq. (2.24) of Part I in all the Fourier modes on the grid (Eq. (2.3) of Part I) evaluated for specific F values. We now do not observe stiffness. Now in all cases we observe that the Lax-Wendroff wavelengths dissipate more rapidly than those in the analytical solution do, but very little for low F-numbers, as the right panel of Fig. 31 confirms. The Lax-Wendroff grid function has just one overdamped regimen. Next, a more in-depth explanation of this effect is found.

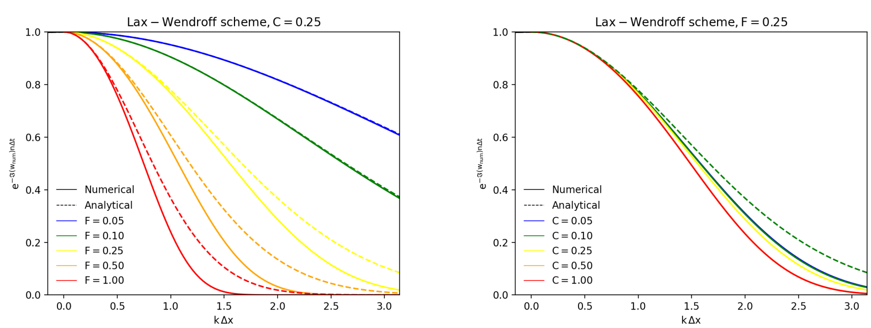

Figure 31: The same as Fig. 3 but for the Lax-Wendroff scheme.

Alternatively, since the exact growth factor in one of the Fourier modes is equal to $\exp(-\alpha\,k^2\,\Delta t)$, the Lax-Wendroff relative amplitude error, Eq. (2.29) of Part I, is given by

$$\delta A = e^{\alpha\,k^2\,\Delta t}\sqrt{[1-2\,F-C^2+(2\,F+C^2)\,\cos{(k\Delta x)}]^2+(C\sin{(k\Delta x)})^2}-1, \tag{2.95}$$

Received: August 04, 2025

International Journal of Applied Mathematics
Volume 38 No. 4s, 2025
ISSN: 1311-1728 (printed version); ISSN: 1314-8060 (on-line version)

In Fig. 32 we show this error in all the Fourier modes on the grid (Eq. (2.3) of Part I) evaluated for a specific and illustrative value of F (indicated in the legend) with low and high C-constant values, and vice versa; where we observe (apart from the region of instability) that almost all the modes, but especially those of high frequency (say, the worst modes), are over-damped (in close agreement with the overdamped regimen from Eq. (2.94)) and, consequently, the Lax-Wendroff scheme is going to lose some accuracy.

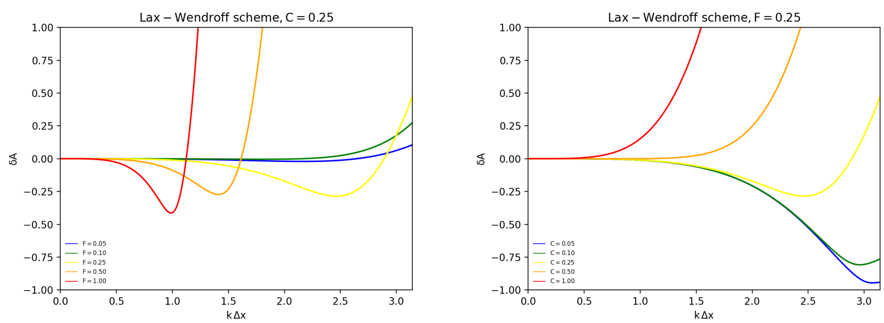

Figure 32: The same as Fig. 4 but for the Lax-Wendroff scheme.

On the other hand, by applying the discrete Fourier series grid solution of Eq. (2.1) of Part I to the Lax-Wendroff modified equation (2.89) truncated up to the five-order derivatives, then we see that the dispersive term is given by

$$\exp\left\{ i\,k\,\left[x - v\,t + \frac{1}{6}(C - 6\,F\,C - C^3)\,\frac{(\Delta x)^3}{\Delta t}\,k^2\,t \right] \right\}, \qquad (2.96)$$

implying the dispersive phase velocity shown in Fig. 33, where we find that the instantaneous velocity flips sign when the stability threshold (Eq. (2.92)) is reached. Specifically, for $C = 0.25$ we find in the left panel of the Fig. 33 a numerical propagation speed smaller than the physical one, but shifting closer to the physical one with increasing F's. This leads to the very striking fact that the instantaneous velocity flips sign once a threshold is reached, when the numerical speed reaches exact value at $F = 0.47$ with

International Journal of Applied Mathematics
Volume 38 No. 4s, 2025
ISSN: 1311-1728 (printed version); ISSN: 1314-8060 (on-line version)

almost no damping (see the blue and green lines in the left panel in the Fig. 31) implying instability. In contrast, for a constant F number of $F = 0.25$ we find in the right panel of the Fig. 33 a numerical propagation speed greater than the physical one and shifting farther away from the physical one with increasing C's, but now while the damping is strong enough (see the right panel in the Fig. 31) to prevent unstable numerical growth. More on this later.

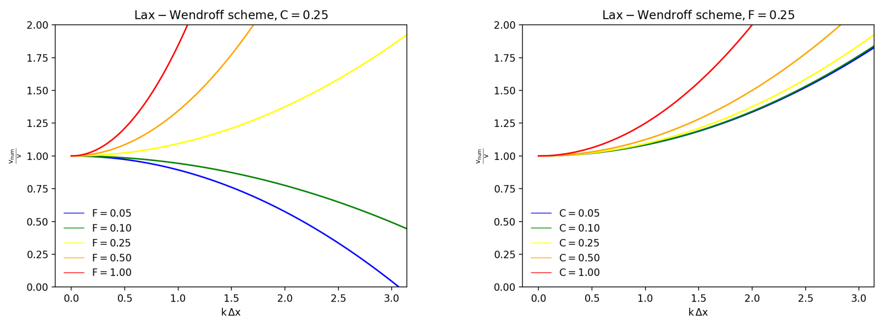

Figure 33: The same as Fig. 5 but for the Lax-Wendroff scheme.

Alternatively, from the von Neumann's complementary analysis point of view, the numerical phase component of the Lax-Wendroff growth factor, Eq. (2.15), is given by

$$\phi = \arctan\left(\frac{\Im(G)}{\Re(G)}\right) = \arctan\left[\frac{-C\,\sin(k\Delta x)}{1 - 2\,F - C^2 + (2\,F + C^2)\,\cos(k\Delta x)}\right], \tag{2.97}$$

which again we very carefully show in the Fig. 34 using the two-argument arctangent.

Consistent with Fig. 33, the upper left panel of Fig. 34 shows us that for $F < 0.47$ we have lagging shift, the relative phase error is smaller than 0 (see the lower left panel of Fig. 34), indicating a numerical propagation speed smaller than the physical one; but shift closer to the line $\delta\phi = 0$ up to the stability threshold is reached when we have no dispersion error, the relative phase shift error flips sign and the Fourier modes have just the opposite, i.e. leading shift.

Received: August 04, 2025

International Journal of Applied Mathematics
Volume 38 No. 4s, 2025
ISSN: 1311-1728 (printed version); ISSN: 1314-8060 (on-line version)

In contrast, and also consistent with Fig. 33, the left panels of Fig. 34 show that for a constant F number of $F = 0.25$ we have leading shift but also shift closer to the line $\delta\phi = 0$, although without reaching it because of damping.

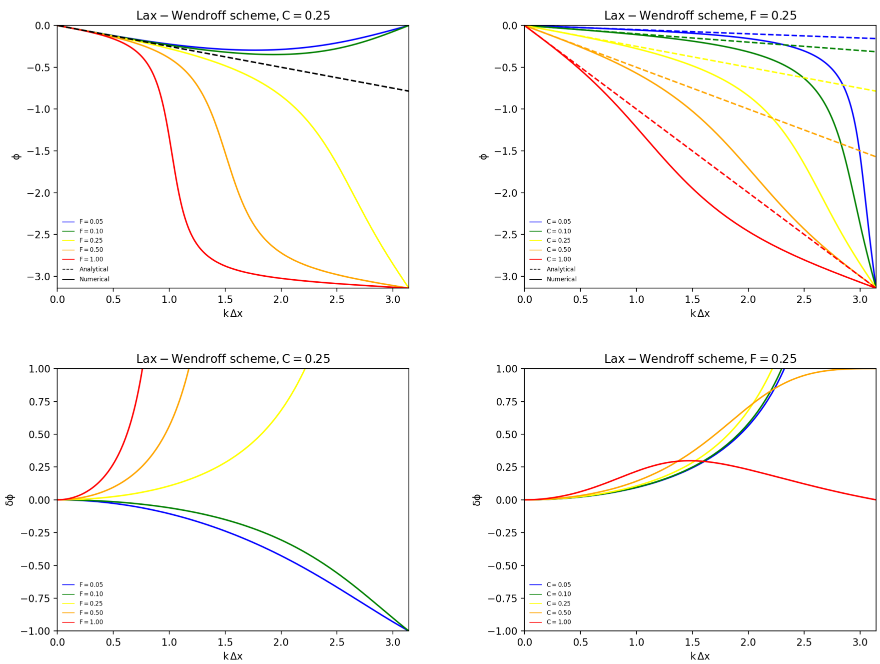

Figure 34: The same as Fig. 6 but for the Lax-Wendroff scheme. We use the `atan2` function, as defined in `Python`.

We thus show that the dispersive numerical behavior of Lax-Wendroff scheme is completely different to that shown in the Part II.

2.8.5 Monotonicity

Finally, from the Eq. (2.12) the coefficients of the new solution are $F + 0.5\,C + 0.5\,C^2$, $1 - 2\,F - C^2$ and $F - 0.5\,C + 0.5\,C^2$. That is, they are all positive in the stability region, left panel of the Fig. 29. Hence, this Lax-Wendroff scheme behaves monotonically.

Received: August 04, 2025

International Journal of Applied Mathematics
Volume 38 No. 4s, 2025
ISSN: 1311-1728 (printed version); ISSN: 1314-8060 (on-line version)

2.9 The Molenkamp's 1967 single-step implicit algorithm

2.9.1 Construction

In 1967 Molenkamp [12] considered the same discretization as Courant, Isaaccson and Rees did (Eq. (2.45)), but evaluating the space derivatives forwards in time; i.e.,

$$\frac{T_j^{n+1}-T_j^n}{\Delta t}=-v\frac{T_j^{n+1}-T_{j-1}^{n+1}}{\Delta x}+\alpha\frac{T_{j-1}^{n+1}-2T_j^{n+1}+T_{j+1}^{n+1}}{(\Delta x)^2}, \quad (2.98)$$

which is reformulated in Table 1.

2.9.2 Consistency and order of accuracy

We firstly analyze the consistency of the scheme using the Hirt's method. Substituting each value of T at points other than point (x_j, t^{n+1}) in the scheme in a Taylor series around the value T_j^{n+1} at that point (x_j, t^{n+1}), i.e. we substitute Eqs. 2.6, 2.12 and 2.13 of Part I in Eq. (2.98), gives

$$\frac{\partial T}{\partial t}+v\frac{\partial T}{\partial x}-\alpha\frac{\partial^2 T}{\partial x^2}=\frac{v\,\Delta x}{2}\frac{\partial^2 T}{\partial x^2}+\frac{\Delta t}{2}\frac{\partial^2 T}{\partial t^2}+\cdots . \quad (2.99)$$

We then see from that equation, which is not the modified equation, that the right hand side vanishes when $\Delta t\to 0$ and $\Delta x\to 0$ and therefore the Molenkamp's scheme of calculation is consistent. In addition, this side goes to zero as the first power of Δt and the first power of Δx, implying that the scheme is of first order accuracy in both time and space as well. Indeed, this result further verifies what would otherwise be expected because the way this scheme is based on Taylor series expansions.

We furthermore provide here the evolution equation with only space derivatives, i.e. the modified equation. In order to achieve it, we firstly find expressions for $\frac{\partial^2 T}{\partial t^2}$, $\frac{\partial^3 T}{\partial t^3}$ and $\frac{\partial^4 T}{\partial t^4}$, and secondly (be careful with this) for $\frac{\partial^2 T}{\partial x\partial t}$, $\frac{\partial^3 T}{\partial x^2\partial t}$ and $\frac{\partial^4 T}{\partial x^3\partial t}$, by differentiating

Received: August 04, 2025

International Journal of Applied Mathematics
Volume 38 No. 4s, 2025
ISSN: 1311-1728 (printed version); ISSN: 1314-8060 (on-line version)

Eq. (2.99); all of which we use systematically to eliminate the time derivatives in it. This implies that the modified equation associated with the Molenkamp's scheme, the equation of the grid function from Molenkamp's difference equation, is:

$$\begin{aligned}
&\frac{\partial T}{\partial t} + v\frac{\partial T}{\partial x} - \alpha\frac{\partial^2 T}{\partial x^2} = \frac{C + C^2}{2}\frac{(\Delta x)^2}{\Delta t}\frac{\partial^2 T}{\partial x^2} \\
&+ \frac{1}{6}(-C - 6\,F\,C - 3\,C^2 - 2\,C^3)\frac{(\Delta x)^3}{\Delta t}\frac{\partial^3 T}{\partial x^3} \\
&+ \frac{1}{24}(2\,F + C + 12\,F^2 + 12\,F\,C + 8\,F\,C^2 + 5\,C^2 + 4\,C^3)\frac{(\Delta x)^4}{\Delta t}\frac{\partial^4 T}{\partial x^4} \\
&+ \mathcal{O}((\Delta x)^5),
\end{aligned} \tag{2.100}$$

which is one of two ways to next not only calculate the local error but also estimate the stability (see below). Notice that this modified equation reduces to Eq. (2.91) of Part II when $F \to 0$, as it must be.

2.9.3 Stability

We secondly analyze the stability using the von Neumann's method. Substituting a term of Eq. (2.1) of Part I into each term in Eq. (2.12) we get the complex valued growth factor (Eq. (2.15) of Part I) associated with the Molenkamp's scheme:

$$G = \frac{1}{1 + 2\,F + C - (2\,F + C)\,\cos(k\Delta x) + i\,C\sin(k\Delta x)}, \tag{2.101}$$

whose magnitude component takes the form

$$|G| = \frac{1}{\sqrt{[1 + 2\,F + C - (2\,F + C)\,\cos(k\Delta x)]^2 + (C\sin(k\Delta x))^2}}, \tag{2.102}$$

which satisfies Eq. (2.16) of Part I for the end values of $\cos(k\Delta x)$:

1. for the case of $k\Delta x = \pi$, we have $|G| = \frac{1}{1+4\,F+2\,C} < 1$; and

Received: August 04, 2025

International Journal of Applied Mathematics
Volume 38 No. 4s, 2025
ISSN: 1311-1728 (printed version); ISSN: 1314-8060 (on-line version)

2. for the limiting case $k\Delta x \to 0$, we have (neglecting high-order terms)

$$\lim_{k\Delta x \to \pi} |G| = 1 - \frac{1}{2}\,(2\,F + C + C^2)\,(k\Delta x)^2 < 1. \tag{2.103}$$

Thus, the Molenkamp's scheme is stable for the diffusion-advection equation, as corresponds to an implicit scheme and as Fig. 35 confirms.

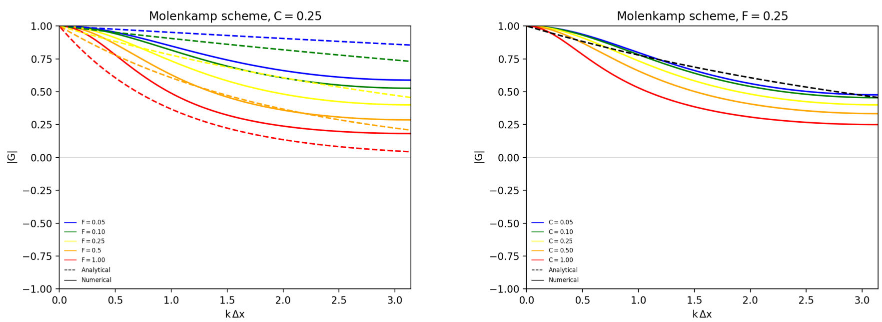

Figure 35: The same as Fig. 2 but for the Molenkamp's scheme.

2.9.4 Accuracy

We thirdly investigate how accurate, both in magnitude and in phase, the numerical solution is using the von Neumann's analysis.

On the one hand, by applying the discrete Fourier series grid solution of Eq. (2.1) of Part I to the Molenkamp's modified equation (2.100) including terms up to the next-to-leading order, the damping term of the numerical solution becomes (see Eq. (2.27) of Part I):

$$\exp\Big\{\Big[\frac{1}{2}(-2\,F - C - C^2)\,\frac{(\Delta x)^2}{\Delta t} + \frac{1}{24}(2\,F + C + 12\,F^2 + 12\,F\,C + 8\,F\,C^2 + 5\,C^2 + 4\,C^3)\,\frac{(\Delta x)^4}{\Delta t}k^2\Big]k^2\,\Delta t\Big\}. \tag{2.104}$$

Received: August 04, 2025

International Journal of Applied Mathematics
Volume 38 No. 4s, 2025
ISSN: 1311-1728 (printed version); ISSN: 1314-8060 (on-line version)

Like its analytical counterpart (see Eq. (2.24) of Part I), we (again) notice that there is a little dissipation for $k = 0$ and it will be greater at higher wavenumbers. We now present the search for stiffness in the left panel of Fig. 36 by comparing Eq. (2.104) to Eq. (2.24) of Part I in all the Fourier modes on the grid (Eq. (2.3) of Part I) evaluated for specific F values. We now do not observe stiffness. All next-to-leading terms (the second sum of the exponent) in Eq. 2.104 are indeed anti-damping. In all cases, we observe that the Molenkamp's long wavelengths dissipate more slowly (indeed, too slowly) that those in the the analytical solution do, and do so equally for progressively higher values of F. The Molenkamp's grid function has also just one underdamped regimen. Next, a more in-depth explanation of this effect is found. The right panel of Fig. 36 shows the same for specific C values. Next, a more in-depth explanation of this effect is found.

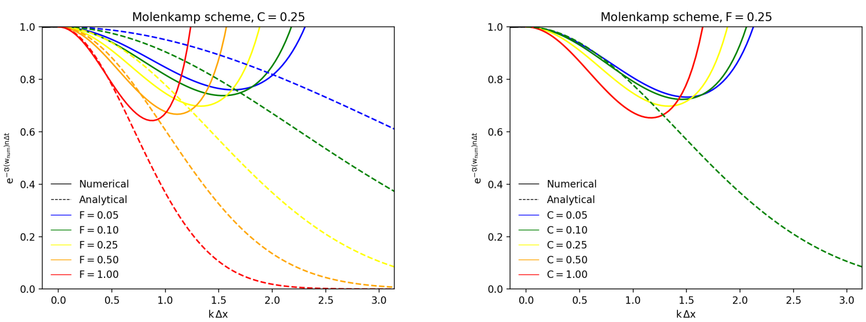

Figure 36: The same as Fig. 3 but for the Molenkamp's scheme.

Alternatively, since the exact growth factor in one of the Fourier modes is equal to $\exp(-\alpha\, k^2\, \Delta t)$, the Molenkamp's relative amplitude error, Eq. (2.29) of Part I, is given by

$$\delta A = \frac{e^{\alpha\, k^2\, \Delta t}}{\sqrt{[1 + 2\,F + C - (2\,F + C)\,\cos\,(k\Delta x)]^2 + (C\sin\,(k\Delta x))^2}} - 1, \tag{2.105}$$

In the left panel of Fig. 37 we show this error in all the Fourier modes on the grid (Eq. (2.3) of Part I) evaluated for for a specific

International Journal of Applied Mathematics
Volume 38 No. 4s, 2025
ISSN: 1311-1728 (printed version); ISSN: 1314-8060 (on-line version)

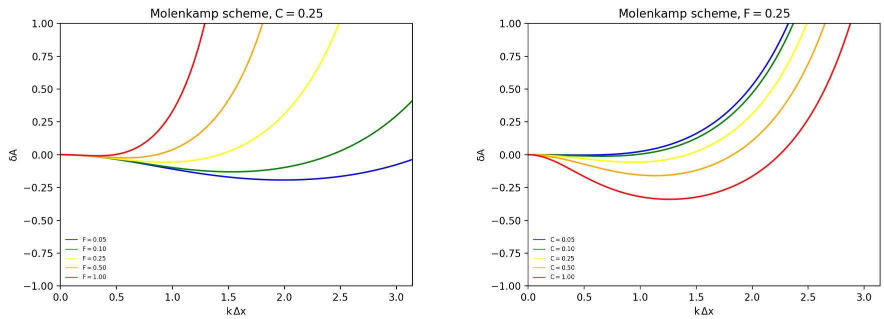

Figure 37: The same as Fig. 4 but for the Molenkamp's scheme.

and illustrative value of F (indicated in the legend) with low and high constant C values, where we observe that almost all the modes, but especially those of high frequency (say, the worst modes), are excesively under-damped (in agreement with the underdamped regimen from Eq. 2.104) and, consequently, the Molenkamp's scheme is going to lose a lot of accuracy. In fact (as the right panel of Fig. 37 confirms) we need very low values of F for high computational efficiency from this dissipative point of view.

We thus show that the dissipative numerical behavior of Molenkamp's scheme is very different to that shown in the Part II and very similar to Laasonen's in this paper.

On the other hand, by applying the discrete Fourier series grid solution of Eq. (2.1) of Part I to the Molenkamp's modified equation (2.100) truncated up to the five-order derivatives, then we see that the dispersive term is given by

$$\exp\left\{i\,k\,\left[x - v\,t + \frac{1}{6}(C + 6\,F\,C + 3\,C^2 + 2\,C^3)\,\frac{(\Delta x)^3}{\Delta t}\,k^2\,t\right]\right\}, \tag{2.106}$$

implying the dispersive phase velocity shown in Fig. 38; where we find a numerical propagation speed much lower than the physical one causing phase lag, but shifting away from the physical one as C increases for fixed F and likewise as F increases for fixed C. This leads to the fact that the instantaneous velocity does not flip sign

Received: August 04, 2025

International Journal of Applied Mathematics
Volume 38 No. 4s, 2025
ISSN: 1311-1728 (printed version); ISSN: 1314-8060 (on-line version)

because the numerical speed never reaches exact value, implying the Molenkamp's scheme don't have instability issue. More on this later.

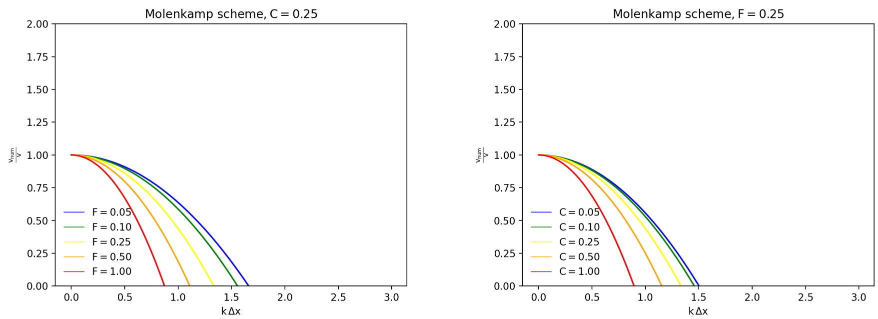

Figure 38: The same as Fig. 5 but for the Molenkamp's scheme.

Alternatively, from the von Neumann's complementary analysis point of view, the numerical phase component of the Molenkamp's growth factor, Eq. (2.15), is given by

$$\phi = \arctan\left(\frac{\Im(G)}{\Re(G)}\right) = \arctan\left(\frac{-C\,\sin(k\Delta x)}{1+2\,F+C-(2\,F+C)\,\cos(k\Delta x)}\right), \tag{2.107}$$

which we show in the Fig. 39.

We find that the (dispersive) behavior is similar to that using the Laasonen's scheme for fixed F. Indeed, the upper right panel of Fig. 39 shows us that for all values of C we have leading shift, the relative phase error is less than 0 (see the lower right panel of Fig. 39), indicating a numerical propagation speed smaller than the physical one; but shift away from the line $\delta\phi = 0$, implying again the Laasonen's scheme don't have instability issue, either. However, let's not forget that the Laasonen's dispersive behavior with increasing C's is better than that using the Molenkamp's scheme (see the right panels of Fig. 39).

We thus show that the dispersive numerical behavior of Molenkamp's scheme is very similar to that shown in the Part II.

Received: August 04, 2025

International Journal of Applied Mathematics
Volume 38 No. 4s, 2025
ISSN: 1311-1728 (printed version); ISSN: 1314-8060 (on-line version)

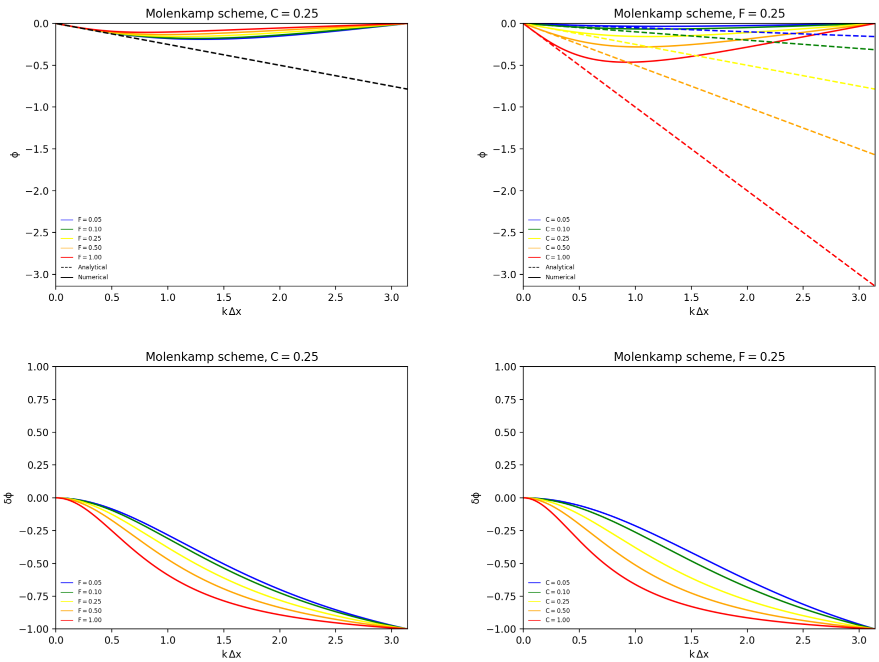

Figure 39: The same as Fig. 6 but for the Molenkamp's scheme.

2.9.5 Monotonicity

The Molenkamp's scheme is an implicit scheme. Since T_j^{n+1} depends only on T_j^n, then we cannot use the convex combination technique. Therefore we must demonstrate Eq. (2.31) of Part I. From Eq. (2.98) (see Table 1) we also get

$$(-F - C)\, T_{j-2}^{n+1} + (1 + 2\,F + C)\, T_{j-1}^{n+1} - F\, T_j^{n+1} = T_{j-1}^n, \quad (2.108)$$

which subtracted from Eq. (2.98) gives

$$\begin{aligned} T_j^{n+1} - T_{j-1}^{n+1} = T_j^n - T_{j-1}^n + F\,(T_{j+1}^{n+1} - T_j^{n+1}) \\ + (F + C)\,(T_{j-1}^{n+1} - T_{j-2}^{n+1}) \\ - (2\,F + C)\,(T_j^{n+1} - T_{j-1}^{n+1}), \end{aligned} \quad (2.109)$$

and if in this equation we take the absolute value of both sides, use the triangle inequality on the right-side and sum the two sides

Received: August 04, 2025

International Journal of Applied Mathematics
Volume 38 No. 4s, 2025
ISSN: 1311-1728 (printed version); ISSN: 1314-8060 (on-line version)

over all j then we get Eq. (2.31) of Part I. Hence, the Laasonen's scheme is monotone and does not introduce oscillations.

2.10 The Runchal's 1977 single-step semi-explicit scheme

2.10.1 Construction

In 1977 Runchal [15] considered the same discretization as Courant, Isaaccson and Rees did (Eq. (2.45)), but using the Crank-Nicolson scheme for the diffusion part; i.e.,

$$\frac{T_j^{n+1}-T_j^n}{\Delta t} = -v\frac{T_j^n - T_{j-1}^n}{\Delta x} + \alpha\left(\frac{1}{2}\right)\left(\frac{T_{j-1}^{n+1}-2T_j^{n+1}+T_{j+1}^{n+1}}{(\Delta x)^2} + \frac{T_{j-1}^n - 2T_j^n + T_{j+1}^n}{(\Delta x)^2}\right), \tag{2.110}$$

which is reformulated in Table 1.

2.10.2 Consistency and order of accuracy

We firstly analyze the consistency of the scheme using the Hirt's method. Substituting each value of T at points other than point (x_j, t^n) in the right hand side of Eq. (2.110) in Table 1 in a Taylor series around the value T_j^n at that point (x_j, t^n), around the value T_j^{n+1} at the point (x_j, t^{n+1}) in the left hand side, and finally expanding the value T_j^{n+1} around (x_j, t^n), i.e. we substitute Eqs. 2.6, 2.12 and 2.13 of Part I in Eq. (2.110), gives

$$\frac{\partial T}{\partial t}+v\frac{\partial T}{\partial x}-\alpha\frac{\partial^2 T}{\partial x^2} = \frac{v\,\Delta x}{2}\frac{\partial^2 T}{\partial x^2}-\frac{\Delta t}{2}\frac{\partial^2 T}{\partial t^2}-\frac{v\,(\Delta x)^2}{6}\frac{\partial^3 T}{\partial x^3}-\frac{(\Delta t)^2}{6}\frac{\partial^3 T}{\partial t^3}+\cdots . \tag{2.111}$$

which is the same equation as that of the Courant-Isaacson-Rees scheme. We then see from that equation, which is not the modified equation, that the right hand side vanishes when $\Delta t \to 0$ and $\Delta x \to$

International Journal of Applied Mathematics
Volume 38 No. 4s, 2025
ISSN: 1311-1728 (printed version); ISSN: 1314-8060 (on-line version)

0 and therefore the Runchal's scheme of calculation is consistent. In addition, this side goes to zero as the first power of Δt and the first power of Δx, implying that the scheme is of first order accuracy in both time and space as well.

We furthermore provide here the evolution equation with only space derivatives, i.e. the modified equation. In order to achieve it, we firstly find expressions for $\frac{\partial^2 T}{\partial t^2}$ and $\frac{\partial^3 T}{\partial t^3}$, and secondly (be careful with this) for $\frac{\partial^2 T}{\partial x \partial t}$ and $\frac{\partial^3 T}{\partial x^2 \partial t}$, by differentiating Eq. (2.111); all of which we use systematically to eliminate the time derivatives in it. This implies that the modified equation associated with the Runchal's scheme, the equation of the grid function from Runchal's difference equation, is:

$$
\begin{aligned}
&\frac{\partial T}{\partial t} + v\frac{\partial T}{\partial x} - \alpha\frac{\partial^2 T}{\partial x^2} = \frac{C - C^2}{2}\frac{(\Delta x)^2}{\Delta t}\frac{\partial^2 T}{\partial x^2} \\
&+ \left(\frac{-C + 3\,F\,C + 3\,C^2 - 2\,C^3}{6}\right)\frac{(\Delta x)^3}{\Delta t}\frac{\partial^3 T}{\partial x^3} \\
&+ \left(\frac{2\,F + C - 6\,F\,C - 3\,C^2 + 8\,F\,C^2 + 4\,C^3}{24}\right)\frac{(\Delta x)^4}{\Delta t}\frac{\partial^4 T}{\partial x^4} + \mathcal{O}((\Delta x)^5),
\end{aligned}
\tag{2.112}
$$

which is one of two ways to next not only calculate the local error but also estimate the stability (see below).

2.10.3 Stability

We secondly analyze the stability using the von Neumann's method. Substituting a term of Eq. (2.1) of Part I into each term in Eq. (2.12) we get the complex valued growth factor (Eq. (2.15) of Part I) associated with the Runchal's scheme:

$$
G = \frac{1 - F - C + (F + C)\,\cos(k\Delta x) - i\,C\sin(k\Delta x)}{1 + F\,(1 - \cos(k\Delta x))}, \tag{2.113}
$$

Received: August 04, 2025

International Journal of Applied Mathematics
Volume 38 No. 4s, 2025
ISSN: 1311-1728 (printed version); ISSN: 1314-8060 (on-line version)

whose magnitude component takes the form

$$|G| = \sqrt{\frac{[1 - F - C + (F + C)\ \cos(k\Delta x)]^2 + (C \sin(k\Delta x))^2}{[1 + F\,(1 - \cos(k\Delta x))]^2}}, \tag{2.114}$$

which has to satisfy Eq. (2.16) of Part I for the end values of $\cos(k\Delta x)$:

1. for the case of $k\Delta x = \pi$, we have $|G| = \frac{-1+2\,C+2\,F}{1+2\,F}$ which implies
$$C \leq 1;; \tag{2.115}$$
and

2. for the limiting case $k\Delta x \to 0$, we have (neglecting high-order terms)
$$\lim_{k\Delta x \to 0} |G| = 1 - (2\,F + C - C^2)\,(k\Delta x)^2 < 1, \tag{2.116}$$
which implies
$$C^2 - C \leq 2\,F. \tag{2.117}$$

We plot these conditions, Eqs. (2.115) and (2.117), in Fig. 40. Hence, the Runchal's semi-explicit scheme is conditionally stable for the diffusion-advection p arabolic d ifferential eq uation, as Fig. 41 confirms; w hich i s a gain n ot o nly u nexpected b ut a lso nothing sort of a surprise as it does not correspond at all to what is expected from a semi-explicit scheme. Indeed, we find t hat the longest wavelengths retain for their stability the Eq. (2.52), but the shortest ones need a new condition (compare Eq. (2.115) with Eq. (2.50)). We introduce for the first t ime i n t he l iterature this outcome, which profoundly challenge the established understanding of implicit schemes and enrich our comprehension of stability.

2.10.4 Accuracy

We thirdly investigate how accurate, both in magnitude and in phase, the numerical solution is using the von Neumann's analysis.

Received: August 04, 2025

International Journal of Applied Mathematics
Volume 38 No. 4s, 2025
ISSN: 1311-1728 (printed version); ISSN: 1314-8060 (on-line version)

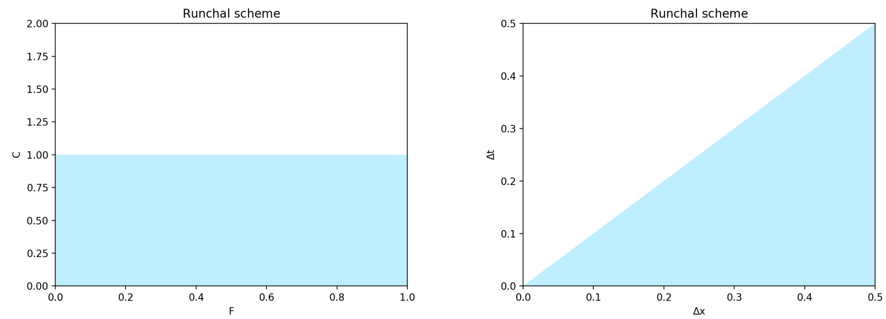

Figure 40: Stability region (by blue colour) of the Runchal's scheme in both FC and resolution planes, using $\alpha = 0.1$ and $v = 1$ as an example.

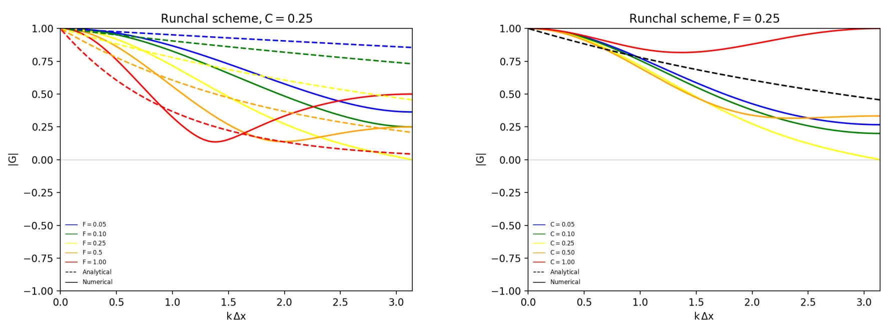

Figure 41: The same as Fig. 2 but for the Runchal's scheme.

On the one hand, by applying the discrete Fourier series grid solution of Eq. (2.1) of Part I to the Runchal's modified equation (2.112) including terms up to the next-to-leading order, the damping term of the numerical solution becomes (see Eq. (2.27) of Part I):

$$\exp\Big\{\Big[\frac{1}{2}(C^2 - C - 2\,F)\,\frac{(\Delta x)^2}{\Delta t} + \frac{1}{24}(-3\,C^2 + 2\,F + C - 6\,F\,C + 8\,F\,C^2 + 4\,C^3)\,\frac{(\Delta x)^4}{\Delta t}k^2\Big]k^2\,\Delta t\Big\}. \tag{2.118}$$

Received: August 04, 2025

International Journal of Applied Mathematics
Volume 38 No. 4s, 2025
ISSN: 1311-1728 (printed version); ISSN: 1314-8060 (on-line version)

Like its analytical counterpart (see Eq. (2.24) of Part I), we (again) notice that there is a little dissipation for $k = 0$ and it will be greater at higher wavenumbers. We now present the search for stiffness in the left panel of Fig. 42 by comparing Eq. (2.118) to Eq. (2.24) of Part I in all the Fourier modes on the grid (Eq. (2.3) of Part I) evaluated for specific F values. We now do not observe stiffness. Now in all cases we observe that the Runchal's wavelengths dissipate more rapidly than those in the analytical solution do but much less with increasing F. The Runchal's grid function has just one overdamped regimen but only for small F number; and the opposite for a constant F number of $F = 0.25$, as the right panel of Fig. 42 confirms. Next, a more in-depth explanation of this effect is found.

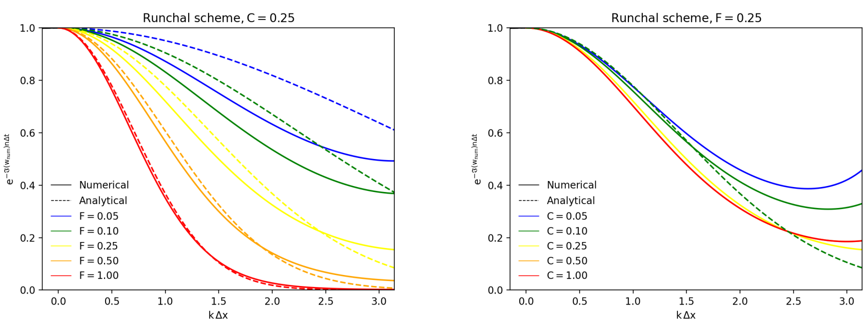

Figure 42: The same as Fig. 3 but for the Runchal's scheme.

Alternatively, since the exact growth factor in one of the Fourier modes is equal to $\exp(-\alpha\, k^2\, \Delta t)$, the Runchal's relative amplitude error, Eq. (2.29) of Part I, is given by

$$\delta A = e^{\alpha\, k^2\, \Delta t} \sqrt{\frac{[1 - F - C + (F + C)\, \cos{(k\Delta x)}]^2 + (C \sin{(k\Delta x)})^2}{[1 + F\,(1 - \cos{(k\Delta x)})]^2}} - 1, \tag{2.119}$$

In Fig. 43 we show this error in all the Fourier modes on the grid (Eq. (2.3) of Part I) evaluated for a specific a nd illustrative value of F (indicated in the legend) with low and high C-constant

Received: August 04, 2025

International Journal of Applied Mathematics
Volume 38 No. 4s, 2025
ISSN: 1311-1728 (printed version); ISSN: 1314-8060 (on-line version)

values, and vice versa; where we observe (apart from the region of instability) that almost all the modes, but especially those of high frequency (say, the worst modes), are excesively over-damped (in agreement with the overdamped regimen from Eq. (2.118)) and the opposite for a constant F number of $F = 0.25$; and, consequently, the Runchal's scheme is going to lose accuracy.

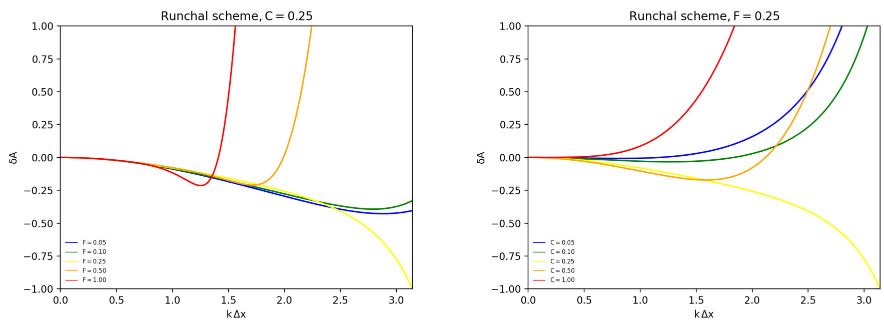

Figure 43: The same as Fig. 4 but for the Runchal's scheme.

We thus show that the dissipative numerical behavior of Runchal's scheme is different to that of Courant-Isaacson-Rees in this study.

On the other hand, by applying the discrete Fourier series grid solution of Eq. (2.1) of Part I to the Runchal's modified equation (2.112) truncated up to the five-order derivatives, then we see that the dispersive term is given by

$$\exp\left\{i\,k\,\left[x - v\,t + \frac{1}{6}(C - 3\,F\,C - 3\,C^2 + 2\,C^3)\,\frac{(\Delta x)^3}{\Delta t}\,k^2\,t\right]\right\}, \tag{2.120}$$

implying the dispersive phase velocity shown in Fig. 44, where we find that the instantaneous velocity flips sign as it corresponds to a scheme that has instability issue. Specifically, in the left panel of the Fig. 44 we find a numerical propagation speed smaller than the physical one (the blue curve) up to the polynomial of Eq. (2.120) cancels out when the numerical speed reaches exact value at $F =$

Received: August 04, 2025

International Journal of Applied Mathematics
Volume 38 No. 4s, 2025
ISSN: 1311-1728 (printed version); ISSN: 1314-8060 (on-line version)

0.12 but while the damping is strong enough (see the right panel in the Fig. 42) to prevent unstable numerical growth. Then the trend reverses and we find a numerical propagation speed greater than the physical one and shifting away from the physical one with increasing F's. The right panel of the Fig. 44 shows the same behavior for a constant F number of $F = 0.25$. More on this later.

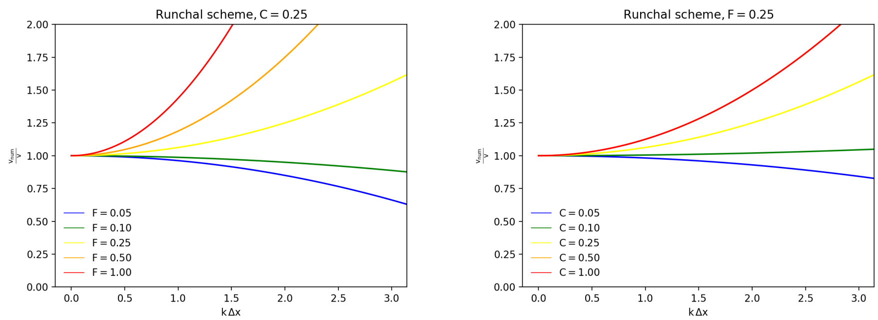

Figure 44: The same as Fig. 5 but for the Runchal's scheme.

Alternatively, from the von Neumann's complementary analysis point of view, the numerical phase component of the Runchal's growth factor, Eq. (2.15), is given by

$$\phi = \arctan\left(\frac{\Im(G)}{\Re(G)}\right) = \arctan\left(\frac{-C\,\sin(k\Delta x)}{1-F-C+(F+C)\,\cos(k\Delta x)}\right), \tag{2.121}$$

which we show very carefully in the Fig. 45. As we already noticed in Crank-Nicolson's scheme, this Eq. (2.121) presents phase jumps and so, to compare the magnitudes of error, we have to evaluate it using the two-argument arctangent.

Therefore, since the exact phase speed is the $-v$, we present in the Fig. 45 both the phase and the numerical relative phase error (see Eq. (2.30) of Part I) of the Runchal's scheme plotted against the phase angle for specific C and F values.

Consistent with Fig. 44, the upper left panel of Fig. 45 shows us that for $F < 0.12$ we have lagging shift, the relative phase error

Received: August 04, 2025

International Journal of Applied Mathematics
Volume 38 No. 4s, 2025
ISSN: 1311-1728 (printed version); ISSN: 1314-8060 (on-line version)

is smaller than 0 (see the lower left panel of Fig. 45), indicating a numerical propagation speed smaller than the physical one; but shift closer to the line $\delta\phi = 0$ up to a threshold is reached when we have no dispersion error, the relative phase shift error flips sign and the Fourier modes have just the opposite, i.e. leading shift; as confirms the left panels of Fig. 45.

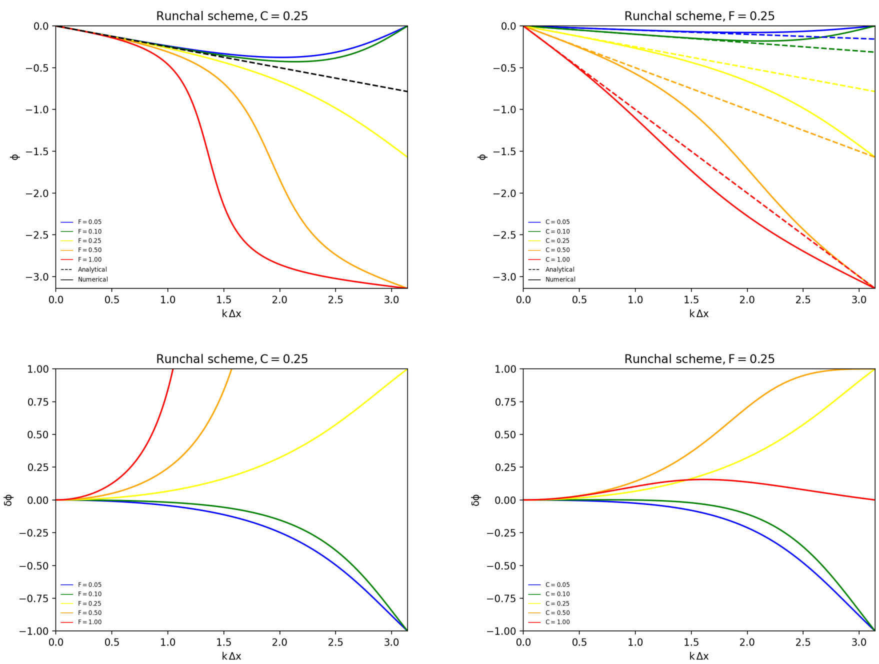

Figure 45: The same as Fig. 6 but for the Runchal's scheme. We use the `atan2` function, as defined in `Python`.

We thus show that the dispersive numerical behavior of Runchal's scheme is similar to that of Courant-Isaacson-Rees in this study.

2.10.5 Monotonicity

Finally, from the Eq. (2.110) the coefficients of the new solution are $-0.5\,F$, $1+F$, $-0.5\,F$, $0.5\,F+C$, $1-F-C$ and $0.5\,F$. Hence,

Received: August 04, 2025

International Journal of Applied Mathematics
Volume 38 No. 4s, 2025
ISSN: 1311-1728 (printed version); ISSN: 1314-8060 (on-line version)

the Runchal's scheme is nonmonotone, i.e. it also may produce spurious oscillations.

2.11 The Lerat's 1979 single-step implicit algorithm

2.11.1 Construction

In 1979 Lerat [11] considered the same discretization as Lax and Wendroff did (Eq. (2.87)), but evaluating the space derivatives forwards in time; i.e.,

$$
\begin{aligned}
T_j^{n+1} = T_j^n - \Delta t\, v\, \frac{T_{j+1}^{n+1} - T_{j-1}^{n+1}}{2\Delta x} + \Delta t\, \alpha\, \frac{T_{j-1}^{n+1} - 2T_j^{n+1} + T_{j+1}^{n+1}}{(\Delta x)^2} \\
+ \frac{1}{2}(\Delta t)^2\, v^2\, \frac{T_{j-1}^{n+1} - 2T_j^{n+1} + T_{j+1}^{n+1}}{(\Delta x)^2},
\end{aligned}
\tag{2.122}
$$

which is reformulated in Table 1.

2.11.2 Consistency and order of accuracy

We firstly analyze the consistency of the scheme using the Hirt's method. Substituting each value of T at points other than point (x_j, t^{n+1}) in the scheme in a Taylor series around the value T_j^{n+1} at that point (x_j, t^{n+1}), i.e. we substitute Eqs. 2.8, 2.12 and 2.13 of Part I in Eq. (2.122), gives

$$
\frac{\partial T}{\partial t} + v\frac{\partial T}{\partial x} - \alpha\frac{\partial^2 T}{\partial x^2} = \frac{v^2\,\Delta t}{2}\frac{\partial^2 T}{\partial x^2} + \frac{\Delta t}{2}\frac{\partial^2 T}{\partial t^2} - \frac{v\,(\Delta x)^2}{6}\frac{\partial^3 T}{\partial x^3} - \frac{(\Delta t)^2}{6}\frac{\partial^3 T}{\partial t^3} + \cdots\,. \tag{2.123}
$$

We then see from that equation, which is not the modified equation, that the right hand side vanishes when $\Delta t \to 0$ and $\Delta x \to 0$ and therefore the Lerat's scheme of calculation is consistent. In addition, this side goes to zero as the first power of Δt and the second power of Δx, implying that the scheme is of first order accuracy in

Received: August 04, 2025

International Journal of Applied Mathematics
Volume 38 No. 4s, 2025
ISSN: 1311-1728 (printed version); ISSN: 1314-8060 (on-line version)

time and second order accuracy in space as well. Indeed, this result further verifies what would otherwise be expected because the way this scheme is based on Taylor series expansions.

We furthermore provide here the evolution equation with only space derivatives, i.e. the modified equation. In order to achieve it, we firstly find expressions for $\frac{\partial^2 T}{\partial t^2}$ and $\frac{\partial^3 T}{\partial t^3}$, and secondly (be careful with this) for $\frac{\partial^2 T}{\partial x \partial t}$ and $\frac{\partial^3 T}{\partial x^2 \partial t}$, by differentiating Eq. (2.123); all of which we use systematically to eliminate the time derivatives in it. This implies that the modified equation associated with the Lerat's scheme, the equation of the grid function from Lerat's difference equation, is:

$$\begin{aligned}\frac{\partial T}{\partial t} + v\frac{\partial T}{\partial x} - \alpha\frac{\partial^2 T}{\partial x^2} &= C^2\frac{(\Delta x)^2}{\Delta t}\frac{\partial^2 T}{\partial x^2} \\ &+ \left(\frac{-C - 6\,F\,C - 5\,C^3}{6}\right)\frac{(\Delta x)^3}{\Delta t}\frac{\partial^3 T}{\partial x^3} \\ &+ \left(\frac{2\,F + 12\,F^2 + 3\,C^2 + 20\,F\,C^2 + 7\,C^4}{24}\right)\frac{(\Delta x)^4}{\Delta t}\frac{\partial^4 T}{\partial x^4} + \mathcal{O}((\Delta x)^5),\end{aligned} \tag{2.124}$$

which is one of two ways to next not only calculate the local error but also estimate the stability (see below). Notice that this modified equation reduces to Eq. (2.102) of Part II when $F \to 0$, as it must be.

2.11.3 Stability

We secondly analyze the stability using the von Neumann's method. Substituting a term of Eq. (2.1) of Part I into each term in Eq. (2.122) we get the complex valued growth factor (Eq. (2.15) of Part I) associated with the Lerat's scheme:

$$G = \frac{1}{1 + 2\,F + C^2 - (2\,F + C^2)\,\cos(k\Delta x) + i\,C\sin(k\Delta x)}, \tag{2.125}$$

Received: August 04, 2025

International Journal of Applied Mathematics
Volume 38 No. 4s, 2025
ISSN: 1311-1728 (printed version); ISSN: 1314-8060 (on-line version)

whose magnitude component takes the form

$$|G| = \frac{1}{\sqrt{[1 + 2\,F + C^2 - (2\,F + C^2)\,\cos(k\Delta x)]^2 + (C\sin(k\Delta x))^2}}, \tag{2.126}$$

which satisfies Eq. (2.16) of Part I for the end values of $\cos(k\Delta x)$:

1. for the case of $k\Delta x = \pi$, we have $|G| = \frac{1}{1+4\,F+2\,C^2} < 1$; and
2. for the limiting case $k\Delta x \to 0$, we have (neglecting high-order terms)

$$\lim_{k\Delta x \to \pi} |G| = 1 - (F + C^2)\,(k\Delta x)^2 < 1. \tag{2.127}$$

Thus, the Lerat's scheme is stable for the diffusion-advection equation, as corresponds to an implicit scheme and as Fig. 46 confirms.

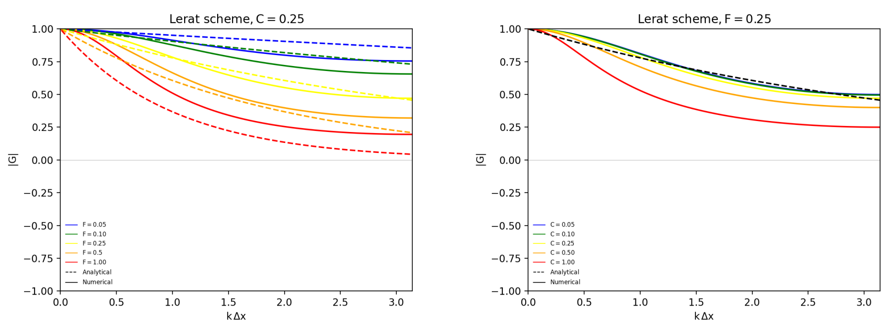

Figure 46: The same as Fig. 2 but for the Lerat's scheme.

2.11.4 Accuracy

We thirdly investigate how accurate, both in magnitude and in phase, the numerical solution is using the von Neumann's analysis.

On the one hand, by applying the discrete Fourier series grid solution of Eq. (2.1) of Part I to the Lerat's modified equation

Received: August 04, 2025

International Journal of Applied Mathematics
Volume 38 No. 4s, 2025
ISSN: 1311-1728 (printed version); ISSN: 1314-8060 (on-line version)

(2.124) including terms up to the next-to-leading order, the damping term of the numerical solution becomes (see Eq. (2.27) of Part I):

$$\exp\left\{\left[(-F-C^2)\,\frac{(\Delta x)^2}{\Delta t}+\frac{1}{24}(2\,F+12\,F^2+20\,F\,C^2+3\,C^2+7\,C^4)\,\frac{(\Delta x)^4}{\Delta t}k^2\right]k^2\,\Delta t\right\}. \tag{2.128}$$

Like its analytical counterpart (see Eq. (2.24) of Part I), we (again) notice that there is a little dissipation for $k=0$ and it will be greater at higher wavenumbers. We now present the search for stiffness in the left panel of Fig. 47 by comparing Eq. (2.128) to Eq. (2.24) of Part I in all the Fourier modes on the grid (Eq. (2.3) of Part I) evaluated for specific F values. We now do not observe stiffness. All next-to-leading terms (the second summand in equation) in Eq. 2.128 are indeed anti-damping. In all cases, we observe that the Lerat's long wavelengths dissipate more slowly (indeed, too slowly) that those in the the analytical solution do, and do so equally for progressively higher values of F. The Lerat's grid function has also just one underdamped regimen. Next, a more in-depth explanation of this effect is found. The right panel of Fig. 47 shows the same for specific C values. Next, a more in-depth explanation of this effect is found.

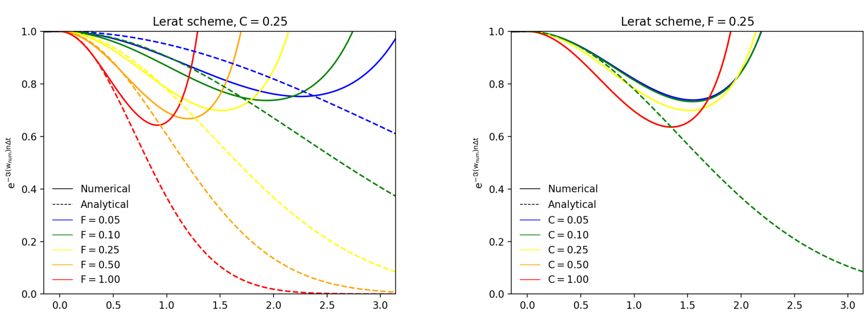

Figure 47: The same as Fig. 3 but for the Lerat's scheme.

Alternatively, since the exact growth factor in one of the Fourier modes is equal to $\exp(-\alpha\, k^2\,\Delta t)$, the Lerat's relative amplitude

Received: August 04, 2025

International Journal of Applied Mathematics
Volume 38 No. 4s, 2025
ISSN: 1311-1728 (printed version); ISSN: 1314-8060 (on-line version)

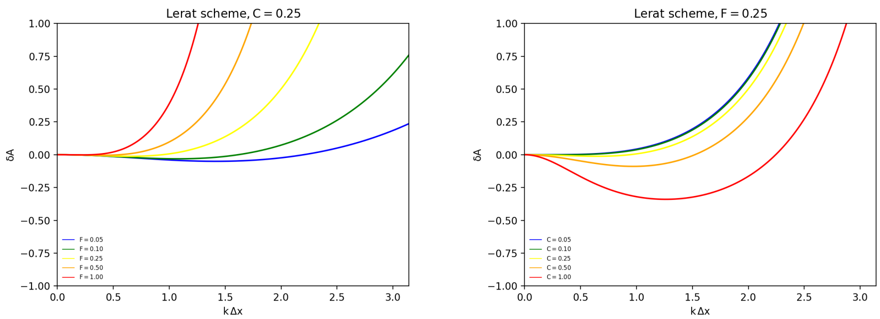

Figure 48: The same as Fig. 4 but for the Lerat's scheme.

error, Eq. (2.29) of Part I, is given by

$$\delta A = \frac{e^{\alpha\, k^2\, \Delta t}}{\sqrt{[1 + 2\, F + C^2 - (2\, F + C^2)\, \cos{(k\Delta x)}]^2 + (C \sin{(k\Delta x)})^2}} - 1, \tag{2.129}$$

In the left panel of Fig. 48 we show this error in all the Fourier modes on the grid (Eq. (2.3) of Part I) evaluated for for a specific and illustrative value of F (indicated in the legend) with low and high constant C values, where we observe that almost all the modes, but especially those of high frequency (say, the worst modes), are excesively under-damped (in agreement with the underdamped regimen from Eq. 2.128) and, consequently, the Lerat's scheme is going to lose a lot of accuracy. In fact (as the right panel of Fig. 48 confirms) we need very low values of F for high computational efficiency from this dissipative point of view.

We thus show that the dissipative numerical behavior of Lerat's scheme is very different to that shown in the Part I and very similar to those of Laasonen and Molenkamp in this paper.

On the other hand, by applying the discrete Fourier series grid solution of Eq. (2.1) of Part I to the Lerat's modified equation (2.124) truncated up to the five-order derivatives, then we see that

Received: August 04, 2025

International Journal of Applied Mathematics
Volume 38 No. 4s, 2025
ISSN: 1311-1728 (printed version); ISSN: 1314-8060 (on-line version)

the dispersive term is given by

$$\exp\left\{i\,k\,\left[x - v\,t + \frac{1}{6}(C + 6\,F\,C + 5\,C^2)\,\frac{(\Delta x)^3}{\Delta t}\,k^2\,t\right]\right\}, \quad (2.130)$$

implying the dispersive phase velocity shown in Fig. 49; where we find a numerical propagation speed much lower than the physical one causing phase lag, but shifting away from the physical one as C increases for fixed F and likewise as F increases for fixed C. This leads to the fact that the instantaneous velocity does not flip sign because the numerical speed never reaches exact value, implying the Lerat's scheme don't have instability issue. More on this later.

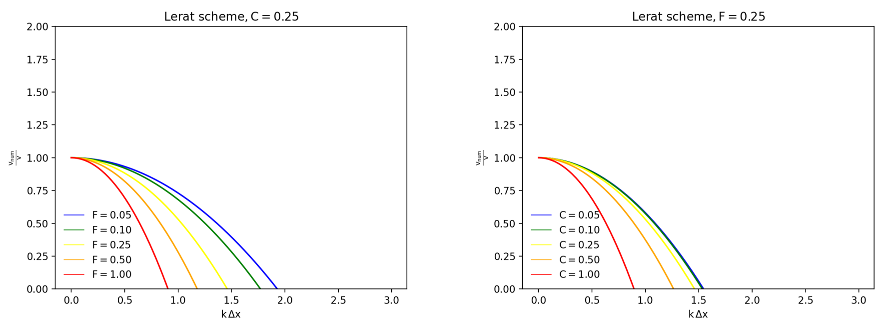

Figure 49: The same as Fig. 5 but for the Lerat's scheme.

Alternatively, from the von Neumann's complementary analysis point of view, the numerical phase component of the Lerat's growth factor, Eq. (2.126), is given by

$$\phi = \arctan\left(\frac{\Im(G)}{\Re(G)}\right) = \arctan\left(\frac{-C\,\sin(k\Delta x)}{1 + 2\,F + C^2 - (2\,F + C^2)\,\cos(k\Delta x)}\right), \quad (2.131)$$

which we show in the Fig. 50.

We find that the (dispersive) behavior is similar to that using the Laasonen's scheme for fixed F. Indeed, the upper right panel of Fig. 50 shows us that for all values of C we have leading shift, the relative phase error is less than 0 (see the lower right panel of

Received: August 04, 2025

International Journal of Applied Mathematics
Volume 38 No. 4s, 2025
ISSN: 1311-1728 (printed version); ISSN: 1314-8060 (on-line version)

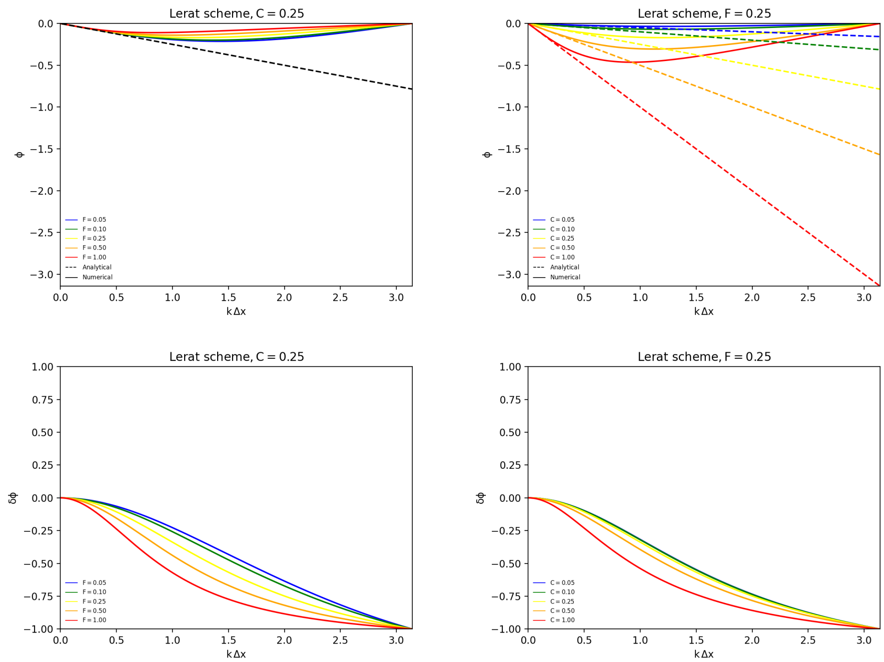

Figure 50: The same as Fig. 6 but for the Lerat's scheme.

Fig. 50), indicating a numerical propagation speed smaller than the physical one; but shift away from the line $\delta\phi = 0$, implying again the Laasonen's scheme don't have instability issue, either. The right panels in the Fig. 50 show the same for fixed F and varying C.

We thus show that the dispersive numerical behavior of Lerat's scheme is very similar to that shown in the Part II and also to those of Laasonen and Molenkamp in this paper.

2.11.5 Monotonicity

Since the Lerat's scheme is implicit the convex combination technique fails to estimate its monotonicity. Therefore we must demonstrate Eq. (2.31) of Part I. From Eq. (2.122) (see Table 1) we also

Received: August 04, 2025

International Journal of Applied Mathematics
Volume 38 No. 4s, 2025
ISSN: 1311-1728 (printed version); ISSN: 1314-8060 (on-line version)

get

$$(-F-0.5\,C-0.5\,C^2)\,T_{j-2}^{n+1}+(1+2\,F+C^2)\,T_{j-1}^{n+1}+(-F+0.5\,C-0.5\,C^2)\,T_j^{n+1}=T_{j-1}^n, \tag{2.132}$$

which subtracted from Eq. (2.98) gives

$$\begin{aligned}T_j^{n+1}-T_{j-1}^{n+1}=T_j^n-T_{j-1}^n&+(F-0.5\,C+0.5\,C^2\,(T_{j+1}^{n+1}-T_j^{n+1})\\&+(F+0.5\,C+0.5\,C^2)\,(T_{j-1}^{n+1}-T_{j-2}^{n+1})\\&-(2\,F+C^2)\,(T_j^{n+1}-T_{j-1}^{n+1}),\end{aligned} \tag{2.133}$$

and if in this equation we take the absolute value of both sides, use the triangle inequality on the right-side and sum the two sides over all j then we get Eq. (2.31) of Part I. Hence, the Lerat's scheme is monotone and does not introduce oscillations.

2.12 The Crouzeix's 1980 single-step semi-explicit scheme

2.12.1 Construction

In 1980 Crouzeix [3] presented the same approximation as Schmidt did, but discretizing the diffusion part in an implicit way, and the other part in an explicit way; i.e.

$$\frac{T_j^{n+1}-T_j^n}{\Delta t}=-v\frac{T_{j+1}^n-T_{j-1}^n}{2\Delta x}+\alpha\frac{T_{j-1}^{n+1}-2T_j^{n+1}+T_{j+1}^{n+1}}{(\Delta x)^2}. \tag{2.134}$$

Table 1 emphasizes that Eq. (2.134) is the semi-explicit counterpart of both the Schmidt's explicit scheme and the Laasonen's implicit scheme.

2.12.2 Consistency and order of accuracy

We firstly a nalyze t he c onsistency o f t he s cheme u sing t he Hirt's method. Substituting each value of T at points other than point

Received: August 04, 2025

International Journal of Applied Mathematics
Volume 38 No. 4s, 2025
ISSN: 1311-1728 (printed version); ISSN: 1314-8060 (on-line version)

(x_j, t^n) in the right hand side of Eq. (2.134) in Table 1 in a Taylor series around the value T_j^n at that point (x_j, t^n), around the value T_j^{n+1} at the point (x_j, t^{n+1}) in the left hand side, and finally expanding the value T_j^{n+1} around (x_j, t^n), i.e. we substitute Eqs. 2.6, 2.12 and 2.13 of Part I in Eq. (2.134), gives

$$\begin{aligned}\frac{\partial T}{\partial t} + v\frac{\partial T}{\partial x} - \alpha\frac{\partial^2 T}{\partial x^2} = &-\frac{\Delta t}{2}\frac{\partial^2 T}{\partial t^2} - \frac{(\Delta t)^2}{6}\frac{\partial^3 T}{\partial t^3} - v\frac{(\Delta x)^2}{6}\frac{\partial^3 T}{\partial x^3} \\ &- \frac{(\Delta t)^3}{24}\frac{\partial^4 T}{\partial t^4} + \frac{\alpha\,(\Delta x)^2}{12}\frac{\partial^4 T}{\partial x^4} + \cdots\,,\end{aligned} \tag{2.135}$$

which is the same equation as that of the Schmidt's scheme. We then see from that equation, which is not the modified equation, that the right hand side vanishes when $\Delta t \to 0$ and $\Delta x \to 0$ and therefore the Crouzeix's scheme of calculation is consistent. In addition, this side goes to zero as the first power of Δt and the second power of Δx, implying that the scheme is of first order accuracy in time and second order accuracy in space as well, as expected by construction.

We furthermore provide here the evolution equation with only space derivatives, i.e. the modified equation. In order to achieve it, we firstly find expressions for $\frac{\partial^2 T}{\partial t^2}$, $\frac{\partial^3 T}{\partial t^3}$ and $\frac{\partial^4 T}{\partial t^4}$, and secondly (be careful with this) for $\frac{\partial^2 T}{\partial x \partial t}$, $\frac{\partial^3 T}{\partial x^2 \partial t}$ and $\frac{\partial^4 T}{\partial x^3 \partial t}$, by differentiating Eq. (2.135); all of which we use systematically to eliminate the time derivatives in it. This implies that the modified equation associated with the Crouzeix's scheme, the equation of the grid function from Crouzeix's difference equation, is:

$$\begin{aligned}\frac{\partial T}{\partial t} + v\frac{\partial T}{\partial x} - \alpha\frac{\partial^2 T}{\partial x^2} = &\frac{-C^2}{2}\frac{(\Delta x)^2}{\Delta t}\frac{\partial^2 T}{\partial x^2} + \left(\frac{-C - 2\,C^3}{6}\right)\frac{(\Delta x)^3}{\Delta t}\frac{\partial^3 T}{\partial x^3} \\ &+ \left(\frac{2\,F + 12\,F^2 + 8\,F\,C^2 - 2\,C^2}{24}\right)\frac{(\Delta x)^4}{\Delta t}\frac{\partial^4 T}{\partial x^4} + \mathcal{O}((\Delta x)^5),\end{aligned} \tag{2.136}$$

which is one of two ways to next not only calculate the local error but also estimate the stability (see below).

Received: August 04, 2025

International Journal of Applied Mathematics
Volume 38 No. 4s, 2025
ISSN: 1311-1728 (printed version); ISSN: 1314-8060 (on-line version)

2.12.3 Stability

We secondly analyze the stability using the von Neumann's method. Substituting a term of Eq. (2.1) of Part I into each term in Eq. (2.12) we get the complex valued growth factor (Eq. (2.15) of Part I) associated with the Crouzeix's scheme:

$$G = \frac{1 - i\,C\sin(k\Delta x)}{1 + 2\,F\,(1 - \cos(k\Delta x))}, \tag{2.137}$$

whose magnitude component takes the form

$$|G| = \sqrt{\frac{1 + (C\sin(k\Delta x))^2}{[1 + 2\,F\,(1 - \cos(k\Delta x)]^2}}, \tag{2.138}$$

which satisfies Eq. (2.16) of Part I for the end values of $\cos(k\Delta x)$:

1. for the case of $k\Delta x = \pi$, we have $|G| = \frac{1}{1+4\,F} < 1$; and
2. for the limiting case $k\Delta x \to 0$, we have (neglecting high-order terms)

$$\lim_{k\Delta x\to 0} |G| = 1 - (2\,F - C^2)\,(k\Delta x)^2 < 1, \tag{2.139}$$

which implies

$$C^2 \le 2\,F; \tag{2.140}$$

We plot this condition, Eq. (2.140), in Fig. 51. Hence, the Crouzeix's semi-explicit scheme is conditionally stable for the diffusion-advection parabolic differential equation, as Fig. 52 confirms; which is the same surprise we found with Runchal's semi-explicit scheme. Indeed, unexpectedly for a semi-explicit scheme, we find that the longest wavelengths retain for their stability the Eq. (2.19), but the shortest ones do not need any condition.

Received: August 04, 2025

International Journal of Applied Mathematics
Volume 38 No. 4s, 2025
ISSN: 1311-1728 (printed version); ISSN: 1314-8060 (on-line version)

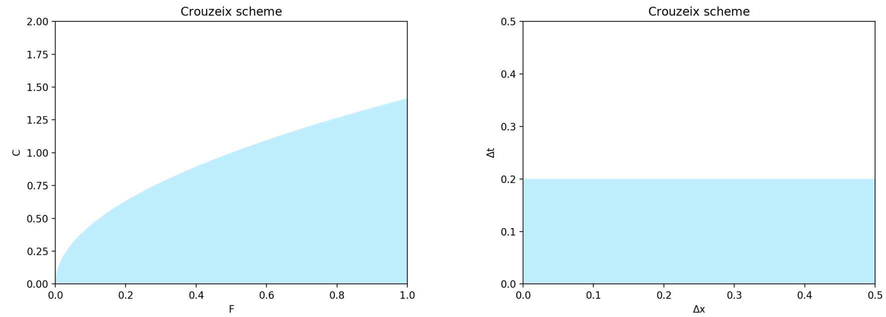

Figure 51: Stability region (by blue colour) of the Crouzeix's scheme in both FC and resolution planes, using $\alpha = 0.1$ and $v = 1$ as an example.

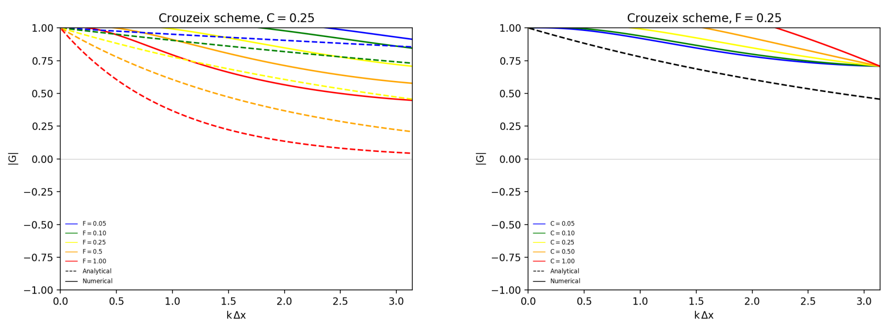

Figure 52: The same as Fig. 2 but for the Crouzeix's scheme.

2.12.4 Accuracy

We thirdly investigate how accurate, both in magnitude and in phase, the numerical solution is using the von Neumann's analysis.

On the one hand, by applying the discrete Fourier series grid solution of Eq. (2.1) of Part I to the Crouzeix's modified equation (2.136) including terms up to the next-to-leading order, the damping term of the numerical solution becomes (see Eq. (2.27) of Part

Received: August 04, 2025

International Journal of Applied Mathematics
Volume 38 No. 4s, 2025
ISSN: 1311-1728 (printed version); ISSN: 1314-8060 (on-line version)

I):

$$\exp\Big\{\Big[(-F+\frac{C^2}{2})\,\frac{(\Delta x)^2}{\Delta t}+\frac{1}{24}(2\,F+12\,F^2+8\,F\,C^2-2\,C^2)\,\frac{(\Delta x)^4}{\Delta t}k^2\Big]k^2\,\Delta t\Big\}. \tag{2.141}$$

Like its analytical counterpart (see Eq. (2.24) of Part I), we (again) notice that there is a little dissipation for $k = 0$ and it will be greater at higher wavenumbers. We now present the search for stiffness in the left panel of Fig. 53 by comparing Eq. (2.141) to Eq. (2.24) of Part I in all the Fourier modes on the grid (Eq. (2.3) of Part I) evaluated for specific F values. We now do not observe stiffness. All next-to-leading terms (the second summand in equation) in Eq. 2.141 are indeed anti-damping. In all cases, we observe that the Crouzeix's long wavelengths dissipate more slowly (indeed, too slowly) that those in the the analytical solution do, and do so equally for progressively higher values of F. The Crouzeix's grid function has also just one underdamped regimen. Next, a more in-depth explanation of this effect is found. The right panel of Fig. 53 shows the same for specific C values. Next, a more in-depth explanation of this effect is found.

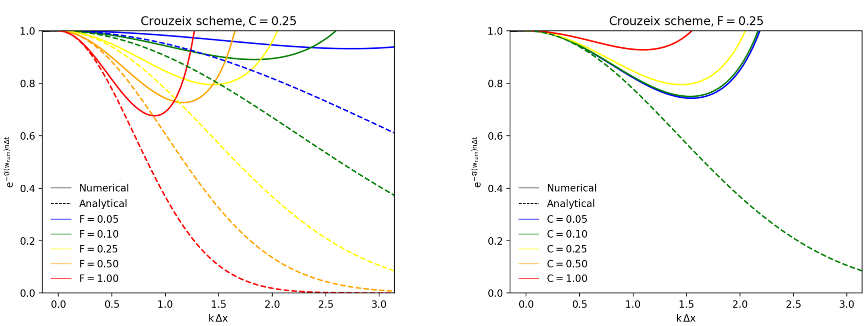

Figure 53: The same as Fig. 3 but for the Crouzeix's scheme.

Alternatively, since the exact growth factor in one of the Fourier modes is equal to $\exp(-\alpha\,k^2\,\Delta t)$, the Crouzeix's relative amplitude

International Journal of Applied Mathematics
Volume 38 No. 4s, 2025
ISSN: 1311-1728 (printed version); ISSN: 1314-8060 (on-line version)

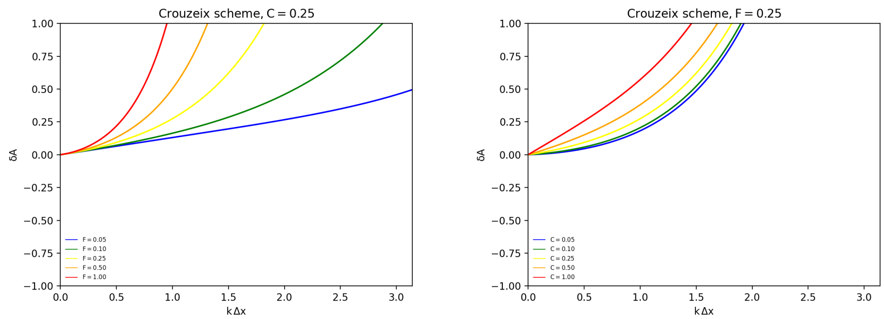

Figure 54: The same as Fig. 4 but for the Crouzeix's scheme.

error, Eq. (2.29) of Part I, is given by

$$\delta A = e^{\alpha\, k^2\, \Delta t} \sqrt{\frac{1 + (C \sin{(k\Delta x)})^2}{[1 + 2\, F\, (1 - \cos{(k\Delta x)}]^2}} - 1, \qquad (2.142)$$

In the left panel of Fig. 54 we show this error in all the Fourier modes on the grid (Eq. (2.3) of Part I) evaluated for for a specific and illustrative value of F (indicated in the legend) with low and high constant C values, where we observe that almost all the modes, but especially those of high frequency (say, the worst modes), are excesively under-damped (in agreement with the underdamped regimen from Eq. 2.141) and, consequently, the Crouzeix's scheme is going to lose a lot of accuracy. In fact (as the right panel of Fig. 54 confirms) we need very low values of F for high computational efficiency from this dissipative point of view.

We thus show that the dissipative numerical behavior of Crouzeix's scheme is very different to that of Schmidt in this study.

On the other hand, by applying the discrete Fourier series grid solution of Eq. (2.1) of Part I to the Crouzeix's modified equation (2.136) truncated up to the five-order derivatives, then we see that the dispersive term is given by

$$\exp\left\{i\, k\, \left[x - v\, t + \frac{1}{6}(C + 2\, C^3)\, \frac{(\Delta x)^3}{\Delta t}\, k^2\, t\right]\right\}, \qquad (2.143)$$

Received: August 04, 2025

International Journal of Applied Mathematics
Volume 38 No. 4s, 2025
ISSN: 1311-1728 (printed version); ISSN: 1314-8060 (on-line version)

implying the dispersive phase velocity, surprisingly not dependent on F (up to second order of accuracy), shown in Fig. 55; where we find a numerical propagation speed much lower than the physical one causing phase lag, but shifting away from the physical one as C increases for fixed F and likewise as F increases for fixed C. This is again not only unexpected but also nothing sort of a surprise as it does not correspond at all to what is expected from a scheme that has the issue of stability. We introduce for the first time in the literature this outcome, which profoundly challenge the established understanding of implicit schemes and enrich our comprehension of stability. More on this later.

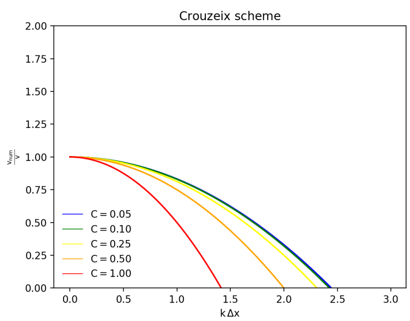

Figure 55: The same as Fig. 5 but for the Crouzeix's scheme.

Alternatively, from the von Neumann's complementary analysis point of view, the numerical phase component of the Crouzeix's growth factor, Eq. (2.137), is given by

$$\phi = \arctan\left(\frac{\Im(G)}{\Re(G)}\right) = \arctan\left(-C\,\sin\left(k\Delta x\right)\right), \qquad (2.144)$$

which we show in the Fig. 56.

We find that the (dispersive) behavior, surprisingly not dependent on F, is similar to that using the Laasonen's scheme for fixed F. Indeed, the upper right panel of Fig. 56 shows us that for all values of C we have leading shift, the relative phase error is less than 0 (see the lower right panel of Fig. 56), indicating a numerical

Received: August 04, 2025

International Journal of Applied Mathematics
Volume 38 No. 4s, 2025
ISSN: 1311-1728 (printed version); ISSN: 1314-8060 (on-line version)

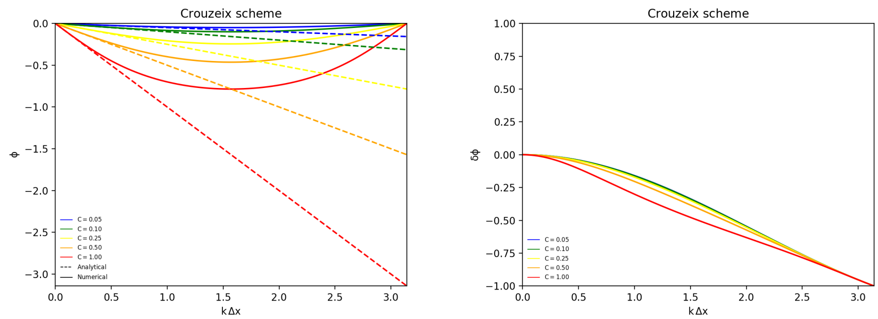

Figure 56: The same as Fig. 6 but for the Crouzeix's scheme.

propagation speed smaller than the physical one; but shift away from the line $\delta\phi = 0$, again challenging the fact that the Crouzeix's scheme has instability issue.

We thus show that the dispersive numerical behavior of Crouzeix's scheme is very diferente to that of Schmidt in this study.

2.12.5 Monotonicity

Finally, from the Eq. (2.134) the coefficients of the new solution are $-F$, $1 + 2F$, $-F$, $0.5C$, 1 and $-0.5F$. Hence, the Crouzeix's scheme is nonmonotone, i.e. it also may produce spurious oscillations.

3 The numerical tests

We illustrate different behaviour of the depending on time instantaneous grid function for a basic example and discuss the consequences and limitations of the proven results. In particular, equipped with a analytical solution, we critically assess the performance, in terms of stability, accuracy, and also convergence, of different numerical solution schemes to solve the advective diffusion. Comparisons with each other are finally commented.

Received: August 04, 2025

International Journal of Applied Mathematics
Volume 38 No. 4s, 2025
ISSN: 1311-1728 (printed version); ISSN: 1314-8060 (on-line version)

Table 2: Parameter space of the schemes analysed in this work, excluding the Richardson's and Du Fort-Frankel unstable schemes.

Author	Order	Stability	Mid frequency accuracy		Oscillations
			Growth factor squared	Phase angle tangent	
Schmidt [16]	$\mathcal{O}(\Delta t + (\Delta x)^2)$	$F \leq 0.5$ $C^2 \leq 2\,F$	$(1 - 2\,F)^2 + C^2$	$\frac{-C}{1-2\,F}$	No
Crank-Nicolson [2]	$\mathcal{O}((\Delta \mathrm{t})^2$	Stable	$\frac{(1-F^2-(0.5\,C)^2)^2+C^2}{((1+F)^2+(0.5\,C)^2)^2}$	$\frac{-C}{1-F^2-(0.5\,C)^2}$	Yes
Laasonen [8]	$\mathcal{O}(\Delta t + (\Delta x)^2)$	Stable	$\frac{1}{(1+2F)^2+C^2}$	$\frac{-C}{1+2\,F}$	No
Courant-Isaccson-Rees [1]	$\mathcal{O}(\Delta t + \Delta x)$	$C \leq 1 - 2\,F$ $C^2 - C \leq 2\,F$	$(1 - 2\,F - C)^2 + C^2$	$\frac{-C}{1-2\,F-C}$	No
Wendroff [19]	$\mathcal{O}(\Delta t + \Delta x)$	$C \leq 1 - 2\,F$	Use Eq. (2.75)	$\frac{1}{F}$	Yes
Lax-Wendroff [10]	$\mathcal{O}((\Delta t)^2 + (\Delta x)^2)$	$C^2 \leq 1 - 2\,F$	$(1 - 2\,F - C^2)^2 + C^2$	$\frac{-C}{1-2\,F-C^2}$	No
Molenkamp [12]	$\mathcal{O}(\Delta t + \Delta x)$	Stable	$\frac{1}{(1+2\,F+C)^2+C^2}$	$\frac{-C}{1+2\,F+C}$	No
Runchal [15]	$\mathcal{O}(\Delta t + \Delta x)$	$C \leq 1$ $C^2 - C \leq 2\,F$	$(1 - F - C)^2 + C^2$	$\frac{-C}{1-F-C}$	Yes
Lerat [11]	$\mathcal{O}(\Delta \mathrm{t} + (\Delta \mathrm{x})^2)$	Stable	$\frac{1}{(1+2\,F+C^2)^2+C^2}$	$\frac{-C}{1+2\,F+C^2}$	No
Crouzeix [3]	$\mathcal{O}(\Delta \mathrm{t} + (\Delta \mathrm{x})^2)$	$C^2 \leq 2\,F$	$\frac{1+C}{1+2\,F}$	$-C$	Yes

Received: August 04, 2025

International Journal of Applied Mathematics
Volume 38 No. 4s, 2025
ISSN: 1311-1728 (printed version); ISSN: 1314-8060 (on-line version)

More specifically, the illustrative application we use is the analytical solution of the representative and challenging Cauchy problem described in the Appendix A on bounded domain size $L = 1.5$, initial condition given in Eq. (A.1), and diffusion coefficient $\alpha = 0.1$ and speed $v = 1$ arbitrary units, which deals with evolving discontinuous derivatives in solution quantity. So the full parameter space of every discretization model, summarized in Table 2, is validated (or otherwise) and compared to exact solution and other numerical solutions with special emphasis on graphical exposition.

Since we want to study the general behavior of the convection–diffusion problem, we construct the grid function assuming only that the Péclet number (ratio of convection to diffusion) equals unity; which implies time step $\Delta t = 0.025$ and spatial step size $\Delta x = 0.1$, i.e. $C = F = 0.25$. This discretization also satisfies the proven demanding stability criteria and, very importantly, ensures the consistency of Crank-Nicolson scheme. The advantage of this natural approach is that all schemes can be used on an equal footing. This is our goal.

3.1 Stability tests

We are now able to extend that Section in three directions. We firstly demonstrate the instability of Richardson and Du Fort-Frankel's schemes.

Here, we use the simplest Schmidt's scheme to compute the lowest time level required by both three-level approximations.

The upper panels of Fig. 57 shows the unacceptable residuals computed with the Richardson's scheme as a consequence of its instability, as explained in Section 2.1.

The lower panels of Fig. 57 shows the same for Du Fort-Frankel's scheme. Indeed, especially in the left lower panel, we see that at first it oscillates and amplifies errors, and then diverges. Its size of the prediction error, measured in RMSE or standard deviation of the residuals is three times greater than the acceptable values.

Received: August 04, 2025

International Journal of Applied Mathematics
Volume 38 No. 4s, 2025
ISSN: 1311-1728 (printed version); ISSN: 1314-8060 (on-line version)

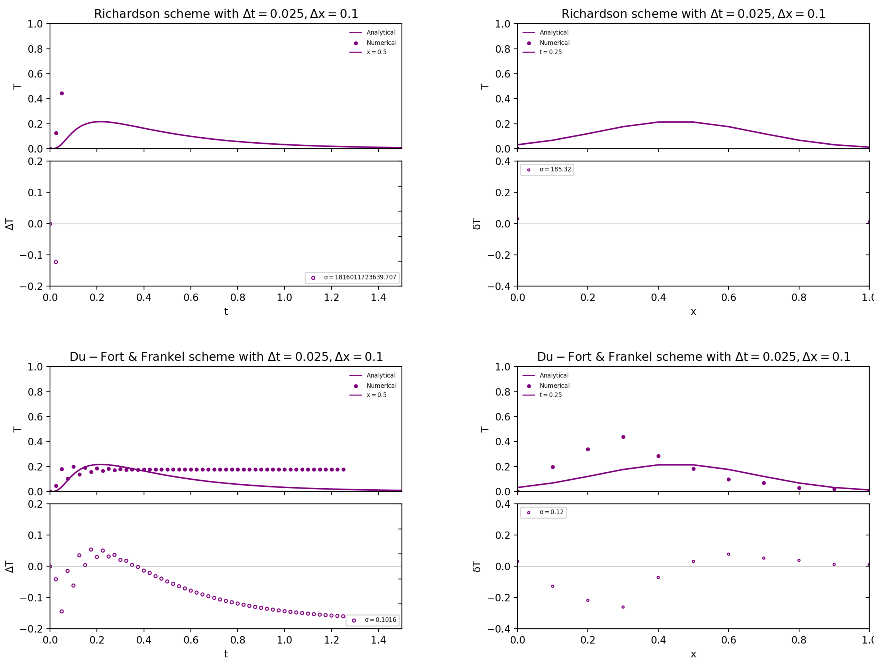

Figure 57: The unstable schemes. Left panels: $T^n_{0.50}$ appears at the top of each panel alongside $T(0.50, t)$, and residual temperatures for the mesh points are shown at the bottom. Right panels: $T^{0.25}_x$ appears at the top of each panel alongside $T(x, 0.25)$ as a evolving function of time until the end of the simulations, and residuals for the mesh points are shown at the bottom.

3.2 Accuracy tests

We secondly demonstrate the accuracy of different schemes. To achieve this, we present in Fig. 58 the results we obtain for first order explicit schemes, namely, Schmidt and Courant-Isaacson-Rees schemes. Fig. 59 presents the results obtained for first order semi-explicit schemes, namely, Wendroff, Runchal and Crouzeix's schemes. Fig. 60 presents the results obtained for fully implicit schemes, namely, Laasonen, Molenkamp and Lerat's schemes. And Fig. 61 presents the results we obtain for second order schemes,

International Journal of Applied Mathematics
Volume 38 No. 4s, 2025
ISSN: 1311-1728 (printed version); ISSN: 1314-8060 (on-line version)

namely, Lax-Wendroff and Crank-Nicolson schemes. Finally, Fig. 62 summarizes all of them, re-presenting the RMSE errors of both first- (undashed) and second-order (dashed) schemes obtained in them.

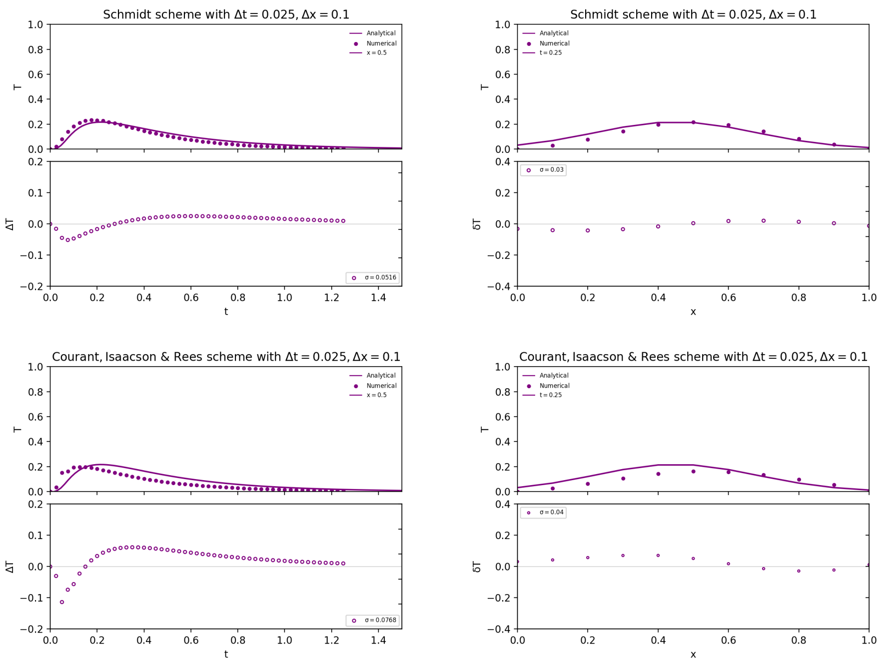

Figure 58: The same as Fig. 57 but for first order explicit schemes.

Our investigation reveals seven important results. First, surprisingly, all numerical solutions are frankly good (especially compared to the numerical solutions found in the investigations of Part I and II).

Second, Wendroff a nd C rouzeix's s chemes p roduce oscillations in their numerical solutions.

Third, Schmidt, Courant-Isaacson-Rees, Wendroff, Runchal and Lax-Wendroff's n umerical s olutions l ead t he e xact s olution. On the contrary, Laasonen, Molenkamp, Lerat and Crouzeix's numerical solutions lag behind the exact solution. In contrast, Crank-

Received: August 04, 2025

International Journal of Applied Mathematics
Volume 38 No. 4s, 2025
ISSN: 1311-1728 (printed version); ISSN: 1314-8060 (on-line version)

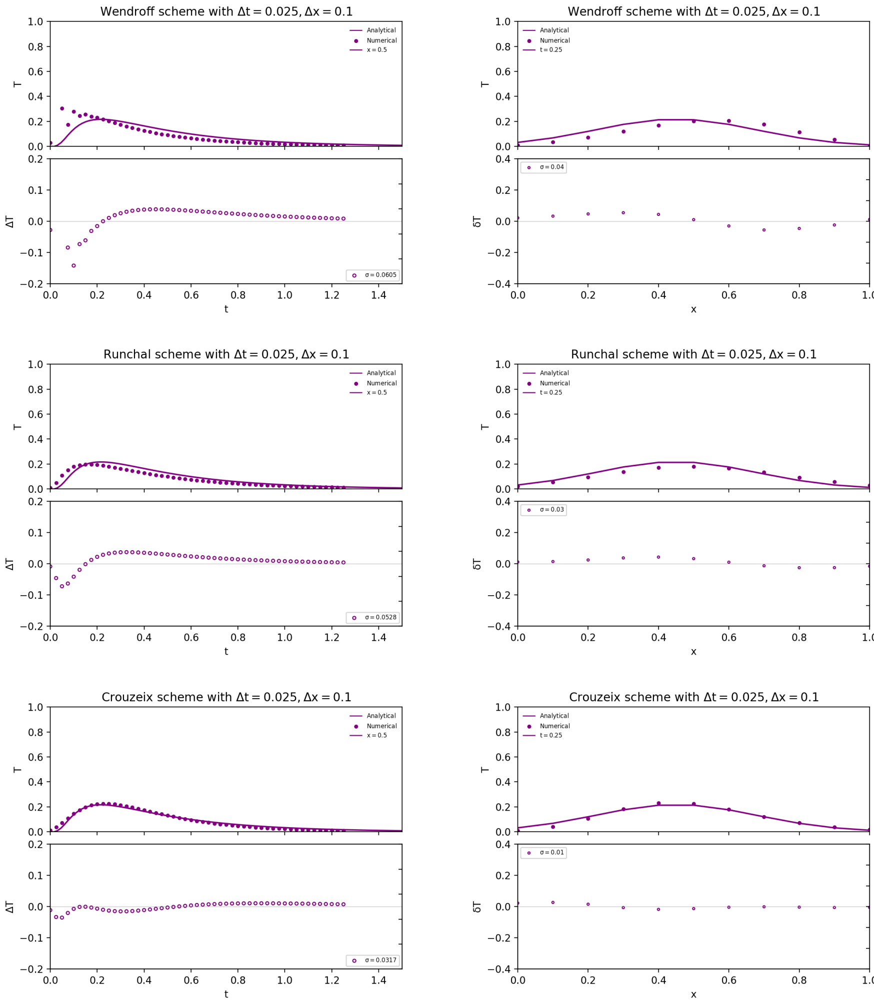

Figure 59: The same as Fig. 57 but for first order semi-explicit schemes.

Nicolson's numerical solution neither lags nor is ahead.

Fourth, Wendroff's numerical solution is the worst at the beginning.

Fifth, Courant-Isaacson-Rees's numerical solution is the worst

Received: August 04, 2025

International Journal of Applied Mathematics
Volume 38 No. 4s, 2025
ISSN: 1311-1728 (printed version); ISSN: 1314-8060 (on-line version)

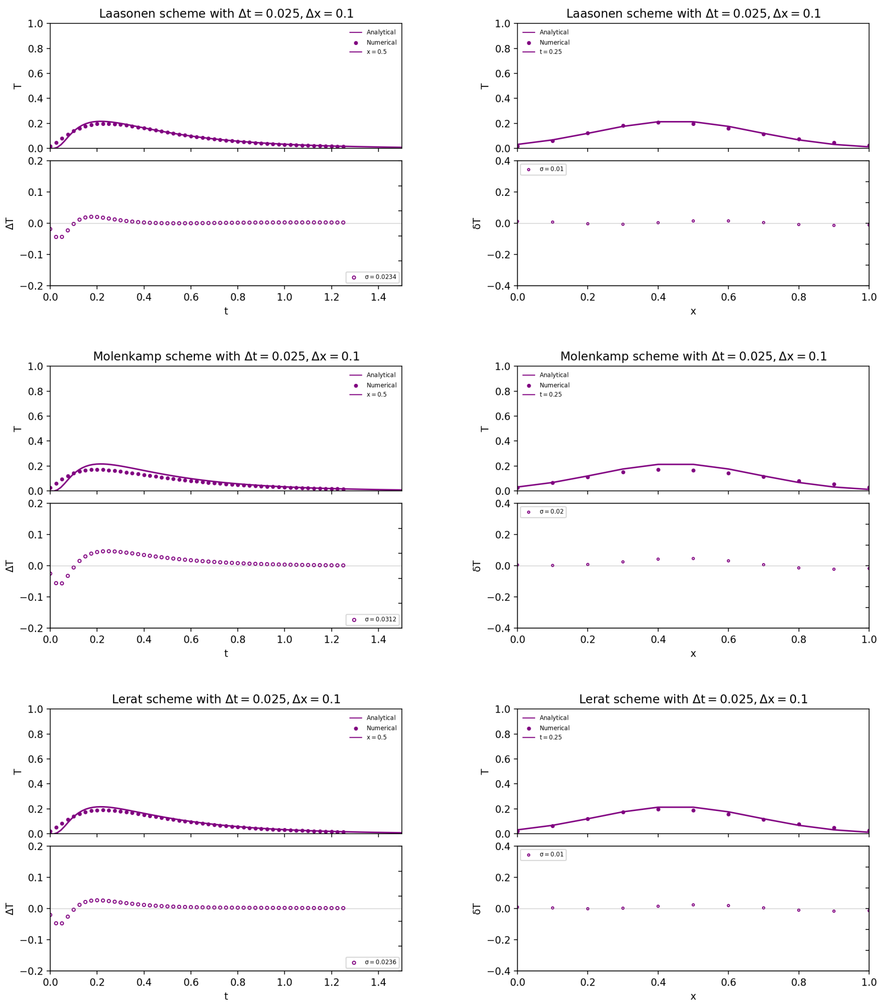

Figure 60: The same as Fig. 57 but for fully implicit schemes.

at the end.

Sixth, qualitatively speaking, explicit schemes are the worst and fully implicit schemes are the best. We should also mention that theres is hardly any difference between the first order and second order schemes (see also Fig. 62).

Received: August 04, 2025

International Journal of Applied Mathematics
Volume 38 No. 4s, 2025
ISSN: 1311-1728 (printed version); ISSN: 1314-8060 (on-line version)

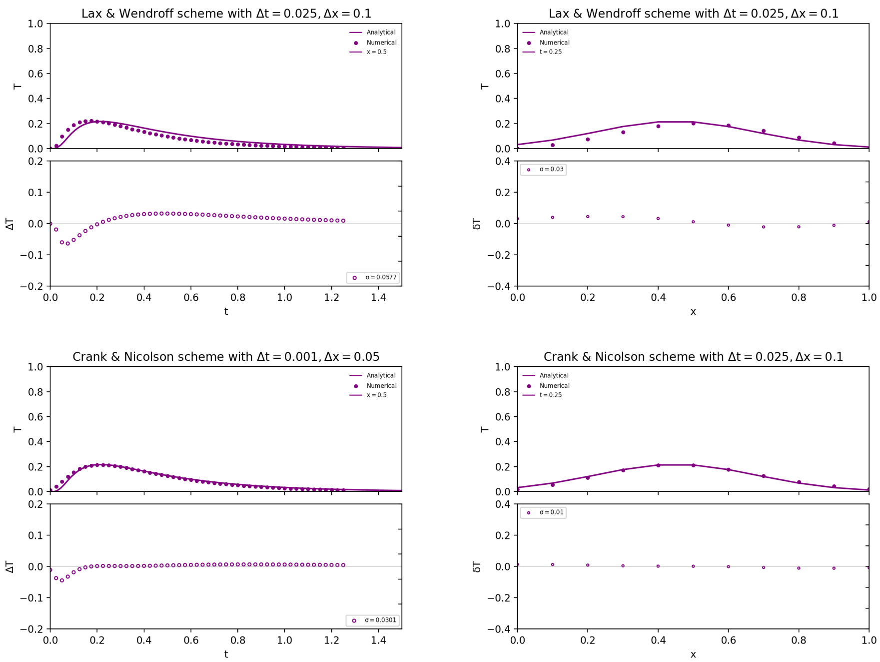

Figure 61: The same as Fig. 57 but for second order schemes.

Seventh, Crank-Nicolson's numerical solution is the most accurate.

Here we offer the following seven respective explanations.

- The convection-diffusion equation combines the effects of these two transport mechanisms and any difference algorithm is also both dissipative and dispersive (unlike what happens in Part II, where we still have diffusive and dispersive algorithms while we only have advective transport).

- Wendroff and Crouzeix's schemes are nonmonotone schemes with little numerical diffusion. Crank-Nicolson and Runchal's schemes are also nonmonotone schemes but with greater numerical diffusion that smooths artificial wiggles into their solutions.

Received: August 04, 2025

International Journal of Applied Mathematics
Volume 38 No. 4s, 2025
ISSN: 1311-1728 (printed version); ISSN: 1314-8060 (on-line version)

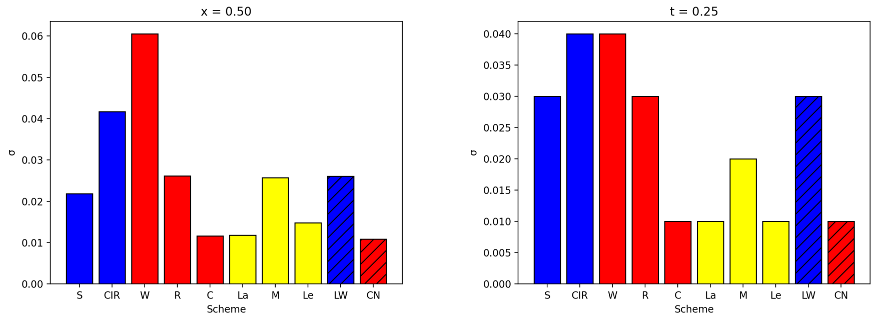

Figure 62: Bar plots with the RMSE errors. The blue bars represent explicit schemes, the red bars represent semi-explicit schemes, the yellow bars represent fully implicit schemes and the dashed bars indicate second-order schemes. It suggests that the dashed bars remain viable.

- The reason is that their relative dispersion errors are positive, negative, or almost zero, respectively.
- Wendroff's scheme has the highest dispersion error.
- Courant-Isaacson-Rees's scheme introduces the greatest numerical diffusion.
- Explicit schemes are the only lead schemes and that involve excessive numerical difusion, which are detrimental to the accuracy of the solution. In contrast, fully implicit schemes are lag and underdamped schemes; as is Crouzeix's scheme, which also provides an excellent numerical solution.

  The fact that there is no difference between first order and second order schemes, which we already found in Part II, is due to the fact that we analyze an analytical Gaussian beam composed of a linear combination of Fourier modes of arbitrarily high frequency and, as we have demonstrated, we do by using numerical schemes just able to poorly resolve a finite number of these modes, up to those in the range $0 \leq$

Received: August 04, 2025

International Journal of Applied Mathematics
Volume 38 No. 4s, 2025
ISSN: 1311-1728 (printed version); ISSN: 1314-8060 (on-line version)

$k\,\Delta x \leq \pi/2$. Indeed, all ten schemes resolve very poorly their high frequency Fourier harmonics. This fact is very significant in those problems where the initial and boundary condition is a non-smooth continuous function rendering their convergence limited.

- Crank-Nicolson's scheme has the lowest dispersion and is minimally underdamped.

3.3 Convergence tests

Lastly, we explore the error convergence of different s chemes. In Part I we already have explained that consistency means that the error at each time step goes to zero as the grid is refined a nd in Section 2 we have estimated the rate that this one-step error goes to zero. Here we investigate global (not local over one time step) rate of convergence, i.e. the overall approximation error.

Since as the discretization is refined, the dimensionless numbers F and C change, the correct way to do a convergence test for a numerical solution of a convection-diffusion equation is to keep the ratio P equal to unity; which implies refining the time step while keeping the spatial grid constant. Thus, Fig. 63 is created when the time step is $\Delta t = 0.025$, then $\Delta t/2 = 0.0125$, then $\Delta t/4 = 0.00625$, etc. with a fixed spatial mesh of $\Delta x = 0.1$.

Our investigation reveals two important results. First, for no scheme do we obtain its order of accuracy when we compute the rate of convergence which we do in l^2-norm error (Eq. (2.5) of Part I), and show in Fig. 63. In fact, we observe in the right panel of Fig. 63 that the second-order schemes are converging at about first order, while the first-order schemes are converging at less than first order.

Second, the order of convergence of all methods degrades when we look at a single point in the domain (for all elapsed time) instead of looking at all points. In fact, the left panel of Fig. 63 shows that the numerical differences decrease very little as the parameters are refined.

Received: August 04, 2025

International Journal of Applied Mathematics
Volume 38 No. 4s, 2025
ISSN: 1311-1728 (printed version); ISSN: 1314-8060 (on-line version)

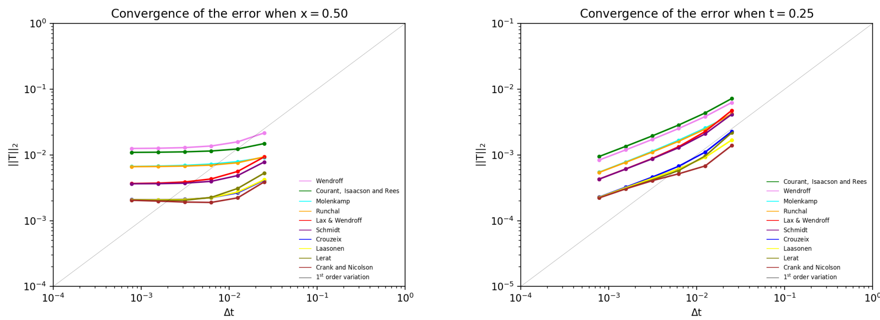

Figure 63: Convergence of the error for the Gaussian wave described in the Appendix A, which we use to rank schemes.

Here we offer the following two respective explanations.

- We have already argued in the sixth item of the previous Section that this result is due to the fact that the analytical solution is nonmonotone. Additionally, Crank-Nicolson scheme, despite being the most accurate, also introduce additional algorithmic oscillations.

- This degradation found in the left panel of Fig. 63 occurs because the spatial and temporal discretizations are intrinsically linked, and refining only one may not improve the overall accuracy if the other is already a limiting factor; i.e., the error associated with the spatial grid spacing become the dominant factor.

Finally, the convergence studies carried out and showed in Fig. 63 (which agrees with Fig. 62) also lead to better ability to discriminate between schemes. And what we find is that, unsurprisingly, Crank-Nicolson scheme of finite difference method provides the most successful description of Eq. (A.1).

Received: August 04, 2025

International Journal of Applied Mathematics
Volume 38 No. 4s, 2025
ISSN: 1311-1728 (printed version); ISSN: 1314-8060 (on-line version)

4 Concluding remarks

The scope of this Part III is exactly to complete the analysis of Parts I and II by studying the combination of advection and diffusion. To achieve this goal, we select and discuss a complete and unbiased sample of schemes for the advection-diffusion parabolic partial differential equation constituted by all those up to second-order in both time and space; which are of topical current interest. In fact, we conduct a comprehensive study of the behavior of each scheme and its implication on the error estimation of each scheme. Moreover, we empirically validate as well as illustrate all of this phenomenology by computation.

To be more precise, the classical Richardson's [14], Schmidt's [16], Crank-Nicolson [2], Laasonen's [8], Courant-Isaacson-Rees [1], Du Fort-Frankel [5], Wendroff's [19], Lax-Wendroff [10], Molenkamp's [12], Runchal [15], Lerat's [11] and Crouzeix's [3] schemes for a advection-diffusion type transport equation have been coherently revised at low and (which is a vital aspect to capture the correct behavior of the system in the regions where the space scale is very small) high wavenumbers by exploiting the power of both the reverse Taylor's analysis and the discrete Fourier's analysis, even though these associated formalisms are not physically equivalent. In fact, this distinction is important because we demonstrate these mode high wavenumbers (smallest scales) always remain poorly constrained. For more clarity, we homogeneously test all the schemes on an equal spatiotemporal discretization. In fact, we highlight the benefits of this framework. Our main conclusions, some of which (those highlighted in italics) are unexpected and reported here for the first time, are summarized below.

1. The pioneering Richardson's numerical scheme for approximating the solution to advection-diffusion linear equation is unstable.

2. The simplest Schmidt's numerical scheme for advection-diffusion differential equation is conditionally stable and conse-

Received: August 04, 2025

International Journal of Applied Mathematics
Volume 38 No. 4s, 2025
ISSN: 1311-1728 (printed version); ISSN: 1314-8060 (on-line version)

quently presents both two stiff regimes and two aceleration regimens.

3. The innovative Crank-Nicolson numerical scheme for the advection-diffusion equation *is conditionally consistent.* It presents only one moderately underdamping regimen and additionally shows moderate numerical dispersion.

4. The curious Laasonen's numerical scheme presents only a regimen which is excessively underdamped and additionally shows significant numerical dispersion.

5. The impressive Courant-Isaacson-Rees scheme for advection-diffusion differential equation is conditionally stable *but presents only one significantly underdamping regimen and practically only one acceleration regimen.*

6. The fascinating Du Fort-Frankel scheme for advective diffusion *is unstable.*

7. The surprising Wendroff's numerical scheme *is first order accurate in both space and time. Besides, it is conditionally stable but presents only one excessively underdamping regimen and practically only one regime of excessive acceleration. We also reveal spurious oscillations in the numerical solution.*

8. The ingenious Lax-Wendroff numerical scheme is conditionally stable and *presents practically only one moderately overdamping regimen*, which is nevertheless able to explain its two aceleration regimens.

9. The strange Molenkamp's numerical scheme presents only one excessively underdamping regimen and additionally exhibits only one acceleration regime.

10. The intriguing Runchal's numerical scheme *is conditionally stable, presents moderate damping and nevertheless shows two*

Received: August 04, 2025

International Journal of Applied Mathematics
Volume 38 No. 4s, 2025
ISSN: 1311-1728 (printed version); ISSN: 1314-8060 (on-line version)

acceleration regimes. We also reveal spurious oscillations in the numerical solution.

11. The elaborated Lerat's numerical scheme presents practically only one excessively underdamping regimen and exhibits only one acceleration regime explaining its stability.

12. The peculiar Crouzeix's numerical scheme *is conditionally stable, nevertheless presents only one excessively underdamping regimen and additionally shows only one acceleration regime. We also reveal spurious oscillations in the numerical solution.*

Despite its simplicity, this has however been a challenging project which contains numerous different scenarios. Indeed, the focus of the present paper was in rich variety of physical effects and numerical artifacts not explored in the original literature, which are expressly relevant for high accuracy or data systematics. Overall, our findings, we believe, should help researchers entering the field, while contributing to the ongoing efforts to refine our understanding of the diffusive advection.

Statements and Declarations

- Competing interests

  The author has no conflicts to disclose.

- Data availability

  No new data were created or analysed in this study.

A The damping and traveling Gaussian wave analytical solution as a test case

As a continuation of Part II, to test numerical codes case by case, in this paper we also select the linear one-dimensional advective

Received: August 04, 2025

International Journal of Applied Mathematics
Volume 38 No. 4s, 2025
ISSN: 1311-1728 (printed version); ISSN: 1314-8060 (on-line version)

diffusion problem

$$\begin{cases} \frac{\partial T}{\partial t} = -v\,\frac{\partial T}{\partial x} + \alpha\frac{\partial^2 T}{\partial x^2} & x \in (0,\,L),\, t > 0, \\ T(x,\,0) = e^{-200\,(x-0.2)^2} & x \in (0,\,L). \end{cases} \tag{A.1}$$

subject to a Gaussian initial condition and homogenous Dirichlet boundary conditions.

Based on the separation of variables technique, after transforming Eq. (A.1) into a diffusion equation, we obtain the following superposition solution:

$$T(x,t) = \frac{0.035355}{\sqrt{0.00125 + \alpha\,t}} e^{-\frac{2.5\,(0.2+t-v\,x)^2}{0.00125+v\,t}} \tag{A.2}$$

Additionally, we represent this explicit solution in Figure 64 for values of α and v equal to 0.1 and 1 arbitrary units, respectively, to graphically visualize how the initial profile translates to the right at constant speed with changing shape — which has to be simulated by the numerical solutions.

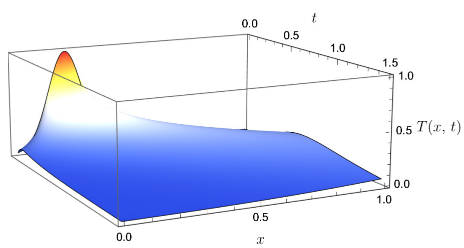

(a) 3-dimensional plot of $T(x,t)$

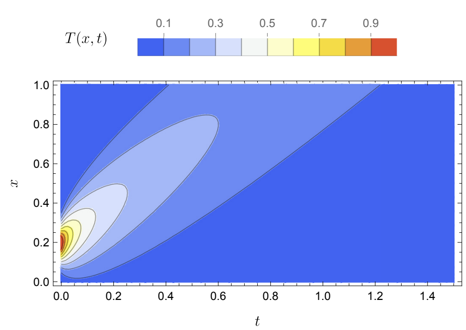

(b) Contour plot of $T(x,t)$

Figure 64: Representation of the analytical temperature distribution given by Eq. (A.2). The pseudo-colours indicate the temperature values. The contour lines are drawn at specific intervals of 0.1 units.

International Journal of Applied Mathematics
Volume 38 No. 4s, 2025
ISSN: 1311-1728 (printed version); ISSN: 1314-8060 (on-line version)

References

[1] R. Courant, E. Isaacson, M. Rees, On the solution of nonlinear hyperbolic differential equations by finite differences, *Communications on Pure and Applied Mathematics*, **5** (1952), 243-255. doi: 10.1002/cpa.3160050303

[2] J. Crank, P. Nicolson, A practical method for numerical evaluation of solutions of partial differential equations of the heat-conduction type, *Mathematical Proceedings of the Cambridge Philosophical Society*, **43** (1947), 50-67. doi: 10.1017/S0305004100023197

[3] M. Crouzeix, Une méthode multipas implicite-explicite pour l'approximation des équations d'évolution paraboliques, *Numerische Mathematik*, **35** (1980), 257-276. doi: 10.1007/BF01396412

[4] B. Cushman-Roisin, Analytical, linear stability criteria for the leap-frog, Dufort-Frankel method, *Journal of Computational Physics*, **53(2)** (1984), 227-239. doi: 10.1016/0021-9991(84)90039-1

[5] E. C. Du Fort and S. P. Frankel, Stability Conditions in the Numerical Treatment of Parabolic Differential Equations, *Mathematical Tables and Other Aids to Computation*, **7(43)** (1953), 135-152. doi: 10.2307/2002754

[6] G. Garrido, J. L. G. Pestaña, Revisiting finite difference solutions for heat-type equations. Part I. Diffusive transfer, *International Journal of Applied Mathematics*, **37(6)** (2024), 649-698. doi: 10.12732/ijam.v37i6.6

[7] G. Garrido, J. L. G. Pestaña, Revisiting finite difference solutions for heat-type equations. Part II. Advective transfer, *International Journal of Applied Mathematics*, **37(6)** (2025), 649-698. doi: 10.12732/ijam.v37i6.6

Received: August 04, 2025

[8] P. Laasonen, Über eine Methode zur Lösung der Wärmeleitungs-gleichung, *Acta Mathematica*, **81** (1949), 309-317. doi: 10.1007/BF02395025

[9] P. D. Lax, Weak solutions of nonlinear hyperbolic equations and their numerical computation, *Communications on Pure and Applied Mathematics*, **7** (1954), 159-193. doi: 10.1002/cpa.3160070112

[10] P. D. Lax, B. Wendroff, Systems of conservation laws, *Communications on Pure and Applied Mathematics*, **13**, (1960), 217-237. doi: 10.1002/cpa.3160130205

[11] A. Lerat, Une classe de schémas aux différences implicites pour les systèmes hyperboliques de lois de conservation, *Comptes Rendus Acad. Sc. Paris*, **Sér. A 288** (1979), 1033-1036.

[12] C. R. Molenkamp, Accuracy of Finite-Difference Methods Applied to the Advection Equation, *Journal of Applied Meteorology*, **7(2)** (1967), 160-167. doi: 10.1175/1520-0450(1968)007<0160:AOFDMA>2.0.CO;2

[13] Roger Peyret and Thomas D. Taylor, *Computational Methods for Fluid Flow*, Springer Berlin, Heidelberg (1983). doi: 10.1007/978-3-642-85952-6

[14] L. F. Richardson, The approximate arithmetical solution by finite differences of physical problems involving differential equations, with an application to the stresses in a masonry dam, *Philosophical Transactions of the Royal Society of London, Series A*, **210** (1910), 307-357. doi: 10.1098/rsta.1911.0009

[15] A. K. Runchal, Comparative criteria for finite-difference formulations for problems of fluid flow, *International Journal for Numerical Methods in Engineering*, **11** (1977), 1667-1679. doi: 10.1002/nme.1620111104

[16] E. Schmidt, Über die Anwendung der Differenzenrechnung auf technische Anheiz- und Abkühlungsprobleme, *Beiträge zur Technischen Mechanik und Technischen Physik: August Föppl zum Siebzigsten Geburtstag am 25. Januar 1924*, (1924), 179-189. doi: 10.1007/978-3-642-51983-3_19

[17] S. Sengupta, N. A. Sreejith, P. Mohanamuraly, G. Staffelbach, L. Gicquel, Global spectral analysis of the Lax-Wendroff-central difference scheme applied to Convection-Diffusion equation, *Computers and Fluids*, **242** (2022), 105508. doi: 10.1016/j.compfluid.2022.105508

[18] E. Sousa, The controversial stability analysis, *Applied Mathematics and Computation*, **145** (2003), 777-794. doi: 10.1016/S0096-3003(03)00274-1

[19] B. Wendroff, Finite difference approximations to solutions of partial differential equations, *New York University ProQuest Dissertations Publishing* (1958), 6102619.